Ultra-short solutions of a higher-order nonlinear Schrödinger equation: stability and applicability in dispersion managed systems

Inaugural - Dissertation

zur

Erlangung des Doktorgrades der

Mathematisch-Naturwissenschaftlichen Fakultät

der Heinrich-Heine-Universität Düsseldorf

vorgelegt von

Fabio Mancin

aus Turin

Düsseldorf

2004

Gedruckt mit der Genehmigung der Mathematisch-Naturwissenschaftlichen Fakultät der Heinrich-Heine-Universität Düsseldorf

Referent: Prof. Dr. K.-H. Spatschek
Koreferent: Prof. Dr. Christos N. Likos
Tag der mündlichen Prüfung: 22. Januar 2004

Contents

1 Introduction

1.1 Brief history of solitons

We can say that the history of solitons began in 1834, on the bank of the Edinburgh-Glasgow canal, in Scotland. An engineer by name John Scott Russel was walking along the channel, when he saw something that caught his interest. But let leave to him the description of such curious phenomenon:

"I was observing the motion of a boat which was rapidly drawn along a narrow channel by a pair of horses, when the boat suddenly stopped - not so the mass of water in the channel which it had put in motion; it accumulated round the prow of the vessel in a state of violent agitation, then suddenly leaving it behind, rolled forward with great velocity, assuming the form of a large solitary elevation, a rounded, smooth and well-defined heap of water, which continued its course along the channel apparently without change of form or diminution of speed. I followed it on horseback, and overtook it still rolling on at a rate of some eight or nine miles an hour, preserving its original figure some thirty feet long and a foot to a foot and a half in height. Its height gradually diminished, and after a chase of one or two miles I lost it in the windings of the channel. Such, in the month of August 1834, was my first chance interview with that singular and beautiful phenomenon which I have called the Wave of Translation."

This is what Russel reported to the British Association for the Advancement of Science. This moment began one of the most interesting and involved area of physics research. Russel concentrated his energy on the comprehension of such phenomenon, and after a while he was able to reproduce a model of the channel and he obtained an empirical formula expressing the speed of the wave in terms of its amplitude and the depth of the channel. With this experiment, he found out that the wave's speed is proportional to its amplitude, showing that higher waves travel faster. At that time it was believed that any non-sinusoidal

wave would broaden and decay. The excitement of Russel was caused by the lack of dispersion of the wave in the channel. Only 40 years later, Boussinesq and Rayleigh, independently, were able to derive the expression for the shape and the speed of such waves, but we have to wait until 1895, before to have an equation governing the propagation of shallow water waves. Such result was obtained by two Dutchmen, Korteweg and his student de Vries. This equation was based on the assumption that the width of the wave was big compared with the depth of the water. The Kortweg-de Vries equation, or shortly called KdV equation, has the following form

$$u_z + 6uu_t + u_{ttt} = 0 , \tag{1}$$

and its solution is

$$u = a \, \mathrm{sech}^2[b(t - vz)] . \tag{2}$$

Here $b = \sqrt{\frac{a}{12}}$, $v = 3a$, and a is a free parameter.

The people mentioned until now were the pioneers of a new area of research, which is extensively studied today in a large number of fields. However, after the work of Korteweg and de Vries, few paid attention to these waves for quite some time afterwards. We have to wait until the middle of the last century before this phenomenon returns to catch the interest of many researchers.

The beginning of a new age for solitary waves began in 1955, when Fermi, Pasta, and Ulam described a model for studying the finite heat conductivity of solids. This model consists of a set of masses connected with each other by springs. The masses represent the molecules of the matter, and the springs the forces holding the molecules together. They investigated numerically a one-dimensional lattice, in which all the energy was concentrated in the lowest mode. What

Fermi, Pasta, and Ulam expected was the thermalization of the system, by effect of a redistribution of the entire energy throughout all the modes. This did not happen: they saw the energy flow back and forth throughout all the modes and eventually recollect near the initial state.

This phenomenon was explained 12 years later by two mathematical physicists, Zabusky and Kruskal. They approximated the discreet model of Fermi, Pasta and Ulam by a continuous model, by letting the spacing between the masses approach zero. As a result, the equation that they obtained for wave propagation in the model was the KdV equation. Computer experiments showed that an initial sinusoidal pulse breaks into a train of pulses, which after a certain time recombines to almost reproduce the initial shape. Another interesting results was given by the studying the interaction between these waves: they came out of the collision with their identities intact. Zabusky and Kruskal called such special localized waves, which show particle-like behavior, solitons.

Some years later, in 1973, Hasegawa and Tappert proposed to use soliton pulses in optical communication systems through the balance between dispersion and nonlinearity. They showed that solitons in fibers are governed by the nonlinear Schrödinger equation (NLS), solved one year before by Zakharov and Shabat by using the inverse scattering method. However, at that time, there was neither capability to produce fibers with proper characteristics for this scope, nor to build lasers which could produce very short wavelengths. In 1980, Mollenauer, Stollen and Gordon demonstrated experimentally what Hasegawa and Tapper predicted 7 years before. The propagation of solitons in optical fibers was possible.

In the last 20 years much progress has been made in this field in the last 20 years. Solitons are not only extensively studied for application in optical communication systems or in hydrodynamics, but also in a quite large area of research. They are involved in description of plasmas, protein models, general relativity, high energy physics and solid state physics.

After this excursus in the history of solitons, we would like to briefly resume the most important characteristic of such particular phenomenon:

- existence due to a balance between dispersion and nonlinear effects
- remarkable stability against perturbations
- periodicity of the phase
- particle-like properties (solitons attract or repel each other)
- no changes in shape after collision
- non linear superposition of n-waves

1.2 Motivations: solitons in optical communication

After the experiment of Mollenauer, Stollen and Gordon in 1980, which confirmed the prediction of Hasegawa and Kodama about the possibility to propagate solitons in optical fibers through the balance of nonlinearity and dispersion, a wide number of scientists and private companies concentrated on this new area of research. Optical communication systems require a transmitter, a receiver and a medium for transmitting the encoded information. The transmission rate is measured in bits per second. The information is stored in a series of 0's and 1's, or on's and off's. The original communication system employed pulse trains with width of about one nanosecond, and in order to correct the distortion caused by fiber loss, repeaters were placed every several of tens kilometers. In 1988 Mollenauer and his group had shown that an amplification of the signal could be realized through a process known as Raman scattering (see Sec 1.3) and they were able to propagate a soliton over 6000 km without the need of repeaters. During the last 20 years much progress has been made in developing fibers with

proper characteristics, amplifiers and lasers which could produce very small wavelengths. The development of optical fibers, which are the basis of such systems, had led to a revolution in communication technology. Different techniques are used to transmit and decode signals (e.g. return to zero RTZ, non return to zero NRZ and dispersion phase shift keying DPSK). Soliton transmission is a promising technology for future undersea communication systems, owing specifically to its very high capacity potential (> 40-100 Gbit/s), the possibility of long amplifier/repeater spacing (> 60-100 Km), and increased transmission distances (> 10000 Km) [1]. In order to give an idea of the power of such systems, we can say that a transmission rate of 32 Gbits per second is the equivalent of one half million digitized voice channels in one fiber. Since the rate at which the information can be transmitted depends on the rate of modulation, which is naturally limited by the carrier frequency, it becomes important to investigate the transmission of shot-pulses (femtosecond pulses).

1.3 Linear and nonlinear properties of the dielectric fiber

An optical fiber consists of a central core with refractive index n_1 surrounded by a cladding layer with a slightly lower refractive index ($n_2 < n_1$), and a jacket (with $n_3 < n_2$). If the fiber has a very small cross section, any angle of incidence between the ray and the core-cladding-interface will be smaller than the critical angle ϕ_c, where

$$\phi_c = \arcsin(\frac{n_2}{n_1}) , \tag{3}$$

needed to produce the complete internal reflection of the ray. The material of choice for optical fibers is silica glass formed by fusing $Si0_2$ molecules. The reflective core-cladding index difference Δ defined by

$$\Delta = \frac{n_1 - n_2}{n_1} , \tag{4}$$

is realized by a selective use during the fabrication process. To increase the refractive index of the core dopant such as GeO_2 and P_2O_5 are used, while boron and fluorine are used in order to decrease the reflective index in silica. Additional dopant can be used depending on specific requirements.
The main linear and nonlinear properties of a dielectric fiber responsible for pulse evolution during propagation are: energy loss, chromatic dispersion, Kerr effect and Raman scattering. Next to these effects we would also like to mention Brillouin and modal birefringence [35, 38], which will not be taken into account in this work. In the next few pages we give a brief overview of these phenomena to understand the physical processes which occur inside an optical fiber.

Energy loss

The fiber loss is the main drawback in using optical fibers. This loss is due to several physical phenomena such as Rayleigh scattering, absorption and dispersion. Rayleigh scattering is the major loss mechanism. It occurs because of random fluctuation of the index of refraction in the fiber material, and is measured in units of decibel per unit length. Such local fluctuations in the index of refraction scatter light in all directions. The Rayleigh scattering loss increases as λ^{-4} and thus is dominant at short wavelengths. Even a small amount of impurities can lead to a significant absorption. The most important impurity is the ion OH^- which has an absorption peak near to 1.37 and 1.23 micrometer wavelengths. If P_0 is the power of the entering signal at the beginning of the fiber, the transmitted power P_T after a length L is

$$P_T = P_0\, e^{-\alpha L}\,, \tag{5}$$

where α is the attenuation constant, commonly referred to as the fiber loss. A rigorous discussion of the process would require quantum mechanics, but a classical picture is enough to describe a qualitative model. When electromagnetic waves travel through the dielectric, they interact with electrons which are bounded to the nucleus. The incident wave will move the electrons away from their equilibrium positions creating a dipole. Then, the electron will be attracted again from the protons to the nucleus, and this will originate an oscillating dipole. We can imagine such oscillating dipoles like little antennas, which emit electromagnetic waves in all directions at the same frequency of the incident light. This effect is called Rayleigh scattering and it responses to the attenuation of the signal through the fiber.

Absorption occurs when the electrons do not release the same fraction of energy that has excited them. This can happen when the oscillations of the dipole are damped out because of molecular vibrations.

Chromatic dispersion

A wave propagates along the fiber at a certain group velocity v_g. Since the speed of the wave depends on the index of refraction, the harmonics which compose the wave will propagate at different speeds, given by $\frac{c}{n(\omega)}$. This phenomenon is known as chromatic dispersion, and contributes to distort the incoming signal (broadening of the pulse). This effect is related to the interaction of the electric field with the bound electrons of the dielectric and can be described by the frequency dependence of the linear index of refraction $n_0(\omega)$. The major contributing factor to $n_0(\omega)$ is the resonance of bound electrons with light wave frequency. Far from the resonance region, the refractive index can be approximated by the Sellmeier equation [2]

$$n^2(\omega) = 1 + \sum_{i=1}^{n} \frac{A_i \omega_i^2}{\omega_i^2 - \omega^2} , \tag{6}$$

where ω_i is the resonance frequency and A_i is the strength of $i-th$ resonance. The effects of dispersion in fibers can be expressed by a Taylor series of the mode-propagation β

$$\begin{aligned} \beta(\omega) &= n(\omega)\frac{\omega}{c} = \\ &= \beta_0 + \beta_1(\omega - \omega_0) + \frac{1}{2}\beta_2(\omega - \omega_0)^2 + ... , \end{aligned} \tag{7}$$

where

$$\beta_m = (\frac{d^m \beta}{d\omega^m})_{\omega=\omega_0} \qquad m = 0, 1, 2, ... \tag{8}$$

β_1 is the inverse of the group velocity of the envelope

$$\beta_1 = \frac{1}{c}(n + \omega\frac{dn}{d\omega}) = \frac{1}{v_g} , \tag{9}$$

and β_2 is responsible for the pulse broadening

$$\beta_2 = \frac{1}{c}(2\frac{dn}{d\omega} + \omega\frac{d^2n}{d\omega^2}) \simeq \frac{\lambda^3}{2\pi c^2}\frac{d^2n}{d\lambda^2} . \tag{10}$$

An important parameter which characterizes the group dispersion is the group dispersion delay D defined as

$$D = -\frac{2\pi c}{\lambda^2}\beta_2 . \tag{11}$$

D is measured as the delay of arrival time in picoseconds of two light pulses with the wavelength separation of one nanometer over the distance of one kilometer. Fiber dispersion plays a crucial role in optical communication systems. However, it is possible to minimize the dispersive characteristics of the fiber by choosing an appropriate core radius and different refractive indices of the core and the cladding.

Kerr effect

A linear relation has been assumed between polarization and the applied field. However, when a large electric field is present in the fiber, nonlinear effects should also be taken into account. The origin of the nonlinear response is related to non-harmonic motion of bound electrons under the influence of an applied field. As a result, the Fourier amplitude of the induced polarization P is not linear in the electric field E, but involves terms at higher order in the electric field amplitude,

$$P = \epsilon_0(\chi^{(1)} \cdot E + \chi^{(2)} : EE + \chi^{(3)} \vdots EEE + ...) , \tag{12}$$

where ϵ_0 is the vacuum permittivity and $\chi^{(i)}$ (i=1,2,...) is the i-th order susceptibility. $\chi^{(i)}$ is a tensor of rank $i+1$. The linear susceptibility $\chi^{(1)}$ represents the dominant contribution to P. The second-order susceptibility $\chi^{(2)}$ is responsible for such nonlinear effects as second-harmonic generation and sum-frequency generation [9]. Since SiO_2 is a symmetric molecule, $\chi^{(2)}$ vanishes for silica glasses. As a result, optical fibers normally do not exhibit second-order nonlinear effects. Most of the nonlinear effects in optical fibers originate from a nonlinear refractive index, which results from the contribution of $\chi^{(3)}$. The refractive index of fibers becomes

$$\widetilde{n}(\omega, |E|^2) \;=\; n(\omega) + n_2|E|^2\,, \tag{13}$$

where $n(\omega)$ is the linear part given by Eq.(6), $|E|^2$ is the optical intensity inside the fiber, and n_2 is the nonlinear-index coefficient related to $\chi^{(3)}$. This is the so called *Kerr effect*. It occurs when the medium becomes anisotropic due to the polarization of the molecules in the presence of an applied electric field. The intensity dependence of the refractive index leads to a large number of interesting nonlinear effects; the two most important and widely studied effects are self-phase modulation (SPM) and cross-phase modulation (XPM). SPM refers to the self-induces phase shift experienced by an optical field during its propagation in optical fibers. XPM refers to the nonlinear phase shift of an optical field induced by a co-propagating field at a different wavelength. The first effect is responsible for spectral broadening of ultrashort pulses [12] and the existence of optical solitons in the anomalous-dispersion regime of fibers [13]. The second one is responsible for asymmetric spectral broadening of co-propagating optical pulses. For optical fields, which are equally intense, the contribution of XPM to the nonlinear phase shift is two times larger compared to that of SPM.

Raman scattering

The nonlinear effects governed by the third-order susceptibility $\chi^{(3)}$ are elastic in the sense that no energy is exchanged between the electromagnetic field and the dielectric medium. Another class of nonlinear effects results from stimulated inelastic scattering in which the optical field transfers part of its energy to the nonlinear medium. Two of those important phenomena are known as stimulated Raman scattering (SRS) and stimulated Brillouin scattering (SBS) and were among the first nonlinear effects studied in optical fibers [14, 15, 16]. The

main difference between the two effects is that optical phonons participate in SRS while acoustic phonons participate in SBS [35].

In presence of some resonance level ω_R of a material, the incident light wave at $\omega = \omega_0$ excites the resonance, shifts down its frequency by ω_R, and reappears at the new frequency called Stokes mode, $\omega_0 - \omega_R$. Such a process is called the *Raman scattering*. This scattering, unlike the Rayleigh scattering, is inelastic. The incident photon loses its energy by the amount $\hbar\omega_R$ although the photon number does not change. The major contribution to the resonance in a fiber comes from the optical phonon having a frequency of $\simeq 10^{13}$ Hz. Since the optical phonon has little momentum ($k_R \simeq 0$), the scattered light propagates at the group velocity v_g evaluated at $\omega_0 - \omega_R$ in the same direction as the incident light. When the frequency beating between the incident and the scattered waves collectively enhance the optical phonon, the scattering process is stimulated and the amplitude of the scattered wave grows exponentially in the direction of propagation. Such a process is called the stimulated Raman scattering (SRS), which plays an important role in the light wave propagation in a fiber. For given pump intensity I_p, the Stokes intensity I_s grows in z according to equation

$$\frac{dI_s}{dz} = g_R I_p I_s \,, \tag{14}$$

where g_R is the gain coefficient which depends on the frequency separation between the pump and the Stokes modes ($g_R = 0$ when $I_p = I_s$). When a short pulse propagates in a fiber, the carrier frequency may serve as the pump and excites lower side band spectra. As a results, the carrier frequency cascades down.

Modal birefringence

Even single mode fibers are actually bimodal due to the presence of optical bire-

fringence. The two degenerate modes are dominantly polarized in two orthogonal directions. Under ideal conditions (perfect cylindrical geometry and isotropic material), a mode excited with its polarization in x-direction, would not couple to the mode with the orthogonal y-polarization state. However, such conditions are very difficult to realize in transmission systems. Even small defects in the geometry or isotropy of the material produce a mixing of the two polarization states by breaking the mode degeneracy. This means that the mode-propagation constant β (see Eq.7) becomes slightly different for the modes polarized in orthogonal directions. This effect is known as *modal birefringence* [3, 4]. The degree of modal birefringence B is defined by

$$B = \frac{|B_x - B_y|}{k_0} = |n_x - n_y| \,, \tag{15}$$

where n_x (n_y) is the index of refraction for the x-polarized (y-polarized) mode. It can be shown [4] that for a given value B, the power between the two modes is exchanged periodically as they propagate inside the fiber with the period L_B defined by

$$L_B = \frac{2\pi}{|\beta_x - \beta_y|} = \frac{\lambda}{B} \,. \tag{16}$$

L_B is generally referred to as the beat length. The axis along which the effective mode index is smaller(larger) is called the fast(slow) axis because the group velocity for the light propagating in that direction is larger(smaller).

Because of fluctuations in the core shape and anisotropy, B is not constant along the fiber but changes. As a result, light launched into the fiber with linear polarization usually acquires arbitrary polarization. However, by artificially introducing large birefringence by means of a proper design of the fiber, it is possible to construct a fiber which allows propagation of only one polarization. Such a fiber

is called a polarization-preserving fiber [3, 4, 5, 6, 7].

Brillouin effect

A fiber material admits also excitation of an acoustic wave, which is quantum mechanically called a phonon. Since the velocity of the phonon v_a is much smaller than the speed of the light c, it has a large momentum, $\hbar k_a$. In this case the scattered wave propagates in the direction opposite to the pump wave. The scattering of a light wave of the acoustic wave is called the *Brillouin scattering* (SBS). While the Raman scattering is a forward scattering, the Brillouin scattering is a backward scattering. If the pump wave is so that the Stokes wave can continuously coexist with the pump, the frequency beating between the pump and the Stokes modes continuously induces the acoustic wave excitation, and the process grows exponentially. For a given pump I_p, the Stokes intensity I_s grows in z following a relation similar to the (14), where instead of the Raman-gain g_R we have the Brillouin-gain coefficient g_B. Because of the back scattering, SBS may become important in the case of a pulse train.

1.4 The higher-order nonlinear Schrödinger equation (HNLSE)

In Sec. 1.3 we have discussed some of the most important linear and nonlinear effects in a dielectric fiber. Now we would like to show how such effects can be described mathematically. For ultrashort pulses with width $T_0 < 0.1$ $[ps]$, or for application of solitons to long-distance communication systems, it is often necessary to include the effects of higher-order terms. The NLS equation including the higher-order terms may be expressed as [17, 45]

$$i\psi_z + a_0\psi + ia_1\psi_t + a_2\psi_{tt} + b|\psi|^2\psi = \tag{17}$$
$$= i(a_3\psi_{ttt} + a_4(|\psi|^2\psi)_t) + a_5\psi(|\psi|^2)_t \quad .$$

$\psi(z,t)$ is a complex function which represents the slowly varying envelope of the electric field. Here a_1, a_2, a_3, a_4, and b are real, while a_0 and a_5 are complex numbers. The real part of the coefficient a_0, $Re(a_0)$, represents the phase velocity, while its imaginary one, $Im(a_0)$, is the damping rate arising from the fiber loss, if $Im(a_0) > 0$, or fiber gain, if $Im(a_0) < 0$. a_1 represents the group velocity. The two terms a_2 and b take into account the chromatic dispersion and Kerr effect, respectively

$$a_2 = -\frac{\beta_2}{2}\,, \tag{18}$$

$$b = \frac{n_2\omega_0}{cA}\,, \tag{19}$$

where β_2 is the second term in the expansion (7), n_2 the Kerr coefficient of the dielectric material, A the effective core area (typical value between 10 and 20 $[\mu m^2]$), c the velocity of the light, and ω_0 the carrier frequency.

Dispersion-induced pulse broadening discussed in Sec. 1.3 is due to the lowest-order GVD (group velocity dispersion), which is proportional to a_2 in the expansion (7). When solitons propagate close to the zero-dispersion point ($\beta_2 \simeq 0$) in optical fibers, or when we have to do with femtosecond pulses, the nonlinear Schrödinger equation must be modified to take into account third order dispersion governed by a_3, which provides an important contribution to the GVD effect

$$a_3 = \frac{\beta_3}{6}\,, \tag{20}$$

where β_3 is the cubic term in the expansion (7). When pulses are injected into an optical fiber at dispersion point zero, we find that the pulses separate in the frequency domain into a portion that propagates in the normal dispersion regime and disperses away, and a portion that propagates in the anomalous dispersion regime and turns into a soliton. This behavior is an example of soliton robustness in optical fibers and also plays an important role in lasers.

The term a_4 is responsible for self-steepening and shock formation at the pulse edge [21, 22, 23, 24, 25, 26, 27, 28, 29]. It can be approximately written in the form

$$a_4 = -\frac{n_2}{cA}, \tag{21}$$

where A is the effective core area, and n_2 is the Kerr coefficient of the dielectric material.

The last term on the right-hand side of Eq.(17), a_5, is responsible for the self-frequency shift [30, 31]. That the spectrum of an ultrashort optical pulse can shift toward long wavelengths (red-shift) was discovered numerically in 1985 [27] and in an experiment of 500 fs pulse transmission in 1986 [30]. The intra-pulse Raman scattering (IRS) is responsible for a spectral shift. When femtosecond pulses propagate in fiber, the carrier frequency may serve as the pump and excites lower band spectra, so that the spectrum is continuously shifted down.
Generally, the imaginary part of a_5 is very small and in most cases ignored [28, 29, 32, 33, 34]. Under such assumption, a_5 can be written in the form

$$a_5 = \frac{n_2\omega_0}{c}T_R, \tag{22}$$

n_2, ω and c have been previously defined, and the Raman gain T_R is estimated to be $\simeq 5\ fs$ [31]. However, the possibility to compensate the effects given by $Re(a_5)$

has already been shown mathematically [36, 37]. In this case, the imaginary part of a_5 becomes the most important term for propagation of optical pulses in transmission systems.

The partial differential equation we are going to consider has the form (17), where a_i (i=0,1,..,4) and b are real, and a_5 is imaginary (all of them are of dispersive type [19, 20]). In this work we limit our attention to a well-defined parameter range, where the master equation is integrable. Eq.(17) is integrable under Sasa [41]

$$3ba_3 = a_2a_4 \ , \tag{23}$$

$$a_4 + 2a_5 = 0 \ , \tag{24}$$

and Hirota conditions [40]

$$a_4 + a_5 \ = \ 0 \ , \tag{25}$$

$$3ba_3 \ = \ a_2a_4 \ . \tag{26}$$

Under Sasa conditions Eq.(17) does not only admit bright and dark solutions, but also a linear combination of them. The stability and other properties of such solutions are the topics of the second chapter.

1.5 Dispersion managed solitons

Due to their applicability on long transmission systems, dispersion-managed (DM) solitons have recently gained considerable interest [81, 82, 83, 84, 85]. A dispersion-compensated map consists of a combination of subsections of fiber with sharply different dispersion characteristics, anomalous and normal. The structure is repeated periodically to make up the entire fiber length. The relevant fundamental equation, governing the dynamics, is the nonlinear Schrödinger equation (NLSE) [35, 38]. The NLS equation, including a non-constant dispersion term, admits soliton-type solutions, called DM solitons [70, 90]. In DM maps, the average dispersion and the nonlinear terms are much smaller than the local dispersion. To compensate the effects of loss during the propagation of the pulse, amplifiers are used (at distances of tens of kilometers).

Solitons, which propagate in a dispersion-managed system, have many advantages compared with conventional pulses. The main advantage is that the average dispersion of the map is substantially lower for a given intensity, so that the Gordon-Haus timing jitter is reduced and the system performance improved. Another important reason is, that a DM bright soliton requires a Gaussian form, which means less susceptibility to mutual interaction between pulses. The phase of DM bright solitons has a quadratic time dependency, the so called chirp. It has been proven, that DM solitons work better than standard solitons with wavelengths division multiplexing (WDM), and show a higher robustness against polarization division multiplexed (PMD), which is likely to limit any high-speed system. Therefore, DM solitons have been actively considered for the next generation of optical communication systems.

Both NLS equation and the unperturbed NLS equation (17) admit dark soliton solutions in normal dispersion regime. DM dark pulses keep a tanh-profile and their phase shows a Gaussian time dependency. While DM bright solitons in a NLS equation show oscillations being observable only on a logarithmic scale, the

oscillations of DM dark solitons are dominant on a linear scale.

Propagation of solitons in communication systems using low dispersion fibers is based on the guiding-center (average) soliton concept [82, 86, 87, 88, 89]. Existence of DM solitons has been proven for average dispersion bigger or equal zero, in case of bright pulses, and smaller or equal zero, in case of dark pulses, respectively. Solitons are not only considered for oceanic systems, but also for shorter terrestrial systems. However, most of the research in DM solitons has been focused on bright pulses. It becomes therefore natural to ask ourself if also DM dark solitons could be applied in long transmission systems and to stress out the advantages and disadvantages of such pulses. This is the main subject of the last part of this work, where several methods are used in order to find out whether periodic DM bright and dark solitons are possible for the perturbed NLS equation (17).

1.6 The subject of the present work

In recent years transmission of ultra-short pulses in optical transmission systems has become of great interest. The aim of this work to investigate the stability, interaction, and applicability in dispersion-managed systems of ultra-short pulses. Here, we concentrate our research on a particular area, where the master Eq.(17) becomes integrable. A full stability analysis of a pulse allows us to predict whether a given solution could be used for practical applications. A measure of the robustness of a pulse is given by its stability against finite perturbations on its characteristics (amplitude, width, chirp, noise and shape), and its sensitivity to changes of the fiber parameters, which are mathematically represented by the coefficients of the master equation.

In the second chapter of this work, we have investigated the stability of a new type of short-pulse solutions of Eq.(17), under Sasa conditions. What makes these solutions interesting is that, when the Sasa conditions are fulfilled, the HNLS equation admits not only a pure bright or dark pulse solutions, but also a linear combination of them. We have reported the stability analysis of bright-like and dark-like pulses in detail. With bright-like(dark-like) we mean a dominant contribution of the bright(dark) part. Such new solutions have shown a very high robustness against amplitude, width, shape, and chirp perturbations. Even when an initial random noise disturbs the initial pulse, no sign of instability has been observed.

Significant results also come from the study of the interaction and the collision between pulses. We have observed that a repulsive force acts between bright-like pulses, while two dark-like pulses form a bound state. On the other hand, when we let both bright-like and dark-like pulses collide, we see that they cross each other preserving their shape. Such particle-like behavior indicates that the solitary waves behave like solitons.

Next, we have investigated the stability of those pulses when the characteristics of the fiber, mathematically represented by the coefficients of the HNLS equation, do not exactly satisfy the condition required for the soliton existence. We have noticed that when the Sasa conditions are not exactly fulfilled, bright-like and dark-like pulses can become strongly unstable. By instability of the pulse we mean that in a few hundreds dispersion lengths, it changes its form so drastically that the receiver is not anymore able to detect it. These new types of solutions have shown a very high instability in case of perturbations on the second order dispersion (GVD), and third-order dispersion (TOD), respectively a_2 and a_3 in Eq.(17). This result implicates that such kind of waves could never be employed for practical systems. On the other hand, if the nonlinear coefficients are touched, the pulse is stable. Results of particular interest are obtained by studying the pulse stability when the term a_5 is disturbed. In fact, in case of bright-like pulses,

the initial distribution changes its characteristics and evolves into a completely new type of solution. This means that other solutions exist even when the Sasa conditions are not exactly fulfilled.

In the third and fourth part of this work we present some analytical methods useful to investigate the stability of bright pulses and their interaction. In particular, we are interested to confirm the results numerically obtained in the previous chapter, and understand whether bright pulses are more stable in other coefficient ranges. We have seen that bright pulses under Hirota conditions (see Sec. 1.4) do not present any instability when the characteristics of the pulse and the coefficients of the master equation are disturbed. Three types of solutions have been studied in detail. In all cases, the analytical results have been compared with direct numerical simulations.
In order to estimate a bit rate for short-pulses, it becomes very important to analyze the interactions of signals during their propagations in a fiber. At this scope we have introduced the Karpman Solv'ev approach (KSA). This method allows us to derive a system of differential equations which describes the evolution of the characteristic of the pulse along the fiber during their interaction. By numerical simulation we have proved a good qualitative agreement of such approach in case of bright pulses under Hirota conditions.

For transmission of signals over long distances, dispersion managed (DM) maps are commonly used. Both, the definition of DM maps and their advantages with respect to standard monomode fibers, have been already discussed in the previous section dedicated to dispersion managed solitons. In the last part of this work, we present four different methods which can be used in order to find periodic bright and dark solutions of a given DM map. To find for these solutions one must search for pulses that, at the end of the fiber, represent the same ampli-

tude and width from the beginning. The first two methods are the variational approach and the integral equation, respectively. When the higher-order terms in the HNLS equation are much smaller with respect to GVD and SPM, these approaches produce very good results. However, they can not be applied with success on DM dark pulses. On the other hand, by employing only numerical methods, we have seen that DM dark solitons for both NLS and HNLS equations exist. In the fourth and last part, a new semi-analytic method has been presented. Even in this case we have succeeded in finding DM dark solitons. The main advantage of the last two methods, with respect to the first two is, that the higher-order terms have not been treated as perturbations. This means that the obtained solutions are very close to the exact solution of the map. The pulses obtained have been propagated over tens dispersion lengths, and at the end of each map no changes in shape have been observed.

2 Stability of bright-like and dark-like pulses

In this first part of the work we investigate a new type of solutions of the higher-order nonlinear Schrödinger equation (17) under Sasa conditions [41]. Those solitary waves are very interesting because their particular form, which is given by a combination of bright and dark pulses. The so far known bright solitary wave solutions were obtained under zero boundary conditions. Additional solutions, describing the evolution of ultra-short light pulses and shocks in optical fibers, were recently presented by Li et al [49]. It was shown that both, bright-like and dark-like soliton solutions, exist in the anomalous and the normal dispersion regions, respectively. As is being demonstrated here, those solutions can be further generalized to a combination of bright and dark solitons.

The master equation we are going to consider has several advantages. First, it takes into account important effects beyond the standard nonlinear Schrödinger (NLS) description, such as third order dispersion (TOD), as well as self-steepening and self-frequency shift arising from stimulated Raman scattering (SRS). Secondly, under Sasa conditions the master equation is integrable and exact analytical solutions of different types are known.

Stability is the natural and most important problem consecutive to any presentation of new solutions. In the present case stability is especially important because of the potential applications in transmission systems of the next generation.

The chapter is organized as follows. We start with the model and the new analytic solutions. Then we demonstrate the stable propagation of those waves by employing appropriate numerical simulation methods. The dynamics will be studied over several thousand dispersion lengths. Successively, we will apply perturbations on some of the characteristic parameters (amplitude, width, phase, shape, and noise) and on the coefficients of the master equation in order to investigate the pulses stability.

Finally, we shall investigate interaction and collision between solitary waves and

we discuss whether the stable solutions show a particle-like behavior.

2.1 New analytical solutions for ultra-short pulses

Ultra-short light-pulses propagation may be described by an equation of the form (17), where a_0 and a_1 have been set to zero

$$\begin{aligned} \psi_z &= i(a_2\psi_{tt} + b|\psi|^2\psi) + a_3\psi_{ttt} + a_4(|\psi|^2\psi)_t \\ &\quad + a_5\psi(|\psi|^2)_t \ . \end{aligned} \tag{27}$$

ψ is the slowly varying envelope of the electric field, depending on space z and time t, respectively. The spatial and temporal partial derivatives are being performed in retarded time coordinates. The left-hand-side of Eq. (27), combined with the first two terms on the right-hand-side, is the standard NLS equation. The additional higher-order terms (a_3, a_4, and a_5) take into account higher-dispersive as well as SRS effects, respectively. To be more specific, a_2, b, a_3, a_4 and a_5, are the real parameters related to SOD, SPM, TOD, self-steepening, as well as self-frequency shift arising from SRS, respectively. The additional last three terms on the right-hand-side of Eq. (27) become important for femtosecond light-pulses, whose durations are shorter than 100 fs [35]. For picosecond light-pulses, such terms can be neglected (leading to the standard NLS equation). A solution of Eq. (27) may be written in the form

$$\psi(z,t) = A(z,t)e^{i\phi(z,t)t} \ , \tag{28}$$

when separating the solution $\psi(z,t)$ into a complex envelope $A(z,t)$ and a linear phase shift $\phi(z,t) = kz - \Omega t$. Inserting the expression (28) into Eq. (27), and removing the exponential term, we obtain the differential equation

$$A_z = i\alpha_0 A + \alpha_1 A_t + i\alpha_2 A_{tt} + i\beta|A|^2 A + \alpha_3 A_{ttt} + \alpha_4 |A|^2 A_t + \alpha_5 A^2 A_t^* \ , \tag{29}$$

where $\alpha_0 = -k - a_2\Omega^2 + a_3\Omega^3$, $\alpha_1 = 2\ a_2\Omega - 3a_3\Omega^3$, $\alpha_2 = a_2 - 3a_3\Omega$, $\alpha_3 = a_3$, $\alpha_4 = 2a_4 + a_5$, $\alpha_5 = a_4 + a_5$, and $\beta = b - a_4\Omega$.

So far the model is quite general (although dissipative as well as driving terms have been excluded already). Now we specialize further by requiring the two Sasa conditions already presented in Sec. 1.4,

$$3ba_3 = a_2 a_4 \ , \tag{30}$$

$$a_4 + 2a_5 = 0 \ . \tag{31}$$

A few words are necessary at this stage. The Sasa conditions (30) and (31) look quite restrictive at the first glance. In addition, when scaling amplitude and time we have some freedom in the choice of the a-coefficients which may be used to better fulfill Eq.(30)-(31). Now we generalize known solutions [49] by making the ansatz

$$A(z,t) = \lambda \tanh[\eta(t - \chi z)] + i\rho \ \mathrm{sech}[\eta(t - \chi z)] \ ; \tag{32}$$

λ and ρ are free parameters (see below). The form includes bright-like as well as dark-like forms. Inserting this ansatz into the basic equation (27) under Sasa conditions (30) and (31) we obtain

$$\eta^2 = \frac{a_4}{3a_3}(\rho^2 - \lambda^2) , \tag{33}$$

$$\chi = -(a_2\Omega + a_4\lambda^2) - a_3\eta^2 , \tag{34}$$

$$\Omega = \frac{b}{a_4} , \tag{35}$$

and

$$k = -\frac{2}{3}\frac{a_2 b^2}{a_4^2} . \tag{36}$$

The intensity of the solution (28) is given by

$$|\psi|^2 = \lambda^2 + (\rho^2 - \lambda^2)\mathrm{sech}^2[\eta(t - \chi z)] . \tag{37}$$

We notice that for $\lambda \neq 0$ the intensity does not vanish for $t \to \pm\infty$. A typical graph is shown in Fig. 1. For $\lambda = 0$ the distribution corresponds to a bright solitary wave, while if $\rho = 0$ to a black one.

From the relations between the coefficients a_i, b and the parameters η, ρ, λ, χ, Ω, k [see expression (33) - (36)] we recognize that the solution can describe a bright-like or a dark-like solitary wave. In order to fulfill the condition $\eta^2 > 0$, the factors $\rho^2 - \lambda^2$ and $\frac{a_4}{3a_3}$ should be simultaneously either bigger or smaller than zero. In the first case (bright-like) we have $\rho > \lambda$ and $a_3 a_4 > 0$. Since the coefficient b is

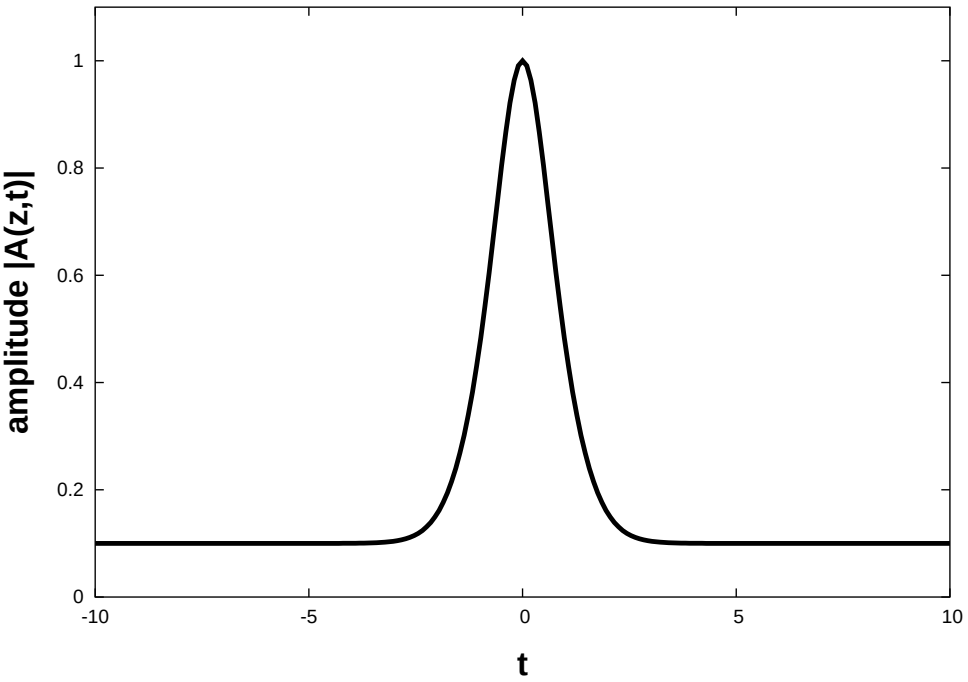

Figure 1: Absolute value $|\psi(z{=}0,t)| \equiv |A(z{=}0,t)|$ of an exact solution (28) of Eq. (27) for $\rho = 1.0$ and $\lambda = 0.1$. The coefficients a_2=0.5, b=1.0, a_3=-0.0083, a_4=-0.0498, and a_5=0.0249 have been chosen.

always positive, in the bright-like case a_2 must be bigger than zero [see Eq. (30)], in agreement with the known case of bright NLS solitons. On the other hand, we call $\rho < \lambda$ and $a_3 a_4 < 0$, requiring $a_2 < 0$, the dark-like case.

When $\lambda \to 0$ or $\rho \to 0$, the solution (32) corresponds to the simple bright or dark solitary wave solution, respectively.

In the next section we start with the stability investigation of the just presented analytical solutions by employing numerical methods.

2.2 Numerical scheme for ultra-short pulses

Because the higher-order terms in Eq.(17) and the particular form of its solutions, it becomes necessary to discuss the numerical scheme that we have adopted. In

this work, and particularly in this chapter, solutions have been take into account which are a combination of even and odd functions with no trivial boundary conditions. The higher-order coefficients are actually small terms, but in case of long propagation distances, they can strongly influence the accuracy of the results. Here, we present the scheme we have used in order to integrate the master equation, and we discuss the boundary problem.
We consider a generalized form of Eq.(17)

$$\psi_z = a_0\psi + a_1\psi_t + a_2\psi_{tt} + b|\psi|^2\psi + a_3\psi_{ttt} + a_4(|\psi|^2\psi)_t + a_5\psi(|\psi|^2)_t \ , \quad (38)$$

where all coefficients a_i (i=0,1,..,5) and b are complex numbers.
Because of the no-trivial form of Eq.(38), the Split-Step Fourier Method has been chosen. A standard scheme to solve such equation is the following. One can rewrite Eq.(38) as

$$\psi_z = (\widehat{L} + \widehat{N})\psi \ , \quad (39)$$

where $\widehat{L}$ is a linear operator which takes into account for dispersion and absorption in a linear medium, and $\widehat{N}$ is a nonlinear operator that governs the effects of fiber nonlinearities. Those operators are

$$\widehat{L} = a_0 + a_1\frac{\partial}{\partial t} + a_2\frac{\partial^2}{\partial t^2} + a_3\frac{\partial^3}{\partial t^3} \ , \quad (40)$$

$$\begin{aligned} \widehat{N} &= b|\psi|^2 + \frac{a_4}{\psi}(|\psi|^2\psi)_t + a_5(|\psi|^2)_t \quad (41) \\ &= b|\psi|^2 + (|\psi|^2)_t(a_4 + a_5) + \frac{a_4}{\psi}|\psi|^2\psi_t \ . \end{aligned}$$

Using the split-step Fourier method we propagate the pulse over a small distance h, by assuming that nonlinear and dispersive effects act independently [35]. Eq.(39) can be rewritten as following

$$\psi(z+h,t) \simeq e^{\frac{h}{2}\widehat{L}} e^{h\widehat{N}} e^{\frac{h}{2}\widehat{L}} \psi(z,t) \, . \tag{42}$$

Because of the symmetric form of the expression (42), this method is known as the symmetrized split-step Fourier method [50]. In the first step the linear operator (40) acts alone ($\widehat{N}=0$) and propagates the field $\psi(z,t)$ for a distance of $\frac{h}{2}$. Then, on the new field only the nonlinear operator (41) ($\widehat{L}=0$) acts over the whole segment length h. Finally, the field is propagated for the remaining length $\frac{h}{2}$ with dispersion only to obtain $\psi(z+h,t)$. The optical field $\psi(z,t)$ is propagated for a distance $\frac{h}{2}$ with dispersion using the FFT algorithm and Eq.(40). The execution of the exponential operator $e^{h\widetilde{L}}$ is carried out in the Fourier domain by using the prescription

$$e^{\frac{h}{2}\,\widehat{L}}\widetilde{\psi}(z,t) = (F^{-1}\, e^{\frac{h}{2}\widehat{D}(i\omega)}\, F)\widetilde{\psi}(z,t) \, , \tag{43}$$

where with F we have indicated the Fourier-transform operation, and with F^{-1} its inverse. Replacing the differential operator $\frac{\partial}{\partial t}$ by $i\omega$, we see that the linear operator (40) in Fourier space becomes just a number

$$\widehat{L}(\omega) = a_0 + ia_1\omega - a_2\omega^2 - ia_3\omega^3 \, . \tag{44}$$

The split-step Fourier method presented is only accurate up to the first order in step size h. When the higher-order terms are not very small or if the propagation distance becomes too long, this kind of integrator does not assure us the necessary accuracy. In order to increase the quality of the results, we should choose a

very small step size h, this means a very long computation time. By adopting a different procedure we can improve the accuracy of our integrator up to the second order in the step size h. The idea is to split the nonlinear step into two steps. In the first one, we consider the nonlinear part

$$\psi_z = b|\psi|^2\psi \ . \tag{45}$$

In the second one, the other two nonlinear terms (Raman terms) are taken into account

$$\psi_z = a_4(|\psi|^2\psi)_t + a_5\psi(|\psi|^2)_t \ . \tag{46}$$

Even in this case we propagate the pulse over a distance h by assuming that linear and nonlinear operators act independently. Let us consider the first nonlinear step, were the coefficient b is a complex number

$$\psi_z = (b_r + ib_i)|\psi|^2\psi \ , \tag{47}$$

with both b_r and b_i real numbers. This equation is solvable and its solution is

$$\begin{aligned} \psi(z+\frac{h}{2},t) &= \widehat{N}(\frac{h}{2}) = \\ &= \psi(z,t)e^{-\frac{1}{2}(1+i\frac{b_i}{b_r})\ln(1-2b_r\frac{h}{2}|\psi_0|^2)} \ . \end{aligned} \tag{48}$$

The solution (48) can just be used when both terms b_r and b_i are different from zero. If this condition is not satisfied, we have to go back to the nonlinear operator $\widehat{N}$, Eq.(41), and exclude the Raman terms.

In the second nonlinear step we consider the last two terms on the right-hand

side of Eq.(38). For this purpose, we consider the Split Step a la Heun. The equation for the Raman terms can be rewritten in the form

$$\psi_z = S(\psi) , \tag{49}$$

where

$$S(\psi) = a_4(|\psi|^2\psi)_t + a_5\psi(|\psi|^2)_t . \tag{50}$$

The step is given by the following expression

$$\begin{aligned} \psi(z+h,t) &= \widehat{R}\psi(z,t) \\ &= \psi(z,t) + \frac{h}{2}(S[\psi(z,t)] + S[\psi(z,t) + hS(\psi(z,t))]) , \end{aligned} \tag{51}$$

and it is valid up to the second order in step size h.
The initial field $\psi(z,t)$ is propagated along the whole segment h by using the following scheme

$$\psi(z+h,t) \simeq e^{\frac{h}{2}\widehat{L}}\ \widehat{N}(\frac{h}{2})\ \widehat{R}(h)\ \widehat{N}(\frac{h}{2})\ e^{\frac{h}{2}\widehat{L}}\psi(z,t) . \tag{52}$$

The advantage of this method compared with most differential schemes is that by using the FFT algorithm [51] the numerical evaluation of Eq.(38) becomes relatively fast [52]. The only disadvantage is that only periodic functions in both real and imaginary part can be integrated. To overcome this problem and make our integrator valid for a larger domain of functions, we present a very useful "trick". If the absolute value of our initial distribution $|\psi(z=0,t)|$ is periodic, we can always transform the non-periodic imaginary and real parts into periodic functions. The new $\widetilde{\psi}$ can be obtained as follows

$$\widetilde{\psi} \;=\; \psi e^{-i\frac{\Delta}{T}t} \tag{53}$$

where T is the domain and Δ is the difference of phase between the two points at the edge of the domain $(-\frac{T}{2}, \frac{T}{2})$. For example, in case of $\psi = \tanh(t)$, $\Delta = \pi$. Substituting the expression (53) into equation (38), we obtain

$$\begin{aligned} \widetilde{\psi}_z \;=\; & \alpha_0\widetilde{\psi} + \alpha_1\widetilde{\psi}_t + \alpha_2\widetilde{\psi}_{tt} + \beta|\widetilde{\psi}|^2\widetilde{\psi} + \alpha_3\widetilde{\psi}_{ttt} + \\ & \alpha_4(|\widetilde{\psi}|^2\widetilde{\psi})_t + \alpha_5\widetilde{\psi}(|\widetilde{\psi}|^2)_t \;, \end{aligned} \tag{54}$$

where the new coefficients are: $\alpha_0 = a_0 + i\phi a_1 - \phi^2 a_2 - i\phi^3 a_3$, $\alpha_1 = a_1 + 2i\phi a_2 - 3\phi^2 a_3$, $\alpha_2 = a_2 + 3i\phi a_3$, $\alpha_3 = a_3$, $\beta = b + i\phi a_4$, $\alpha_4 = a_4$, and $\alpha_5 = a_5$. By employing this algorithm, we have obtained a very good accuracy even for large nonlinear terms and long distance propagation.

Of course, there exists another possibility to integrate functions which do not have periodic real and imaginary parts. That method can be used for odd functions like tanh(t). The idea is to build up an initial distribution formed by two waves defined in two different parts of the domain and with initial different phases, so that we have a continuous and periodic function. A very simple case is the following

$$\psi(t) = \begin{cases} \tanh(t) & \text{if } \; t \geq 0 \\ -\tanh(t) & \text{if } \; t < 0 \end{cases} \tag{55}$$

The split-step Fourier method has been applied to a wide variety of optical problems including wave propagation in the atmosphere [50, 53], graded-index fibers [54, 55], semiconductor lasers [56, 57, 58], unstable resonators [59, 60], and waveguide couplers [61, 62].

For the specific case of pulse propagation in optical fibers, the split-step Fourier

method was first applied in 1973 [38]; its use has become widespread [63, 64] because of its fast execution compared with most finite difference schemes [65]. To integrate systems of differential equations a differential scheme up to the second order has been used.

In the course of this work many other routines have been created and used (e.g. programs for chirp, amplitude and width extrapolation, interpolation, and cut-off).

2.3 Stability of bright pulses

2.3.1 Single bright-like pulse

In order to investigate the stability of bright-like pulses numerically, we have to specify parameters and coefficients. In the following we present results for "typical" parameters and coefficients, i.e. the general conclusions will not depend on the specific values chosen for bright-like or dark-like solutions, respectively. The general conclusions have been checked by analyzing many different simulations. Using as parameters ρ=1.0, λ=0.1, a_2=0.5, and a_3=-0.0083 we are in the bright-like range. The values b=1.0, a_4=-0.0498, a_5=0.0249, and $\Omega = \frac{b}{a_4}$=-20.08 will be also used as typical parameter for dark-like solutions (see section 2.4).

η and χ are determined by Eqs.(33) and (34). From Eq. (37) one can understand the meaning of ρ and λ. They are the maximum amplitude of the pulse and the asymptotic value of the background, respectively. Fig. 1 shows the absolute value $|\psi(z,t)|$ of an exact solution of our system.

We begin the stability analysis by perturbing the amplitude of the imaginary part in Eq.(32). Multiplying the parameter ρ by either the factor p_+=1.1 or p_-=0.9, we increase or decrease the maximum initial value of $|\psi(z{=}0,t)|$ by 10 percent. The simulation results are depicted in Fig. 2. Note that in order to have a fast

and clear idea of the evolution of the perturbed distribution, we have plotted the behavior of the maximum value of $|\psi(z,t)|$ with respect to z. We clearly recognize that the amplified or reduced distributions are going to finally increase or decrease their amplitudes, respectively. In the case p_+ we get the final amplitude $\rho_{new} \simeq 1.2$, whereas in the case p_- the final amplitude is $\rho_{new} \simeq 0.8$. The widths follow the behaviors according to relation (33). Energy is being conserved. From here we conclude that an initial perturbation of ρ leads to the evolution into a new stable solution whose parameter values exactly follow the relations (33)-(36) with a newly determined value of ρ (maximum amplitude).

Next, a similar procedure is applied to the full width at half maximum (FWHM). In this case, the parameter η is multiplied by $p_\pm$. The simulation results are similar to Fig. 2, but now the final amplitudes reach the values: $\rho_{new} \simeq 1.1$ for p_+=0.9, and $\rho_{new} \simeq 0.9$ for p_+=1.1. We again find that the solution evolves into the form (32) with parameters obeying the relations (33) and (36).

In both cases, when initially either the parameter ρ or the parameter η are disturbed, we can draw the same conclusion. In a few hundreds dispersion lengths the pulses modify their amplitudes and widths and the new value of ρ and η satisfy the relation (33). When the energy of the initially perturbed solution is bigger (smaller) than the energy of the original solution, the pulses evolve into a new bound state with larger (smaller) amplitudes. The newly appearing solitary waves are stable, which can be demonstrated by simulations over thousands of dispersion lengths. Note that the relaxation into the new bound state generally occurs around 200-300 dispersion lengths.

Generalizing the previous perturbations, we next start with a smooth initial perturbation being relatively far away from an exact solution. The following expression is used in order to perturb the shape function

$$A(z=0,t) \;=\; \lambda \tanh(\eta t) + i\rho\, e^{\frac{-t^2}{\eta}} \;. \tag{56}$$

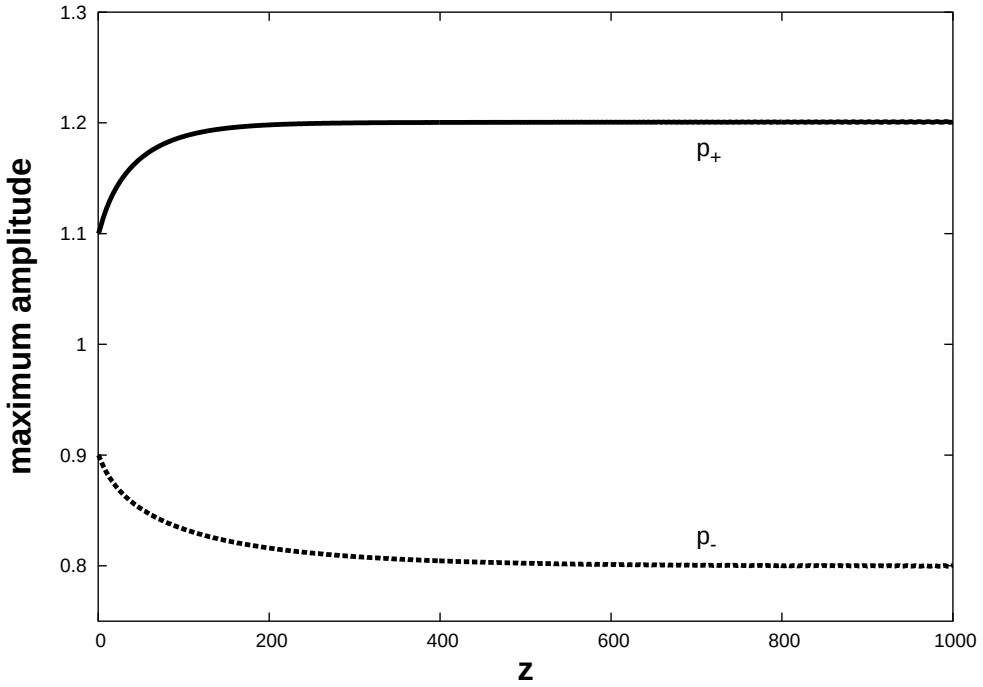

Figure 2: Evolution of the maximum amplitude $|\psi(z,t)|$ with respect to z for the case of an initial perturbation parameter ρ. Case p_+: $\rho(z=0)$=1.1, case p_-: $\rho(z=0)$=0.9. The other parameters are the same as in Fig. 1.

Instead of the sech-shape for the imaginary part of the exact solution we assume initially a Gaussian form. The real part agrees with the exact solution. However, the difference in energy between the exact solution (32) and the initial distribution (56) is very small. The numerical simulations produce results comparable to the previous cases (amplitude and width perturbations). Figure 3 shows the evolution of the maximum amplitude. During the first 300 dispersion lengths, the pulse modifies its amplitude, width, and form, but finally it evolves into a new bound state which is described by Eqs.(28) and (33)-.(36) The oscillations visible for $z >$ 600 are due to numerics. Because the periodic boundary condition used in the integrator, we get reflections from the boundaries back to the center. Note that the oscillations, also occurring in Fig. 2, are smaller since the initial distributions are closer to the final ones in those cases.

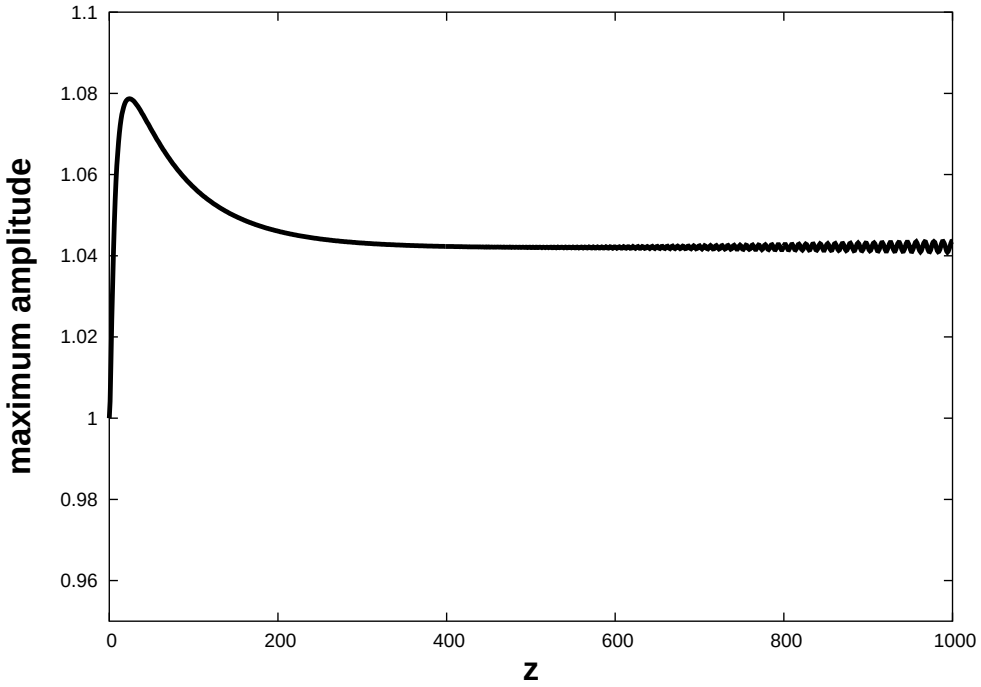

Figure 3: Amplitude evolution of the perturbed solution, Eq.(56). Even in this case the wave evolves around a new bound state.

Until now we have analyzed the stability of Eq. (28) by changing its form. Now we introduce an initial chirp by modifying the exact solution in the form

$$\widetilde{\psi}(z=0,t) \;\; = \;\; \psi(z=0,t)\; e^{ic_1 e^{-c_2 t^2}} \; . \tag{57}$$

Such perturbation produces a change in real and imaginary part, but not in the energy. The form $e^{ic_1 e^{c_2 t^2}}$ is chosen in order to preserve the initial boundary conditions of our initial distribution. The chirp has a Gaussian shape with maximum value at $t = 0$ and decreasing away from the center of the pulse, where only the background is present. For our numerical simulation we have c_1=0.01 and c_2=1.0. We have chosen c_1=0.01 in order to perturb the real part around 10 percent (remember that ρ=1.0 and λ=0.1). In fact, the initial distribution can up to t$\sim \mathcal{O}$ (1) be approximated by

$$(\lambda \tanh[\eta t] + i\rho \operatorname{sech}[\eta t])e^{ic_1} \approx (...)(1 + ic_1) \approx \tag{58}$$
$$\lambda \tanh[\eta t] - c_1\rho \operatorname{sech}[\eta t] + i(\rho \operatorname{sech}[\eta t] + c_1\lambda \tanh[\eta t])$$

For the imaginary part the perturbation is around the 0.1 percent. Under such conditions the numerical simulations do not show the convergence into a new state as was observed in the other three cases. In Fig. 4 is shown the behavior of the maximum of the distribution (57). The amplitude grows constantly but slowly along z, and the pulse does not reach any stable point. After 1000 dispersion lengths the maximum amplitude is increased only by 0.1 percent.

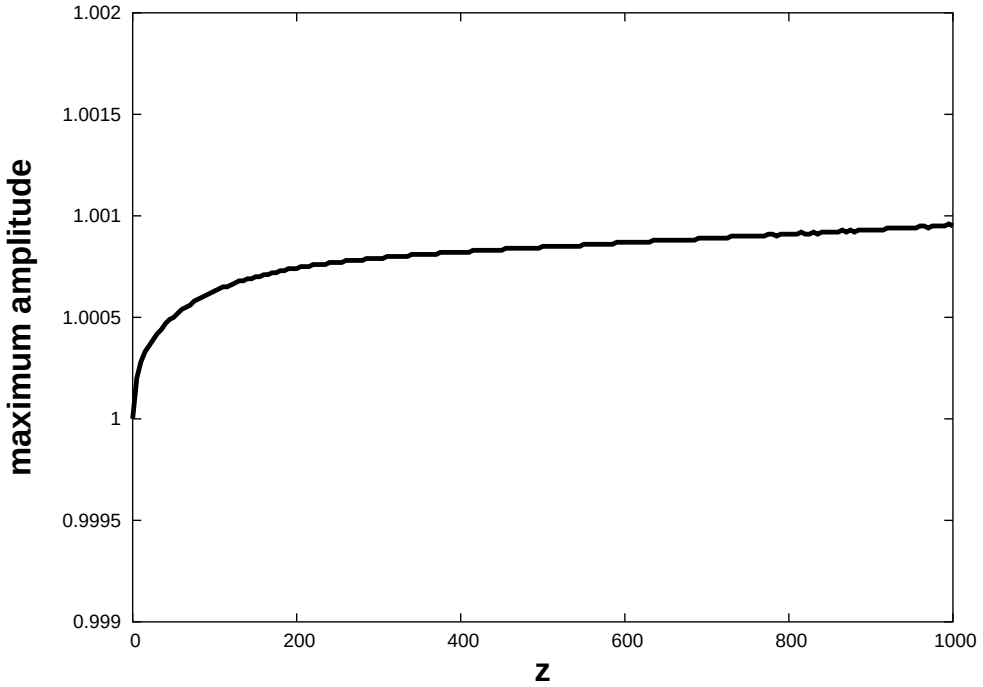

Figure 4: Amplitude evolution of the chirped pulse initially described by Eq.(57). In this case the maximum of the pulse grows very slowly along z.

We conclude the part on stability of bright-like solutions by investigating the robustness of a bright-like pulse under noise perturbations. We have initially added on the solution (28) a random noise with a maximum amplitude of 30 percent

of the background λ. The pulse was propagated over more than one thousand dispersion lengths, and no sign of instability was observed. Even for larger perturbations (up to 50 percent of λ) the wave preserves its form, amplitude, and width. The absolute value of the pulse $|\psi(z,t)|$ is shown in Fig. 5.
One important additional aspect we want to emphasize. The finite tails of the pulses do not show instability.

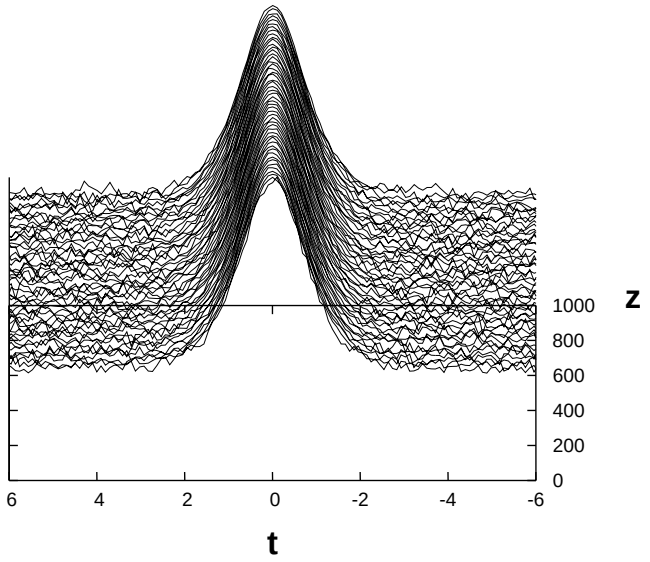

Figure 5: Evolution of $|\psi(z,t)|$ along z for an initial distribution perturbed with random noise. The maximum amplitude of the noise is δ=0.3 λ.

2.3.2 Interaction

An important task is the study of interactions between solitary waves. In this section we present results concerning the propagation of two solitary waves starting at different initial positions. We will follow the propagation over more than 1000 dispersion lengths. The initial distribution is thought as a distribution with two peaks separated by the distance d. To be more specific we choose

$$\mathrm{Real}(A(z,t)) = \begin{cases} \lambda \tanh(\eta_1(t-\frac{d}{2})) & \text{if } t \geq 0 \\ -\lambda \tanh(\eta_2(t+\frac{d}{2})) & \text{if } t < 0 \end{cases} \tag{59}$$

$$\mathrm{Imag}(A(z,t)) = \rho_1 \,\mathrm{sech}(\eta_1(t-\frac{d}{2})) + \rho_2 \,\mathrm{sech}(\eta_2(t+\frac{d}{2})) \,. \tag{60}$$

As one can note, the real part, representing the background, has not been additively composed like the imaginary one. If two pulses are well separated they can be considered as asymptotic soliton solutions of Eq. (29). We consider an initial distribution of the form (60), with $\rho_1 = 1.0$, $\rho_2 = 2.0$ and $\lambda = 0.1$. η_1 and η_2 are determined by relation (33). These parameters will lead to a collision of solitary pulses. In order to elucidate this last point, we write the shape function (32) in the form

$$A(z,t) = |A(z,t)|e^{\phi(z,t)} \,, \tag{61}$$

where

$$\phi(z,t) = \arctan(\frac{\rho \,\mathrm{sech}[\eta(t-\chi z)]}{\lambda \tanh[\eta(t-\chi z)]}) \,. \tag{62}$$

As one can see from Eq.(62), the phase ϕ depends on ρ, λ and η. Of course λ must be the same for every couple of waves, otherwise the background would present a discontinuity. Considering that η and ρ are related to each other by (33), we can argue that the phase ϕ (and the wave's velocity) depends only on the parameter ρ. This means that pulses well separated with same amplitude propagate with the same velocity. Our numerical simulations show that couples of pulses with same amplitude and initial distance $d = 10$ move parallel over one thousand dispersion lengths without interact with each other. Therefore, in order

to avoid initial interactions, we have chosen (for the case $\rho_1 = 1.0$, $\rho_2 = 2.0$) as initial distance $d = 10$. For the just mentioned parameters our simulations show that two pulses move with different and opposite velocity and after circa 200 dispersion lengths they cross each other (see Fig. 6). An important results to point out is that after the collision the form of the two solitary waves is exactly conserved. Such a characteristic particle-like behavior is a prerogative of solitons. The same effect will be observed also in the dark-like case, as one can see in the next section.

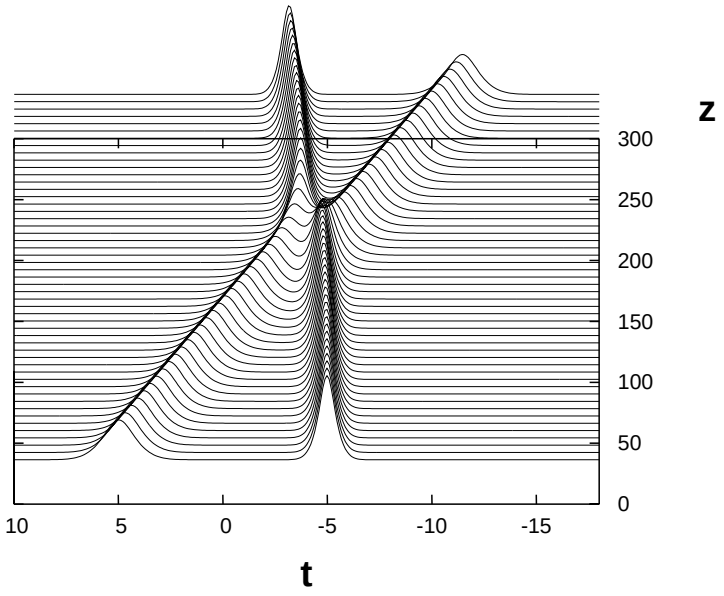

Figure 6: Collision of bright-like pulses. The 3-dimensional picture shows the collision of two solitons with initial distribution (60). ρ_1=1.0, ρ_2=2.0, λ=0.1, d=10, and η_1, η_2 calculated from (33). Any changes have been observed after the collision. Shown is the absolute value of the amplitude

We end the analysis of bright-like solitary waves by investigating the evolution of

a pair of pulses having same amplitude (ρ_1=ρ_2=1.0) and different initial distances (d=7, 6, 5, and 4). As initial distribution was used the expression (60). For such values of d we can not anymore consider the pulses as asymptotic soliton solutions of Eq.(29). When the initial distance between two pulses is large enough ($d = 6$ or 7), the interaction is very small, but decreasing the distance ($d = 4$) one can observe a strong *repulsive* force. For $d = 4$, numerical simulations show a variation of the amplitudes of the two waves along z (see Fig. 7). After 1000 dispersion lengths, the distance between them becomes larger ($d \simeq 11$), while one wave increases its amplitude (by 15.5 percent) the other one decreases it (by 7.6 percent). The two pulses evolves into new bound states which are described by Eqs. (32) and (33)-(36).

2.4 Stability of dark pulses

2.4.1 Single dark-like pulse

The objective of the present section is to complete the stability considerations by investigating the remaining case of dark-like solutions. As we previously saw, a single dark-like is realized when $\lambda > \rho$. Such condition involve $\frac{a_4}{3a_3} < 0$ (Eq.33) and, since $b > 0$, $a_2 < 0$ (Eq.30). Finally, for simulation of dark-like pulses, we have used a_2=-0.5, a_3=0.0083, λ=1.0 and ρ=0.4. The other coefficients of Eq.(27) are the same as in the previous section, while the parameters for the initial distribution are calculated by using (33)-(36). A single dark-like pulse is shown in Fig. 8. In this case the parameter ρ represents the minimum of the hump and λ the asymptotic value of the background.

Similar to the previous section, perturbation on the minimum and on the width of the shape function (32) are produced by multiplying ρ and η by factors $p_\pm$, respectively. In Fig. 9 the evolution of the minimum of a dark pulse is plotted for three different initial cases: $p_+ = 1.1$, 1.2, and 1.3. Multiplication of ρ by

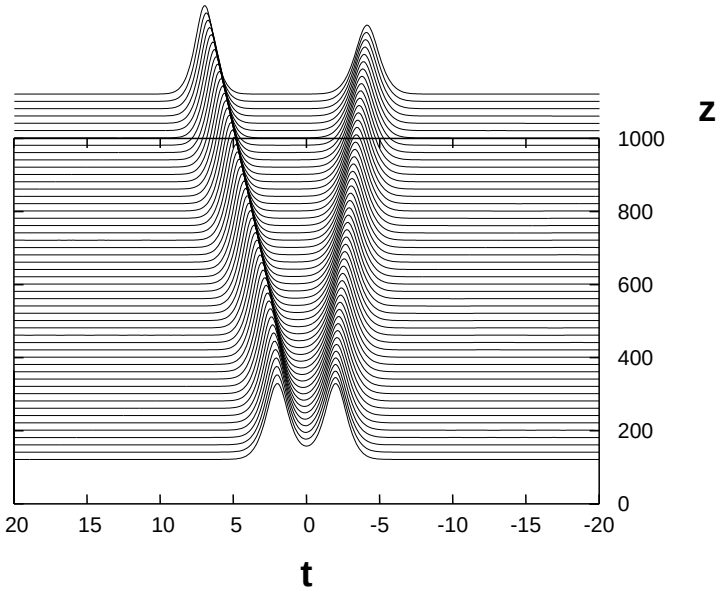

Figure 7: Interaction of bright-like pulses. The initial distance between the solitary waves is $\rho_1 = \rho_2$=1.0, λ=0.1, d=4, and $\eta_1 = \eta_2$ calculated from (33). After 1000 dispersion lengths the distance becomes $d \simeq 11$. The amplitudes of both waves change their values during the propagation.

a factor $p > 1$ means a reduction of the deepness of the humps. For dark-like waves, the convergence into a new stable state is realized in less than one hundred dispersion lengths, much faster than in the bright-like case. Similar results are obtained when ρ is multiplied by $p_- = 0.9,\ 0.8$ and 0.7. In all cases the new solutions exactly represent realizations of the form (32) and the new parameters satisfy the relations (33) and (36).

Even when the parameter η is disturbed, we can draw the same conclusions. Next, we propose the stability analysis of a dark-like pulse by perturbing its shape function. We have substituted the sech-shape of the imaginary part with

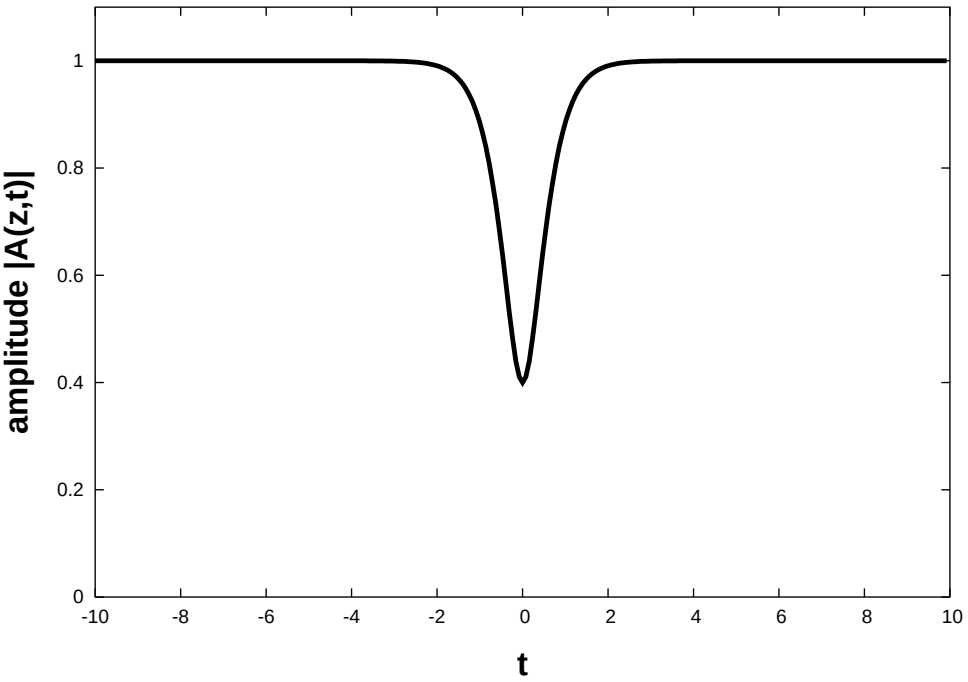

Figure 8: Single dark-like pulse. The figure shows the absolute value of the initial distribution (32) for $\rho = 0.4$ (minimum of the hump), $\lambda = 1.0$ (asymptotic value), and η calculated from (33). The coefficients of Eq. (27) are: a_2=-0.5, b=1.0, a_3=0.0083, a_4=-0.0498 and a_5=0.0249.

a Gaussian by using as initial distribution the expression (56). This substitution changes the shape of the hump but not greatly the total energy. Fig. 10 shows that the convergence into a new state is realized after few hundreds dispersion lengths. The minimum of the hump (ρ) and the new η satisfy relation (33). The pulse regain a sech-shape.

By using Eq.(57), we add a chirp to the exact solution. The distribution (28) is multiplied by $e^{ic_1 e^{-c_2 t^2}}$, where the chirp function has a Gaussian form for the reasons already discussed in a previous section. Two cases considered are: $c_1 = 1.0$, $c_2 = 0.1$ and $c_1 = 1.0$, $c_2 = 1.0$. We have used ρ=0.4, λ=1.0 and η calculated from Eq.(33). In Fig. 11 one can observe what happens when a chirp is initially applied on the exact solution. In both cases the chirped pulse converge into a

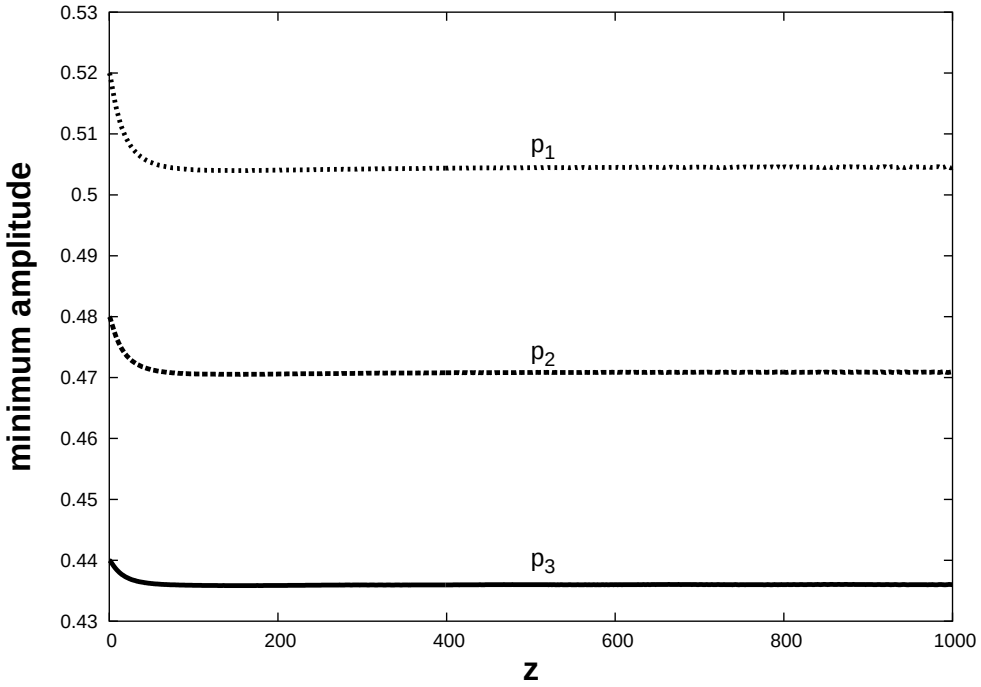

Figure 9: Evolution of the minimum amplitude for three different initial distributions when ρ is multiplied by the factors p_1=1.1, p_2=1.2, p_3=1.3, respectively.

new state. The velocity of such evolution is proportional to the factor c_2, which is inversely proportional to the width of the Gaussian. A small c_2 means to apply the chirp on a larger domain. The parameter c_1 represent the amplitude of the perturbation.

We complete the stability analysis of dark-like pulses by disturbing initially the solution (28) with a random noise. The perturbation was chosen as 5 percent of the background ($\lambda = 1.0$). Figure 12 shows that the dark-like wave is not sensitive to noise perturbations. Increasing the noise amplitude (10 percent of λ) we did not observe any significant modifications of its shape, amplitude and width. The pulse was propagated over one thousand dispersion lengths.

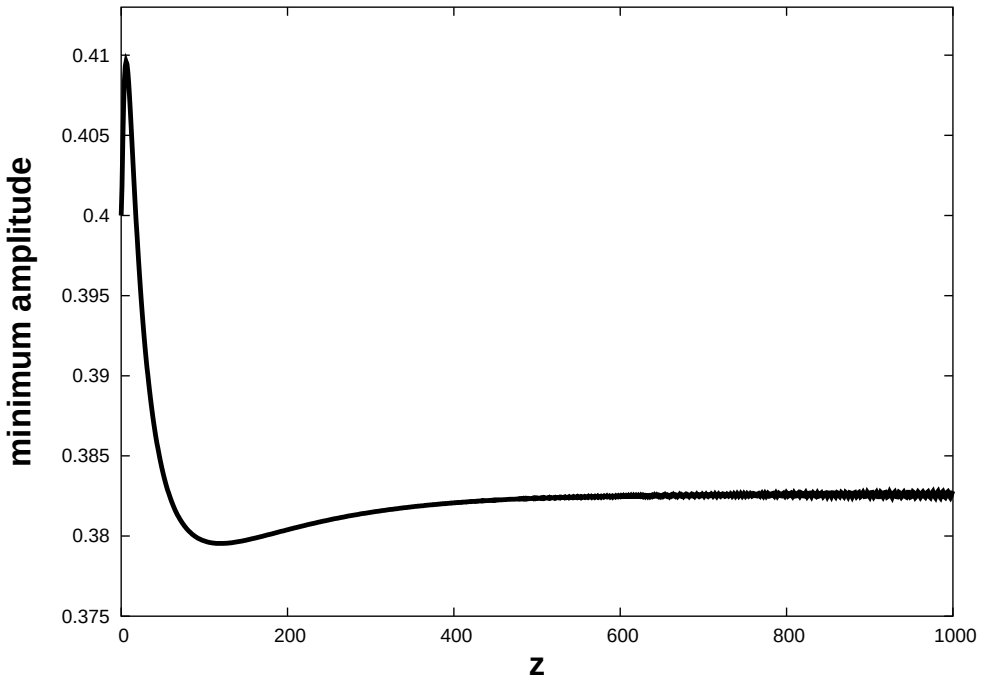

Figure 10: Perturbation of the sech-shape of the exact dark-like solution by using Eq.(56). ρ=1.0, λ=0.1, and η has been obtained from (33).

2.4.2 Interaction

In this section we present the results concerning the propagation of couple of dark-like pulses. We have chosen $\lambda_1 = \lambda_2 = 1$, $\rho_1 = 0.6$, $\rho_2 = 0.1$, and as initial distance $d = 10$. η_1 and η_2 are obtained from relation (33). The initial distribution has form (60). Due to their differences of deepness ($\rho_1 \neq \rho_2$), the two pulses move with a relative velocity different from zero. The initial distance d is large enough to preserve initial interactions. Under such condition, the two pulses can be considered as asymptotic solutions of Eq.(29). The collision was carefully studied over 3000 dispersion lengths. Similar to the bright-like case, the amplitudes and the widths of the two waves are exactly conserved after collision (Fig. 13).

At last, we present results regarding the propagation of a pair of pulses having

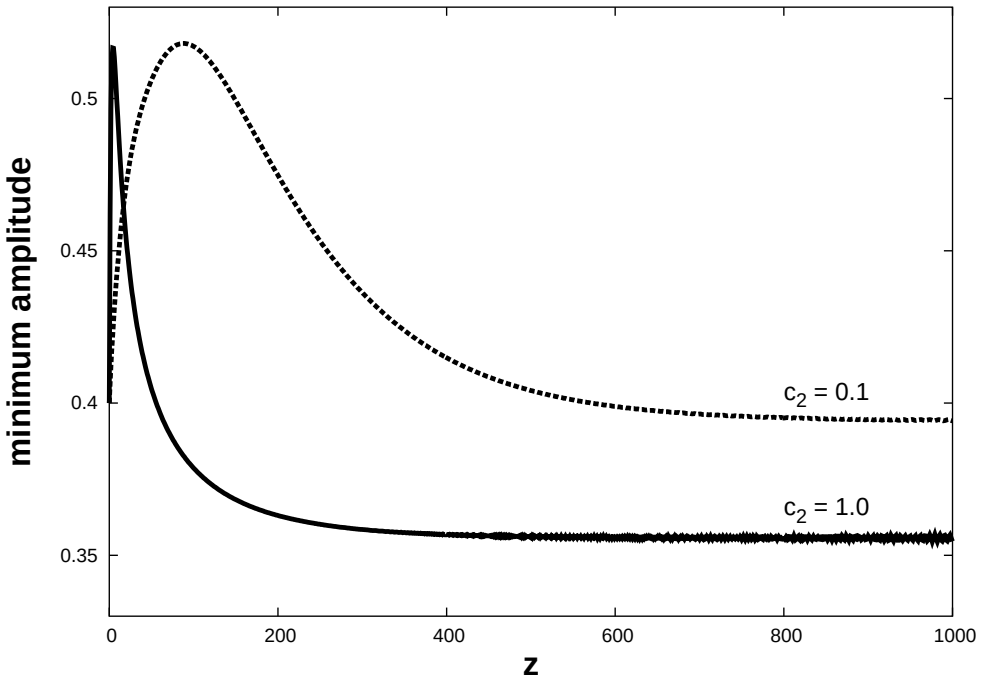

Figure 11: In this picture we show the different behavior of two exact solutions of Eq.(27) disturbed with different initial chirps. Eq.(57) is the initial distribution used in our simulation. In both cases $c_1 = 1.0$, while for c_2 we have used $c_2 = 0.1$ and $c_2 = 1.0$. The minimum value of the amplitude is plotted.

same deepness ($\rho_1 = \rho_2$) and starting very close ($d = 3$). Because reasons previously discussed, in case of short initial distances we can not anymore consider the two pulse (60) as asymptotic solutions of Eq.(29). Numerical simulations show (see Fig. 14) a periodical attraction and repulsion between two dark-like pulses when the initial distribution is chosen according to Eq.(60) $d = 3$ and for $\lambda = 1.0$, $\rho_1 = \rho_2 = 0.4$. A similar phenomenon was already observed for bright pulses in the NLS equation where a new bound state was created by their interaction. In the present case, the shape of the two pulses are not exactly periodic during the propagation. The reason for that behavior, as already discussed in the preceding subsections, is due to the difficulties to create a two-pulse initial distribution. Increasing the distance between the two waves up to $d > 6$, the interaction rapidly

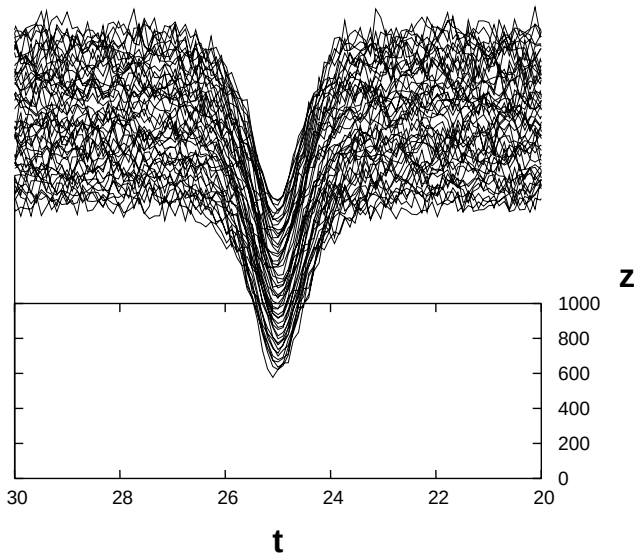

Figure 12: Evolution of a dark-like pulse in the presence of noise with a maximum amplitude δ=0.05 λ, $\lambda = 1.0$.

vanishes.

2.5 Structural stability

For practical applications, it is important to check the stability of pulses when the characteristic of the fibers, mathematically represented by the coefficients of the HNLS equation, do not exactly satisfy the condition for the soliton existence, in our case the Sasa conditions (30) -(31). Therefore, after the investigation of bright-like and dark-like pulses stability under finite perturbations, we propose a brief discussion of the robustness of those pulses when little perturbations are applied on the coefficients of Eq.(27).

First, we consider the bright-like case. As initial distribution we have used the exact bright-like solution (28) of Eq.(27). The parameters (33) - (36) have been

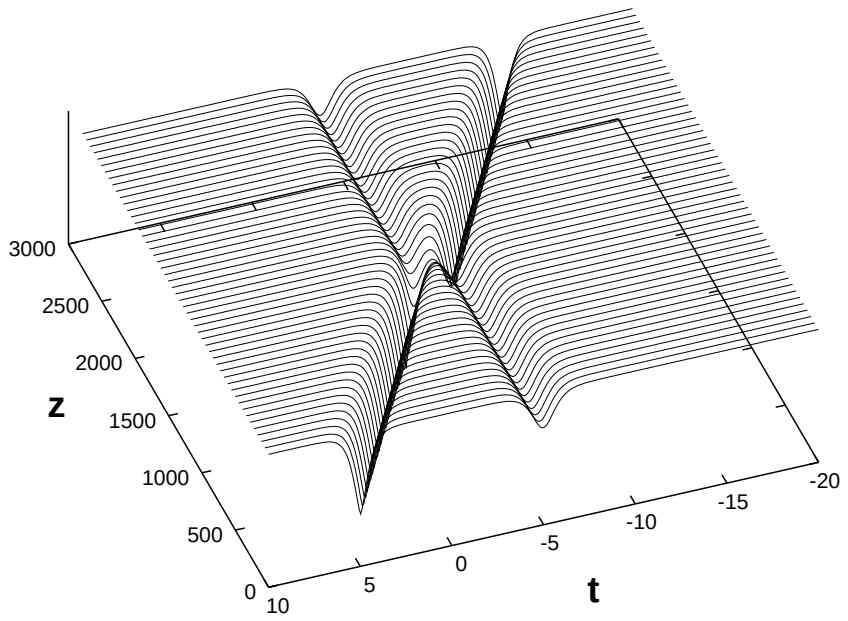

Figure 13: Collision of dark-like pulses for $\rho_1 = 0.6$, $\rho_2 = 0.1$ and initial distance $d = 10$. The 3-dimensional picture shows the collision between two solitary waves solution of equation (27). Shown is the absolute value of the amplitude.

calculated by using $\rho = 1.0$, $\lambda = 0.1$, a_2=0.5, a_1=1.0, a_3=-0.0083, a_4=-0.0498, and $a_5 = 0.0249$. Then, we have applied a perturbation on the coefficients of the master equation . Our numerical simulations show that bright-like pulses become strongly unstable and decay in few tens of dispersion lengths if very little perturbations (order of 5 percent) are applied on a_2 (GVD) and on a_3 (TOD). In case of modification of the two nonlinear coefficients a_4 and b, the pulse does not decay. It produces very strong radiations which move from the central soliton to the boundary. The bright-like pulse changes periodically its amplitude and width without modifying its sech-shape. In Fig. 15 the evolution of the maximum amplitude of the pulse for two different cases (perturbation of

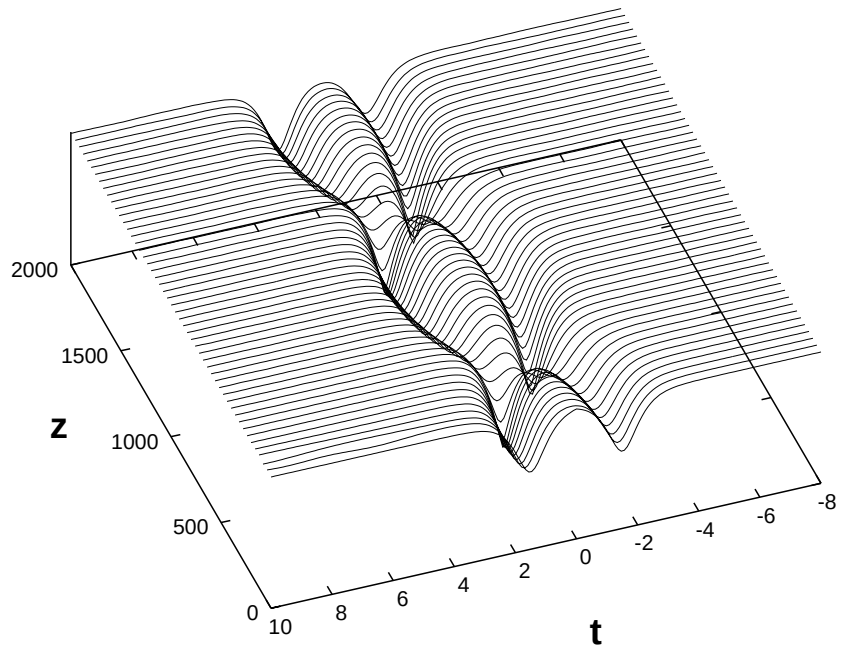

Figure 14: Interaction of dark-like pulses. Initial distance $d = 3$ in the initial distribution (60). Two dark-like pulses interact periodically with each other over 2000 dispersion lengths. Shown is the absolute value of the amplitude.

a_2 and a_4) has been shown.

Bright-like pulses have shown a very particular behavior when the coefficient a_5 in Eq.(27) is disturbed. The evolution of the maximum amplitude of bright-like pulses is shown in Fig. 16. As one can observe, after some thousand dispersion lengths, the pulse reaches a new stable state which has a higher amplitude. The same phenomenon was observed by decreasing a_5 by 5, 10 and 20 percent. In these cases the final states have an amplitude smaller than the initial one. As stronger the perturbation is, as faster the pulse evolves into a new stable state. However, the final state can not be written in form (28). In Fig. 17 the absolute values of the initial distribution ($z = 0$) and the pulse after 5000 dispersion

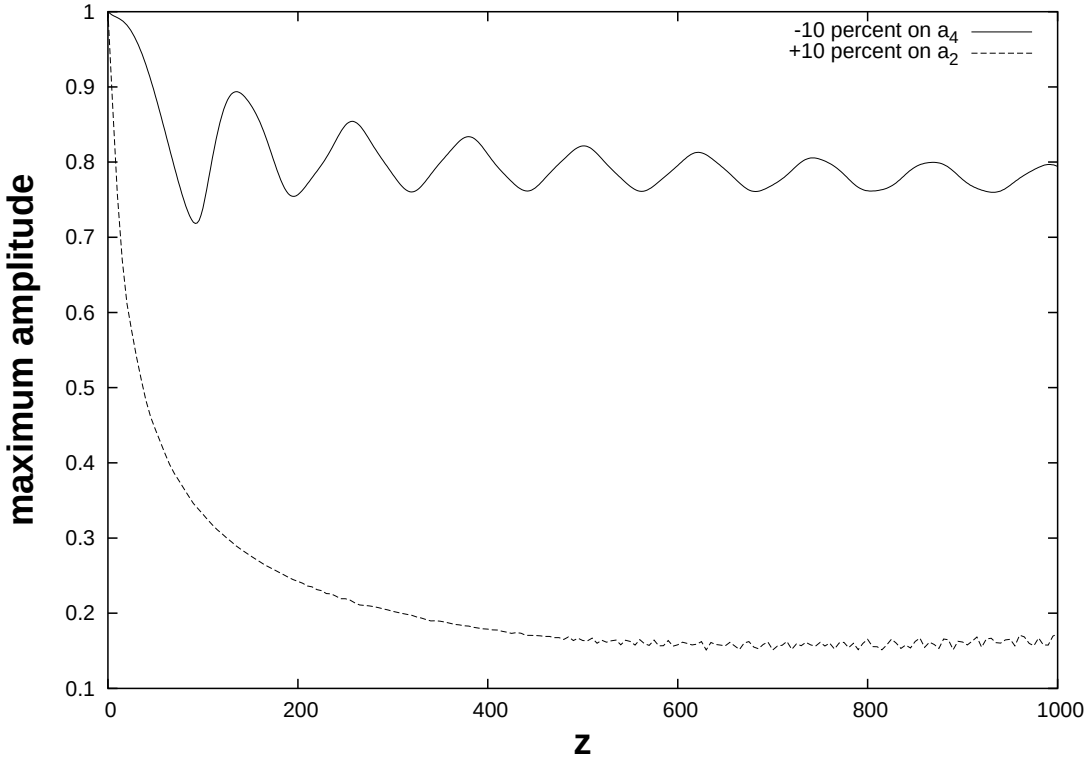

Figure 15: Evolution of the maximum amplitude of the pulse with respect to z for two different cases. A perturbation of 10 percent on the linear term a_2 produces the decay of the pulse, while when the perturbation is applied on the term a_4 the pulse oscillates around an equilibrium point.

lengths are plotted, where the coefficient a_5 has been increased by +20 percent ($0.249 \rightarrow 0.2988$). As one can notice, the pulse changes its amplitude, width and shape, showing two humps on the right and left side of the pulse, but not only this. Another important information about the new stable state is given from its real and imaginary part. Having a look to Eq.(28), we see that the initial distribution has an odd function as real part and an even function as imaginary part. Our new distribution (see Fig. 18) is the combination of two periodic functions. This new state has been propagated over thousand of dispersion lengths and any changes of its shape have been observed. Such result indicates, that when Sasa conditions

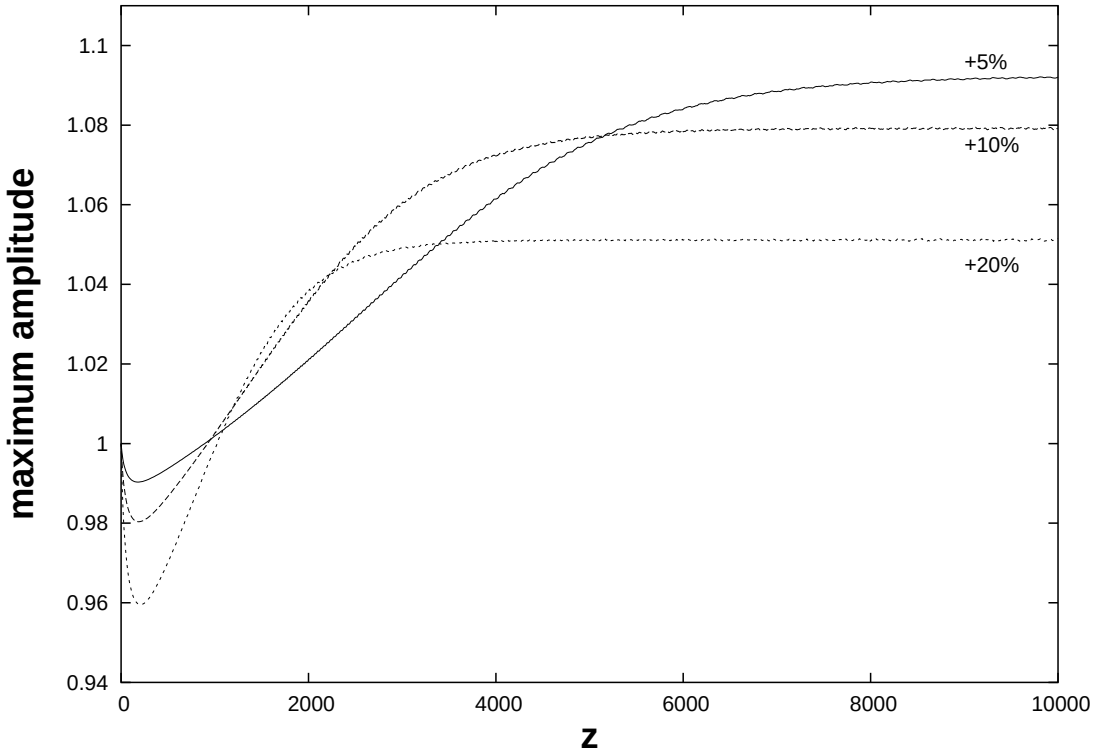

Figure 16: Evolution of the maximum amplitude of the pulse with respect to z. Three cases have been shown: $a_5 = 0.26145$ (+5 percent), $a_5 = 0.2739$ (+10 percent) and $a_5 = 0.2988$ (+20 percent).

are not exactly satisfied, a new kind of solution, which is very different from the (28), exists.

Similar results have been obtained in case of a pure bright pulses, in Eq.(28) $\lambda = 0$. When the background is not present, and the coefficients a_2 and a_3 are disturbed, the bright pulse shows a decay behavior again. In case of perturbation on a_4 and b the radiation from the central soliton to the boundary are not so strong as for the bright-like case, but the oscillating behavior of the evolved state is confirmed. Also the robustness of the pulse against modification of a_5 has been confirmed, but in this case the final state does not represent a new type of solution.

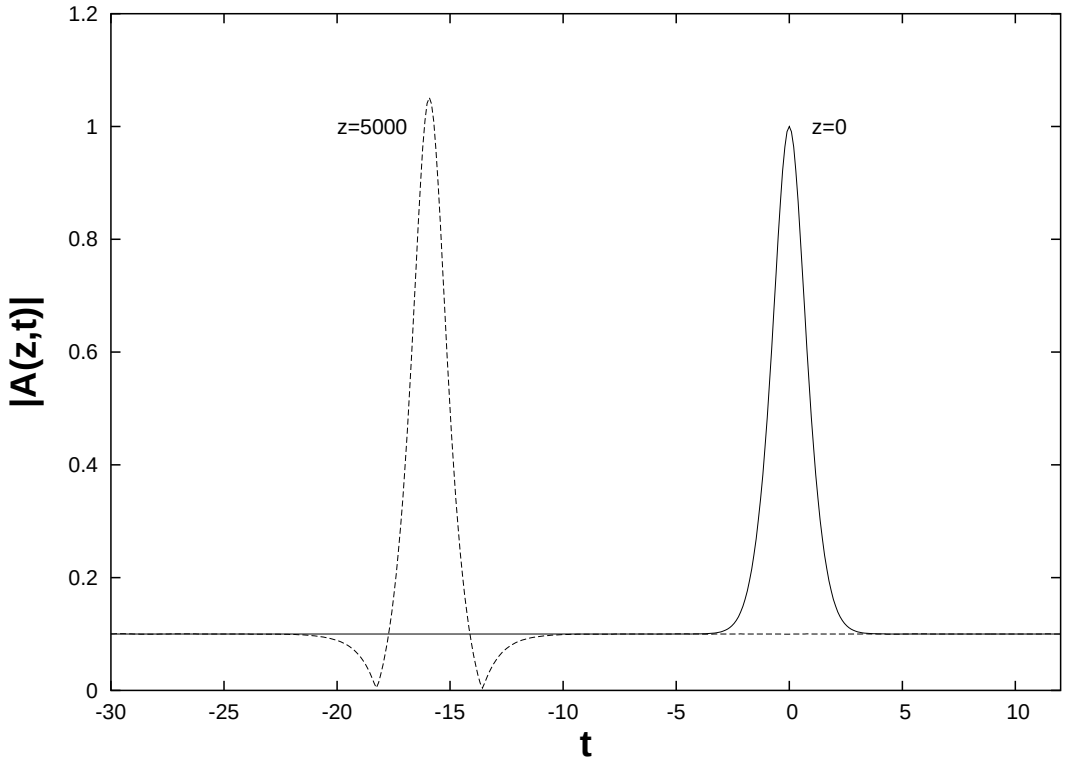

Figure 17: The absolute value of the initial distribution and the evolved pulse $|\psi(z = 5000, t)|$ are shown. The considered case regards perturbation of +20 percent on the Raman term a_5 (see Fig. 16).

Next, we have repeated the same analysis in case of dark-like solitons. Even here, the pulse shows a strong stability dependence on the linear terms a_2 and a_3. If the nonlinear terms are disturbed, the pulse shows a high robustness. Only in the special case $a_{4new} > a_4$, the pulse becomes unstable. In Fig. 19 the evolution of the minimum value of the dark-like pulse has been shown for two different cases: perturbation by +10 percent on both a_5 and b.

In this chapter, we have numerically investigated the robustness of solitary pulses solutions of a higher-order nonlinear Schrödinger equation under non-zero boundary conditions. The results show that the solitary waves are stable under finite perturbations on the pulse characteristics (amplitude, width, shape function,

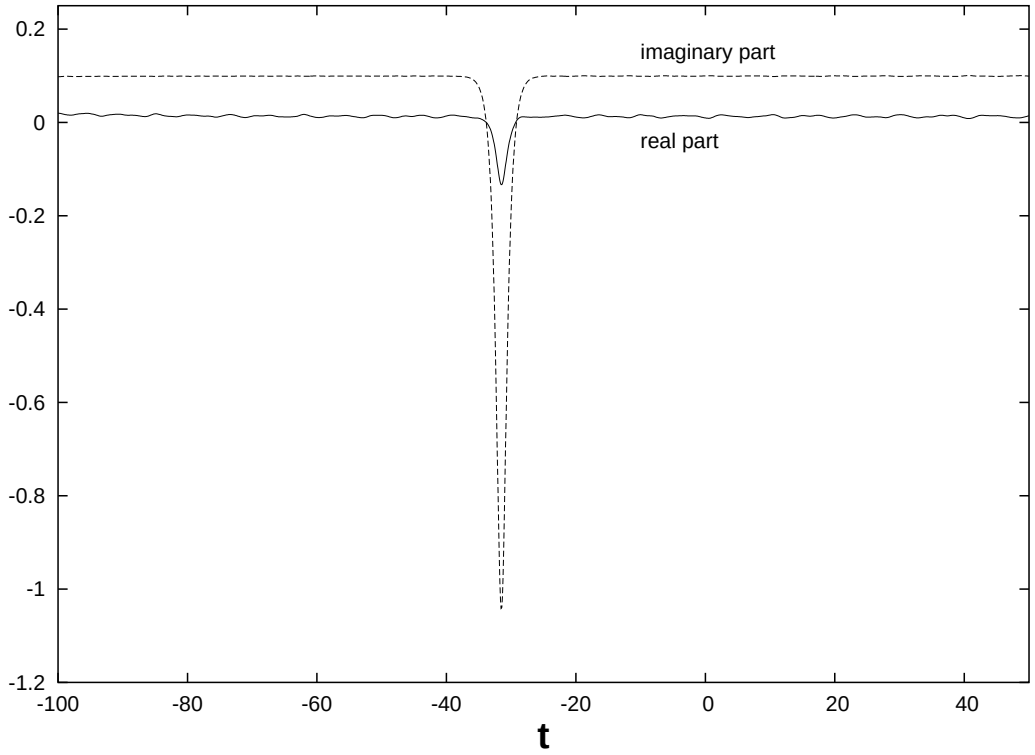

Figure 18: Real and imaginary part of the evolved pulse ($z = 5000$) in case of perturbation of +20 percent on the Raman term a_5. Both real and imaginary parts of the new state are periodic functions.

chirp and noise). In addition we have performed numerical experiments of collision and interaction between two solitary waves. The results indicate that the pulses keep their shapes after the collision. We have seen that a repulsive force acts between two bright-like pulses, while two dark-like pulses having same amplitude create a bound state. All of these characteristics show that those solitary waves behave like solitons. Afterwards we have studied the stability of bright-like and dark-like pulses by disturbing the coefficient of the HNLS equation (27). We have seen that when the conditions on the coefficients (Sasa) are not exactly satisfied, the pulses can become strongly unstable, evolve into a new stable state or into a new type of solution.

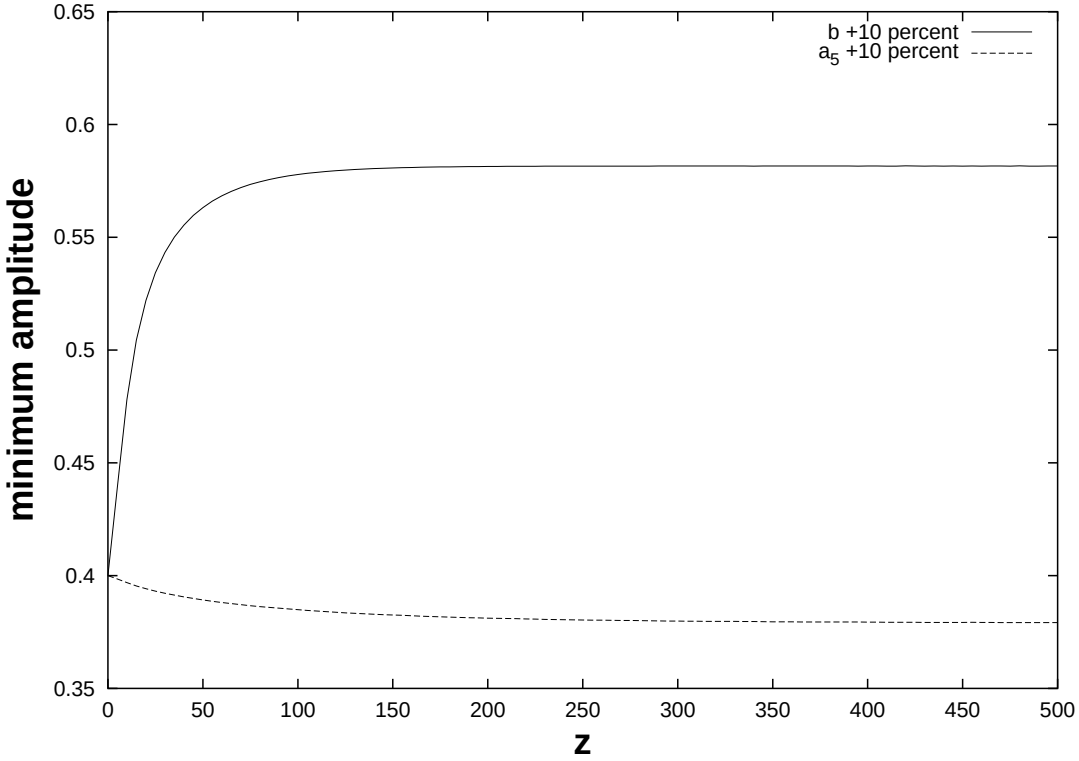

Figure 19: Stability analysis of dark-like solitons. Two cases have been taken into account: perturbation of +10 percent on the coefficient b, and on the coefficient a_5. Evolution of the minimum amplitude of the pulse is shown.

3 Stability Considerations

In the last chapter we have investigated new types of soliton solutions by employing numerical simulations. In this part of the work we present some analytical methods which can be used in order to study the robustness of ultra-short bright pulses.

We employ two analytical approaches (*momentum method, variational approach*) in order to write a system of differential equations which describes the behavior of the signal when finite perturbations are applied on the characteristics of the pulse (amplitude and width) and on the coefficients of the master equation. At the end of each section we compare the analytical model and numerical simulations.

We have seen that an ultra-short light-pulse propagation may be described by the following equation (see Sec. 1.4))

$$i\psi_z + a_2\psi_{tt} + b|\psi|^2\psi = i(a_3\psi_{ttt} + a_4(|\psi|^2\psi)_t + a_5\psi(|\psi|^2)_t) , \qquad (63)$$

where, all coefficients are real numbers. A general bright solution of Eq.(63) is [42, 43, 44, 69]

$$\psi(z,t) = \rho \,\mathrm{sech}(\eta(t-\chi z))e^{i(kz-\Omega t)} , \qquad (64)$$

where amplitude ρ, width η, frequency shift Ω, velocity χ and phase k, are related to the coefficients of Eq.(63) by the following relations

$$\rho = \eta\sqrt{\frac{6a_3}{3a_4+2a_5}} , \qquad (65)$$

$$\Omega = \frac{a_2(3a_4 + 2a_5) - 3ba_3}{6a_3(a_4 + a_5)} , \tag{66}$$

$$\chi = a_3(3\Omega^2 - \eta^2) - 2a_2\Omega , \tag{67}$$

$$k = a_2(\eta^2 - \Omega^2) + a_3\Omega(\Omega^2 - 3\eta^2) . \tag{68}$$

Here, we consider two particular solutions of Eq.(63) already introduced in Sec.1.4. If the Sasa conditions (30)-(31) are satisfied, the pulse parameters (65)-(68) become (33)-(36), where $\lambda = 0$, and the solution (64) is equivalent to the (28).
When the coefficients of Eq.(63) satisfy the Hirota conditions (see Eqs.25 and 26 in Sec. 1.4), amplitude and width are expressed by the same parameter (65), $\rho = \eta$ and Ω becomes an arbitrary number (66). For bright pulses under Hirota conditions the relation between the perturbation terms becomes: $a_4 = 6a_3$, $a_5 = -6a_3$.
In the next section, we are going to consider three types of bright solutions of Eq.(63).

3.1 Stability of a single pulse

The first analytical method we apply in order to investigate the stability of a bright pulse solution of Eq.(63), is the well known variational approach. By using this method we are able to get a set of ordinary differential equations which describes the behavior of a pulse along z when small finite perturbations are applied on the starting distribution (64) or on the coefficients of the master equation.
We can rewrite the equation (63) as

$$i\psi_z + a_2\psi_{tt} + b|\psi|^2\psi \;=\; i\varepsilon R(\psi,\psi^*)\;, \tag{69}$$

where R includes third order dispersion (TOD), self-steepening and self-frequency shift arising from stimulated Raman scattering (SRS)

$$R(\psi,\psi^*) \;=\; a_3\psi_{ttt} + a_4(|\psi|^2\psi)_t + a_5\psi(|\psi|^2)_t\;. \tag{70}$$

The left-hand side of Eq.(69) can be rewritten in the Lagrangian form, with the action defined as

$$\begin{aligned} S &= \int_{-\infty}^{\infty} L_0\; dt\; dz \\ &= \int_{-\infty}^{\infty} (\frac{i}{2}(\psi\psi_z^* - \psi^*\psi_z) + a_2|\psi_t|^2 - \frac{b}{2}|\psi|^4)\; dt\; dz\;. \end{aligned} \tag{71}$$

The right-hand side of Eq.(69) will be treated as a perturbation.
If we consider the case $R(\psi,\psi^*) = 0$, we can write the unperturbed NLS equation as

$$\frac{\delta L_0}{\delta\psi^*} \;=\; 0\;, \tag{72}$$

where

$$\frac{\delta L_0}{\delta\psi^*} \;=\; \sum_n (-1)^n \frac{\partial^n}{\partial t^n}\frac{\partial L_0}{\partial\psi^*_{nt}} - \frac{\partial}{\partial z}\frac{\partial L_0}{\partial\psi^*_z}\;. \tag{73}$$

As trial function we choose the following form

$$\psi(z,t) \;=\; \rho\;\mathrm{sech}(\eta(t-T_0))^{1+iC}e^{i(\Omega(t-T_0)-k)}\;. \tag{74}$$

Any pulse is characterized by its amplitude ρ, width η, chirp β, position T_0, frequency shift Ω and phase k. Inserting (74) into (71) and integrating we obtain

$$\begin{aligned} < L > &= \int_{-\infty}^{\infty} L_0 \; dt \\ &= \frac{\rho^2}{\eta}(C\frac{\eta_z}{\eta} + 2(\Omega T_{0z} + k_z) - 2C_z(\ln(2) - 1) \\ &\quad -\frac{2}{3}a_2\eta^2(1 + C^2) - 2a_2\Omega^2 + \frac{2}{3}\rho^2 b) \; . \end{aligned} \tag{75}$$

From the Euler equations

$$\frac{\partial < L >}{\partial \varphi} - \frac{d}{dz}\frac{\partial < L >}{\partial \varphi_z} = 0 \; , \tag{76}$$

one can derive the equations which describe the evolution of the parameters $\varphi(z) = A(z)$, $\eta(z)$, $C(z)$, $\Omega(z)$, $T_0(z)$ and $k(z)$ for the unperturbed case $R(\psi, \psi^*) = 0$ (NLS equation) [70, 71, 72, 73, 74].
In order to include the perturbation R(ψ,ψ^*), we calculate

$$\begin{aligned} \frac{\partial < L >}{\partial \varphi} &= \int_{-\infty}^{\infty} (\frac{\delta L_0}{\delta \psi}\frac{\partial \psi}{\partial \varphi} + \frac{\delta L_0}{\delta \psi^*}\frac{\partial \psi^*}{\partial \varphi})dt \\ &= \int_{-\infty}^{\infty} 2 \; Re(i\varepsilon R\frac{\partial \psi^*}{\partial \varphi})dt \; , \end{aligned} \tag{77}$$

where

$$\frac{\delta L_0}{\delta \psi^*} = i\varepsilon R(\psi, \psi^*) \; . \tag{78}$$

Inserting the (75) into (76), adding the integrals (77), and solving the system, we get the following set of differential equations

$$\rho_z = \frac{2}{3}\rho\eta^2 C(a_2 + 3a_3\Omega) , \tag{79}$$

$$\eta_z = \frac{4}{3}\eta^3 C(a_2 + 3a_3\Omega) , \tag{80}$$

$$\Omega_z = \frac{8}{15}\eta^2 C\rho^2(a_4 + a_5) , \tag{81}$$

$$C_z = -\frac{4}{3}(1 + C^2)\eta^2(a_2 + 3a_3\Omega) + \frac{2}{3}\rho^2(b + a_4\Omega) , \tag{82}$$

$$T_{0z} = (3a_3 + +2a_2)\Omega + a_3\eta^2(1 + C^2) - \frac{3a_4 + 2a_5}{3}\rho^2 , \tag{83}$$

$$\begin{aligned} k_z = \frac{1}{3}(&\rho^2(2b(-2 + \ln(2)) + (2a_5 + a_4(-1 + 2\ln(2)))\Omega) + \\ &a_2(\eta^2(5 + C^2(3 - 4\ln(2)) - 4\ln(2)) - 3\Omega^2) - \\ &6a_3\Omega(2\eta^2(-1 + \ln(2) + C^2(-3 + 4\ln(2))) + \Omega^2)) . \end{aligned} \tag{84}$$

Those equations describe the evolution of the parameters ρ, η, Ω, T_0, C and k with respect to z. Of course, if the initial parameters and the coefficients exactly satisfy the conditions (65-68) (the initial chirp is $C = 0$), the right-hand side of Eqs.(79-83) vanishes.

The same problem can be analyzed by employing another well known method, the momentum method.

For this purpose we choose a trial bright function in the form:

$$\psi(z,t) = A\ \mathrm{sech}(\eta(t-T_0))e^{i(C(t-T_0)^2+\Omega(t-T_0)+k)}\ . \tag{85}$$

The only difference between Eq.(74) and Eq.(85) is the shape of the chirp. The set of equations obtained in this case is

$$\rho_z = -2\rho C(a_2+3a_3\Omega)\ , \tag{86}$$

$$\eta_z = -4C\eta(a_2+3a_3\Omega)\ , \tag{87}$$

$$\Omega_z = -2C\frac{6a_3(-15\eta^4+C^2\pi^4)+5\eta^2(12a_4+(a_4+2a_5)\pi^2)A^2}{15\eta^2\pi^2}\ , \tag{88}$$

$$C_z = \frac{4(a_2+3a_3\Omega)(\eta^4-C^2\pi^2)-2\eta^2(b+a_4\Omega)\rho^2}{\pi^2}\ , \tag{89}$$

$$T_{0z} = 2a_2\Omega+a_3(\eta^2+3\Omega^2+\frac{C^2\pi^2}{\eta^2})-\frac{1}{3}(3a_4+2a_5)\rho^2\ , \tag{90}$$

$$\begin{aligned} k_z = {} & \frac{1}{6}(a_2(4\eta^2-6\Omega^2)+6a_3\Omega(\eta^2-2\Omega^2-\frac{C^2\pi^2}{\eta^2})+ \\ & (-5b+a_4\Omega+4a_5\Omega)\rho^2)\ . \end{aligned} \tag{91}$$

Even here we have a set of differential equations which describes the evolution of the parameters along z. Because the different ansatz we do not expect an

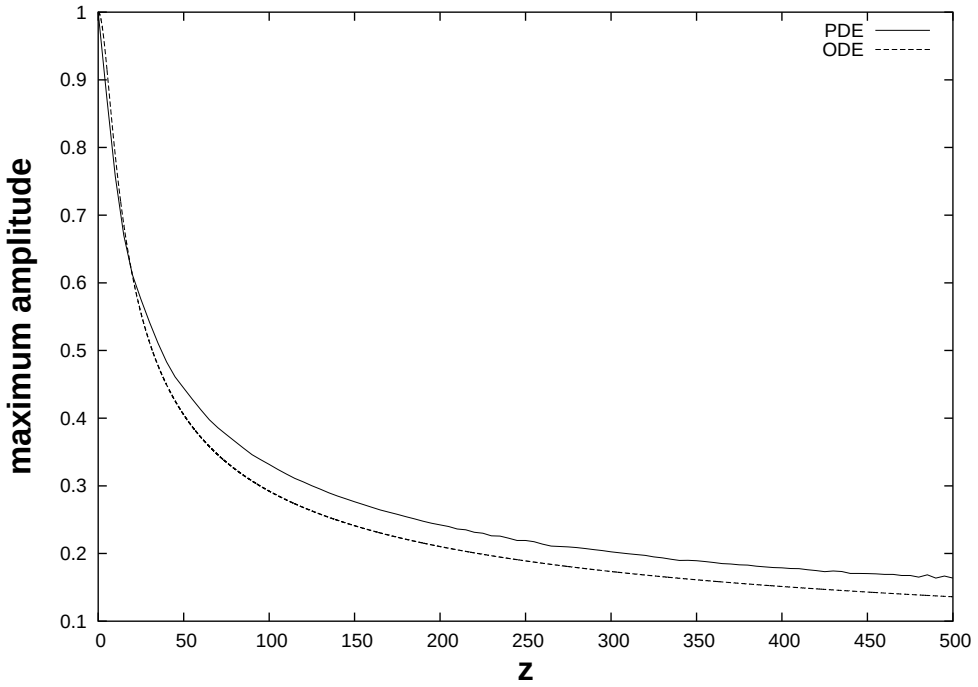

Figure 20: Both ODE model and direct integration of Eq.(63) show the decay of the maximum amplitude of the pulse. The linear parameter a_2 has been increased by +10 percent so that the Sasa conditions are not exactly satisfied.

identical correspondence between the two systems, but only a qualitative agreement. Important to remember is that in deriving the set of differential equations (79)-(84) and (86)-(91) no restriction on the coefficients of the master equation (63) have been taken into account.

First, we investigate the stability of bright pulses which satisfy the Sasa conditions (30) and (31). As initial distribution we consider the exact bright solution (28) of Eq.(27). The width (33) and frequency shift (35) have been calculated by using $\rho = 1.0$, $\lambda = 0.0$ (bright pulse), a_2=0.5, a_1=1.0, a_3=-0.0083, a_4=-0.0498, and $a_5 = 0.0249$. The initial position, phase and chirp are equal zero.
When a little perturbation is applied on the amplitude or on the width of the initial distribution (28), direct numerical simulations of Eq.(63) show that the

pulse evolves into a new stable state really close to the initial one. Such result is confirmed by our ODE models. In fact, when the Sasa conditions are satisfy and the initial parameters ρ and η are disturbed, the right-hand side of both systems (79)- (84), and (86)-(91) vanishes.

Even when the Sasa conditions are not exactly satisfied, PDE and ODE simulations show a good qualitative agreement in estimating the pulse behavior. In Fig. 20 the comparison of ODE models with direct simulation of Eq.(63), in case of perturbation on the linear coefficient a_2 (+10 percent), is shown. In this case the pulse decay in few hundreds of dispersion lengths. The same phenomenon appears when a_3 is disturbed. By perturbing the two nonlinear terms b and a_4 we observe a different behavior. The pulse radiates away part of its energy and starts to oscillate around an equilibrium point. The signal is not sensitive to any variations of the term a_5. Here the pulse evolves into a new stable state by following a similar behavior already seen in case of amplitude and width perturbations (see fox example Fig. 2 in Sec. 2.3.1).

Now, we use the ODE models and a direct numerical simulations of the master equation in order to investigate the stability of bright pulses under Hirota conditions, (25) and (26). The initial distribution (64) has been defined by using, in Eqs.(65)-(68), $a_2 = 0.5$, $b = 1$, $a_3 = -0.01$ $a_4 = -0.06$ and $a_5 = 0.06$. Since in this case both amplitude and width are described by the same parameter and the frequency shift is arbitrary, we can choose $\rho = \eta = 1$ and $\Omega = 0$. In the ODE model the initial chirp has been considered equal zero. When a finite perturbation is applied on the initial amplitude or width, the pulse radiates part of its energy and starts to oscillate quite smoothly around an equilibrium point. Fig. 21 shows the behavior of the maximum amplitude of the pulse when the initial width is multiplied by factor 0.9. Same oscillating behavior has been observed when the Hirota conditions are not satisfied anymore and the linear term a_2 or the nonlinearity b are disturbed. On the other hand, the pulse does not show any

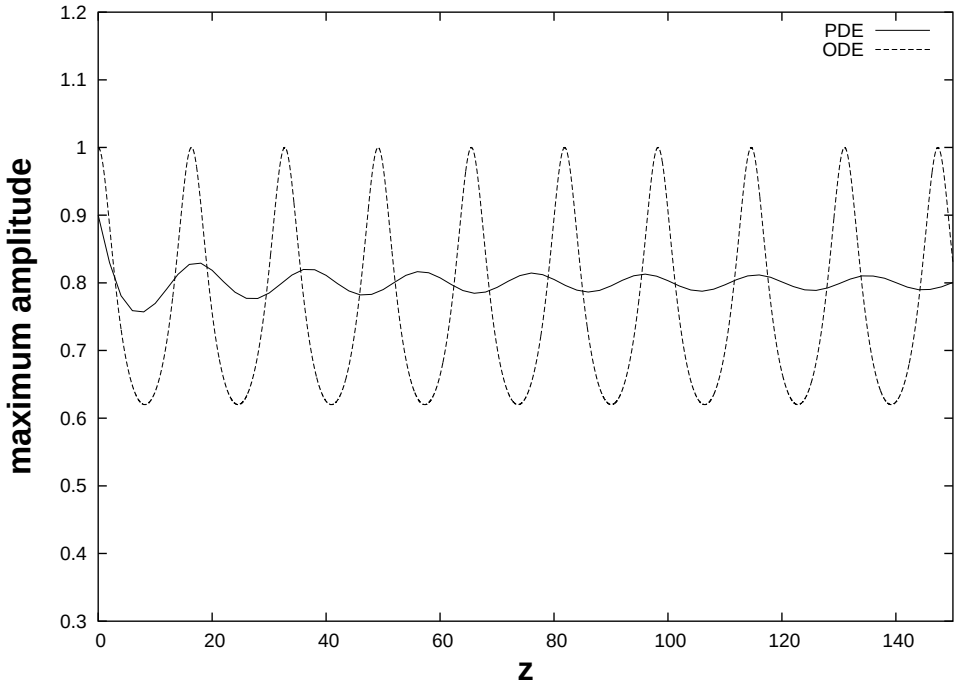

Figure 21: Amplitude evolution in case of perturbed width ($\eta = 0.9$). A comparison of direct integration of Eq. (63) and ODE model is shown. The parameters of the fiber and pulse are (Hirota conditions) : $a_2 = 0.5$, $b = 1$, $a_3 = -0.01$, $a_4 = -0.06$, $a_5 = 0.06$.

changes of its amplitude and width when small perturbations are applied on the other three coefficients a_3, a_4, and a_5.

From this analysis we have seen that bright pulses under Hirota conditions are more robust with respect to pulses which satisfy Sasa conditions. Using the two systems (79)-(84) and (86)-(91) we are able to study the stability of any bright solution (64) of Eq.(63). At last we report the results obtained for a bright pulse solution existing in a coefficient range far from both Sasa and Hirota conditions. The terms $a_2 = 0.5$, $b = 1$, $a_3 = -0.0154321$, $a_4 = -0.06$, $a_5 = 0.04$ have been chosen. From this set of coefficients, using the Eqs.(65-66) and setting $\eta = 1$, we get the initial parameters $\rho = 0.96225$ and $\Omega = -2.0$. The initial position, phase, and chirp are equal zero.

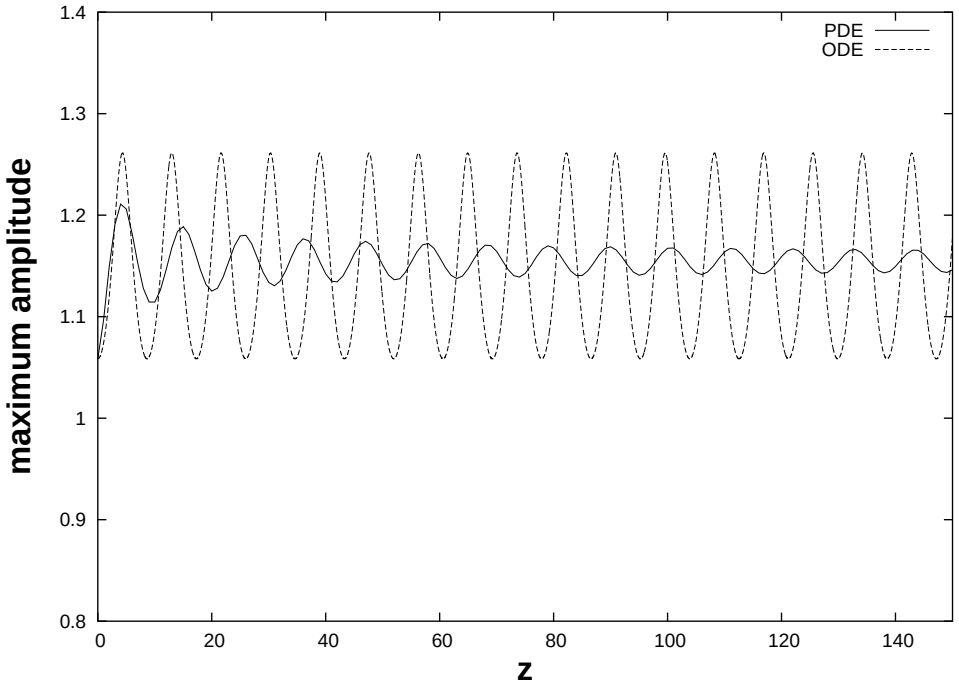

Figure 22: Evolution of the maximum amplitude of a perturbed bright pulse (+10 percent on the amplitude ρ) far from both Sasa and Hirota conditions. The fiber and pulse parameters are : $a_2 = 0.5$, $b = 1$, $a_3 = -0.0154321$, $a_4 = -0.06$, $a_5 = 0.04$, $\eta = 1$, $\rho = 0.96225$ and $\Omega = -2.0$.

When amplitude and width are disturbed, the pulse behaves like the one under Hirota conditions. It radiates part of its energy from the central soliton to the boundary and oscillates smoothly around an equilibrium point. Fig. 22 shows the evolution of the maximum amplitude of the pulse with respect to z for the case of an initial perturbation on the amplitude ρ (+10 percent). The pulses show a good robustness even when the coefficients a_i (i=1,2,3,4,5) and b are disturbed. In particular, they are very stable against perturbations on the nonlinear term a_5. In this case no changes in shape have been observed. However, if the other terms are disturbed, the pulse behaves as it was for finite perturbations on its amplitude and width. The differences between ODE and PDE simulations, that one can observe in Figs. 22 and 21, are due to the following reason. Having a look at the

right-hand side of Eq.(63), one can see that all the higher-order terms are not of dissipative type and therefore the system conserves its energy along z. While for PDE simulation part of the energy of the pulse can be dispersed away along the domain, this can not happen within the ODE simulation. The total energy is kept in the ODE model producing strong oscillations on the parameters. It would be different for driving systems in which damping and amplification terms are included and the energy in excess is dissipated.

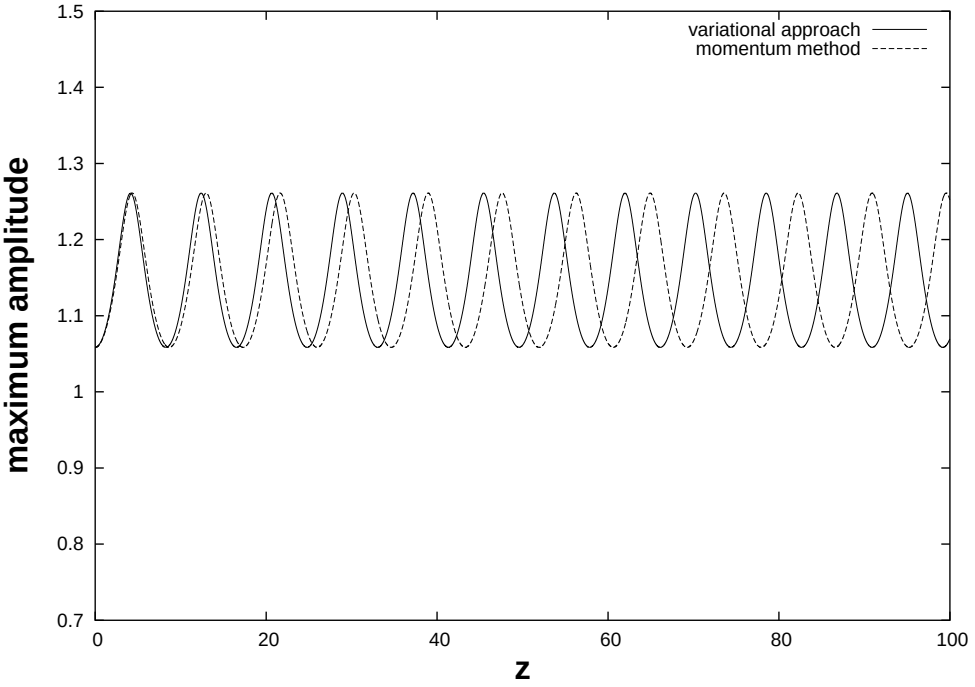

Figure 23: Comparison of variational approach and momentum method. The case presented is the same as in Fig. 22, where the amplitude ρ of a bright pulse far from both Sasa and Hirota conditions was disturbed by an increase of its amplitude.

The discrepancy between ODE and PDE models depend of the perturbation that we apply: the more we disturb the pulse the higher the amplitude of the oscillations will be.

To conclude this section we would like to remark the qualitative equivalence of

the two systems of equations (79)-(84) and (86)-(91). In Fig. 23 a comparison of variational approach and momentum method is shown. The case considered is the same as in Fig. 22. The only difference between those two models consists in a different phase of the oscillations.

In this chapter we have presented two analytical methods which can qualitatively describe the behavior of bright pulses when finite perturbations are applied on the parameters of the pulse (amplitude, and width) and on the coefficients of the master equation. This kind of analysis is important in order to check the real possibility to use ultra-short pulses in optical communication systems. Three types of bright solutions have been considered. In all cases, the analytical results have been compared with direct numerical simulations. We have seen that bright pulses under Hirota conditions are more robust with respect to those under Sasa conditions, specially when the second order dispersion a_2 and the third order dispersion a_3 are disturbed.

4 Soliton-soliton interaction

4.1 The Karpman Solv'ev approach (KSA)

An important task for high bit rates in optical transmission systems, is the studying of pulse interactions during their propagation along the fiber. In Sec. 2.4.2 and 2.5.2, we have numerically discussed the interaction of bright-like and dark-like soliton solutions of a HNLS equation under Sasa conditions. Here, we introduce a very useful analytic method, the Karpman-Solov'ev approach (KSA) [75]. This method has been developed at the beginning of the 80's and during the 90's it has been used for the studying of third order effects (TOD) effects [77] and intra-pulse Raman scattering (IRS) during pulse interaction [78].

The main idea of KSA is to choose a superposition of Schrödinger solitons as a trial function and to derive ordinary differential equations for the soliton parameters which are driven by the interaction as well as the perturbation terms

$$\psi(z,t) \;=\; \sum_{i=1}^{n} 2\eta_n \mathrm{sech}(2\eta_n(t-T_n))e^{i(k_n+2\Omega_n(t-T_n))}\,, \tag{92}$$

where the amplitudes and widths η_n, positions T_n, frequency shift Ω_n, and phases k_n are slowly varying functions of z. From such ansatz it is clear that KSA cannot accurately describe processes which are generating radiations (dispersive waves) and that change the shape of a pulse.

The perturbed nonlinear Schödinger equation is the same as the one considered in the last chapter (see Eq.63) with $a_2 = 0.5$ and $b = 1$:

$$i\psi_z + \frac{1}{2}\psi_{tt} + |\psi|^2\psi \;=\; i\varepsilon R(\psi)\,. \tag{93}$$

Since in the ansatz (92) there is only one parameter to describe both amplitude and width, we would be able to study only particular solutions of the HNLS

equation. The solution (64) and the ansatz (92), taken for $n = 1$, are equivalent in case of $\rho = \eta$. In Sec. 3.1, we have seen that a bright pulse with same value of amplitude and width is solution of Eq.(63) only if the Hirota conditions (25) and (26) are fulfilled. To write a more general ansatz and to derive an ODE system by following the procedure outlined in [75], is a very difficult problem which will not be discussed here. In this chapter we limit our study on bright pulses under Hirota conditions.

The evolution of the soliton parameters along z is given by the following relations [76]

$$\frac{d\eta_n}{dz} = N_n^{(0)}(\psi) + \sum_{p>0} N_n^{(p)}(\psi) , \tag{94}$$

$$\frac{d\Omega_n}{dz} = M_n^{(0)}(\psi) + \sum_{p>0} M_n^{(p)}(\psi) , \tag{95}$$

$$\frac{dT_n}{dz} = 2\Omega_n + \Xi_n^{(0)}(\psi) + \sum_{p>0} \Xi_n^{(p)}(\psi) , \tag{96}$$

$$\frac{d\delta_n}{dz} = 2(\Omega_n^2 + \eta_n^2) + X_n^{(0)}(\psi) + \sum_{p>0} X_n^{(p)}(\psi) , \tag{97}$$

$$X_n^{(p)}(\psi) = 2\Omega_n \Xi_n^{(p)} + D_n^{(p)}(\psi) , \tag{98}$$

where $N_n^{(p)}(\psi)$, $M_n^{(p)}(\psi)$, $\Xi_n^{(p)}(\psi)$, $X_n^{(p)}(\psi)$, and $D_n^{(p)}(\psi)$, for $p = 0$, take into account the mixing terms arising from the left-hand side of Eq.(93), the NLS

equation. The contribution given for $p > 0$ includes the perturbations represented by the right-hand side of Eq.(93). The right-hand side of Eqs.(94)-(97) is determined by [75]

$$N_n^{(p)}(\psi) = \frac{1}{2}\int_{-\infty}^{\infty} \frac{dz_n}{\cosh(z_n)} Re(R_n^{(p)}(\psi)e^{-i\phi_n}) , \tag{99}$$

$$M_n^{(p)}(\psi) = \frac{1}{2}\int_{-\infty}^{\infty} \frac{dz_n \sinh(z_n)}{\cosh^2(z_n)} Im(R_n^{(p)}(\psi)e^{-i\phi_n}) , \tag{100}$$

$$\Xi_n^{(p)}(\psi) = \frac{1}{4\eta_n^2}\int_{-\infty}^{\infty} \frac{dz_n\ z_n}{\cosh(z_n)} Re(R_n^{(p)}(\psi)e^{-i\phi_n}) , \tag{101}$$

$$D_n^{(p)}(\psi) = \frac{1}{2\eta_n}\int_{-\infty}^{\infty} \frac{dz_n\ (1 - z_n tanh(z_n))}{\cosh(z_n)} Im(R_n^{(p)}(\psi)e^{-i\phi_n}) , \tag{102}$$

where $p = 0, 1, 2, 3, ...$; and $z_n = 2\eta_n(t - T_n)$.

First, we consider the unperturbed NLS equation ($\varepsilon = 0$). In this case the soliton interaction is given by the nonlinear term $|\psi|^2\psi$, which includes the following overlapping terms

$$i\varepsilon_{mn} R_{mn}^{(0)}(\psi_n) = i(\psi_m^*\psi_n^2 + 2\psi_m\psi_n\psi_n^*) . \tag{103}$$

Here, we consider the simple case of two pulses ($m, n = 1, 2,\ m \neq n$). The equations for the soliton parameters are [75]

$$\frac{d\eta_n}{dz} = (-1)^n 16\eta^3 e^{-2\eta r}\sin(\phi) , \tag{104}$$

$$\frac{d\Omega_n}{dz} = (-1)^n 16\eta^3 e^{-2\eta r}\cos(\phi) , \tag{105}$$

$$\frac{dT_n}{dz} = 2\Omega_n + 4\eta e^{-2\eta r}\sin(\phi) , \tag{106}$$

$$\frac{dk_n}{dz} = 2(\eta_n^2 + \Omega_n^2) + 8\eta e^{-2\eta r}(\Omega\sin(\phi) + 3\eta\cos(\phi)) , \tag{107}$$

where $\phi = 2\Omega r + \Psi$, $\Psi = k_2 - k_1$, $\eta = \frac{\eta_1+\eta_2}{2}$, $\Omega = \frac{\Omega_1+\Omega_2}{2}$, and $r = T_1 - T_2$.
r is the distance between the solitons and Ψ their relative phase. In deriving the Eqs.(104)-(107) it has been assumed that the fluctuations of amplitudes and velocities are small with respect to their average values ($|\Omega_1 - \Omega_2| << \Omega$, $|\eta_1 - \eta_2| << \eta$) and that their relative distance is not too small ($\eta r >> 1$). Single soliton propagation can be easily recovered by Eqs.(104)-(107) as soon as the distance r becomes large enough. In fact, the exponential factor $e^{-2\eta r}$ regulates the strength of the interaction which depends on the distance between the pulses. If we assume $r >> 1$, $k_n = 0$ and $\Omega(z = 0) = 0$ as initial conditions, we have in a first approximation

$$\frac{d\eta_n}{dz} = \frac{d\Omega_n}{dz} = \frac{dT_n}{dz} = 0 , \tag{108}$$

$$\frac{dk_n}{dz} = 2\eta_n^2 . \tag{109}$$

The only parameter of Eq.(92) which depends on z is the phase [38]: $k_n(z) = 2\eta_n^2 z + const.$

4.2 The perturbed NLS equation

Now, adding the third-order dispersion and two Raman terms to the NLS equation, we consider the case $\varepsilon \neq 0$. As perturbation we assume the same form as in Eq.(70)

$$R^{(1)}(\psi,\psi^*) = a_3\psi_{ttt} + a_4(|\psi|^2\psi)_t + a_5(|\psi|^2)_t\psi \ . \tag{110}$$

Overlapping contributions due to the two nonlinear terms are not taken into account. Inserting Eq.(110) into the integrals of Eqs.(99-102), we calculate the contribution of the perturbation on the n-soliton. Following the procedure outlined in the previous section, and using in Eqs.(99)-(102) the perturbation (110), we obtain the following system of differential equations

$$\frac{d\eta_n}{dz} = (-1)^n 16\eta^3 e^{-2\eta r}\sin(\phi) \ , \tag{111}$$

$$\frac{d\Omega_n}{dz} = (-1)^n 16\eta^3 e^{-2\eta r}\cos(\phi) \ , \tag{112}$$

$$\frac{dT_n}{dz} = 2\Omega_n + 4\eta e^{-2\eta r}\sin(\phi) + 4a_3(\eta_n^2 + 3\Omega_n^2) - 4a_4\eta_n^2 - \frac{8}{3}a_5\eta_n^2 \ , \tag{113}$$

$$\begin{aligned}\frac{dk_n}{dz} = {} & 2(\eta_n^2 + \Omega_n^2) + 8\eta e^{-2\eta r}(\Omega\sin(\phi) + 3\eta\cos(\phi)) + \\ & 16a_3\Omega_n(\Omega_n^2 - \eta_n^2) - \frac{16}{3}a_5\Omega_n\eta_n^2 \ .\end{aligned} \tag{114}$$

The soliton-soliton interaction is taken into account at the first order through the overlapping terms. Eqs.(113) and (114) reflect that the soliton acquires a velocity and a phase velocity due to TDO (a_3) and SRS (a_4 and a_5).

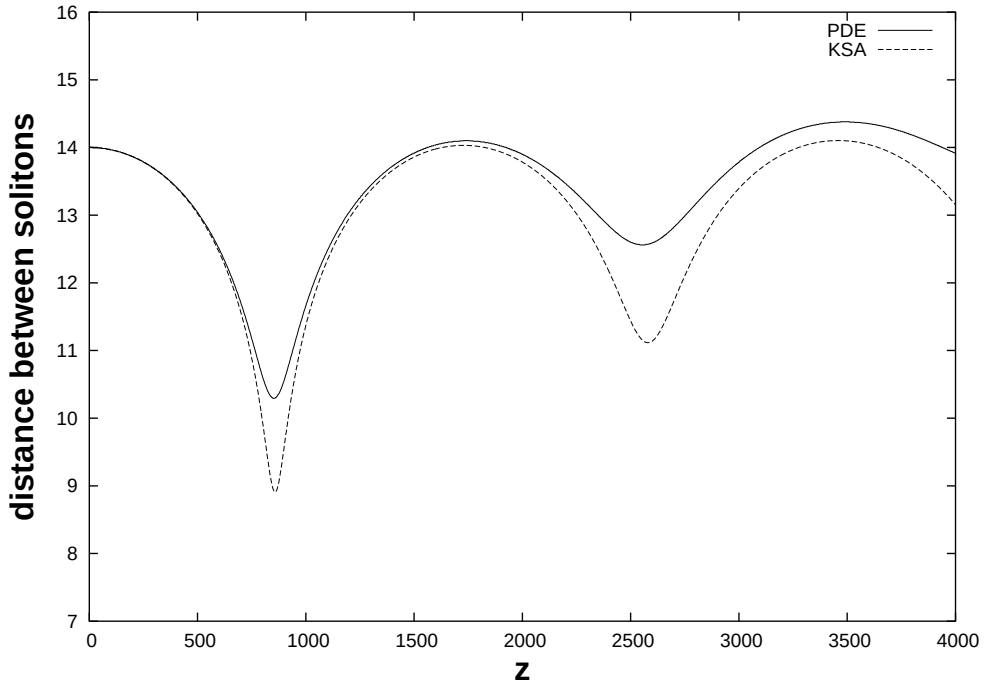

Figure 24: Soliton distance evolution as result of the direct integration of Eq.(93) (PDE) and KSA theory. Initial distance $r = 14$, $a_3 = -0.05$, $a_4 = -0.3$, and $a_5 = 0.3$.

The Eqs.(111)-(114) have been derived under the following assumptions [77]:

a) Dispersive radiation can be neglected.

b) The solitons keep their sech-shape with a fixed relation between width and amplitude.

c) The relative fluctuations in the amplitudes and the velocities are small.

d) The separation between the pulses are not too small.

Now we compare the KSA with direct integration of Eq. (93). We remember that under Hirota conditions amplitude and width are described by the same parameter ($\rho = \eta$ in expression (64)) and the frequency shift Ω becomes arbitrary. All the pictures showed in this section refer to the case with initial distribution (92), where $\eta_{1,2} = \frac{1}{2}$, $\Omega_{1,2} = 0$ and $\delta_{1,2} = 0$.

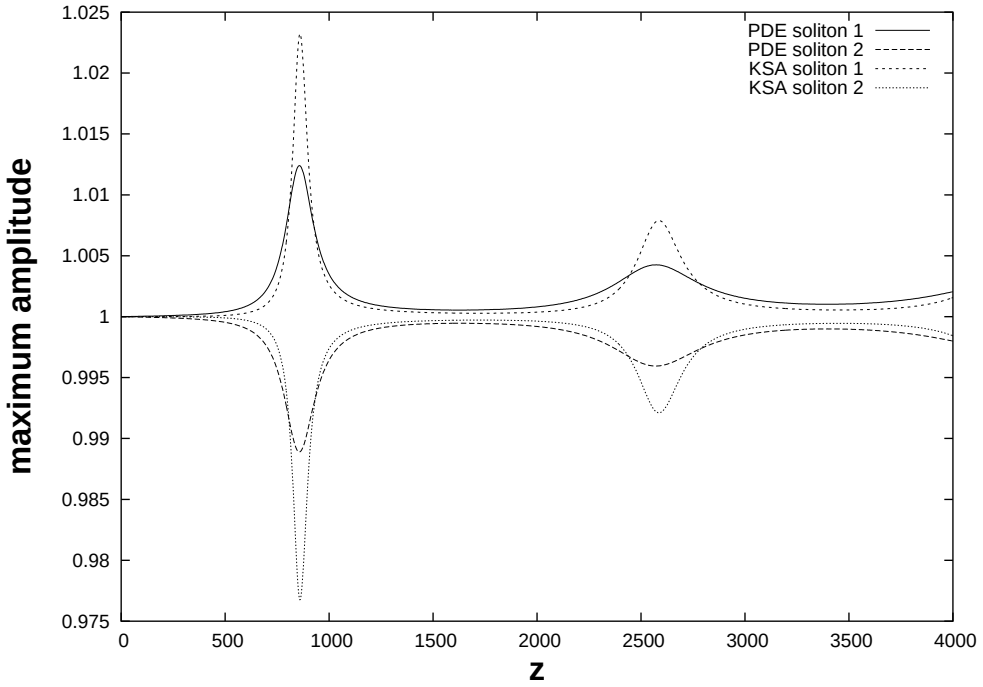

Figure 25: The soliton maximum amplitude evolution as function of the distance is plotted. The parameter values and the initial conditions are the same as those of Fig. 24.

The KSA model gives good results if the perturbation terms are small and the distance between the solitons remains large enough during the propagation. In order to check whether the analytical method and the numerical simulations agree, different initial distances (T_1 and T_2) and higher-order terms (a_3, a_4 *and* a_5) have been chosen. In general we have seen that if the minimum distance between two solitons never goes under $r \simeq 7$ we obtain very good results (even for large perturbation terms). Therefore, it is not possible to study the case where two solitons form a bound state like it happens in case of NLS equation [38].

For our simulations we have chosen a large initial distance between the two pulses and relative large higher-order terms: $r = 14$, $a_3 = -0.05$, $a_4 = -0.3$, and $a_5 = 0.3$. Figs. 24 and 25 show the good qualitative agreement between the analytical description and numerical simulation. Even if the soliton-soliton inter-

action is taken into account only at the first order, the KSA can predict very well the behavior of the pair of pulses. In Fig. 24 we observe the soliton separation evolution with respect of z, while in Fig. 25 the behavior of the maximum amplitudes of a pair of solitons is shown. As one can notice, the ODE model keeps off from the PDE when the distance r is getting smaller (around $z = 850$ and $z = 2600$).

In this chapter, interaction between bright pulses under Hirota conditions have been analytically investigated by employing the Karpman Solv'ev approach. From this analysis we have seen that the presence of higher-order terms gives a significant contribution to the dynamics of the pulse interaction. In fact, in case of the unperturbed NLS equation, two bright solutions close to each other produce a bound state, while in presence of higher-order terms this does not happen. In particular we have proven that under Hirota conditions a repulsive force acts between brighto pulses, see Fig. 24. The analytical description has shown a very good qualitative agreement with the numerical simulations.

5 Dispersion managed bright and black pulses

For the application of signals in long transmission systems, dispersion managed (DM) maps are commonly used. A dispersion compensated map consists of a combination of fibers with sharply different dispersion characteristics, anomalous and normal. The advantages of DM systems with respect to conventional systems have been discussed in Sec. 1.5. What we require for practical application is, that an input pulse could be detected by the receiver at the end of a line. In this chapter we are going to introduce different methods useful to find DM bright and dark solitons for the higher-order nonlinear Schrödinger equation (17). The existence of DM bright solitons, for both perturbed and unperturbed NLS equation, have been proved by several authors, but very few results have been obtained for the dark case.

First, we consider a method already introduced in Sec. 3.2, the variational approach. We discuss advantages and disadvantages of this method and we compare the results with direct numerical simulation of the master equation. As second, we propose an approach based on an integral equation. Even in this case the applicability of the periodic solutions has been carefully studied. Third, we discuss the possibility to obtain periodic solutions of the map by using only numerical simulations. Finally, at last stage, we present a new useful method which combines numerics and analytics.

Fig. 26 shows the map that we have considered in this chapter. It is composed of three segments: the first and the third have positive group delay parameters D (standard mono mode fibers SMF) and a length $\frac{L}{4}$, and the second one negative value of D (dispersion compensating fibers DCF) with a length of $\frac{L}{2}$.

We remember that the local group delay parameter a_2 is given by

$$a_2 = \frac{\lambda^2 D}{2\pi c}, \tag{115}$$

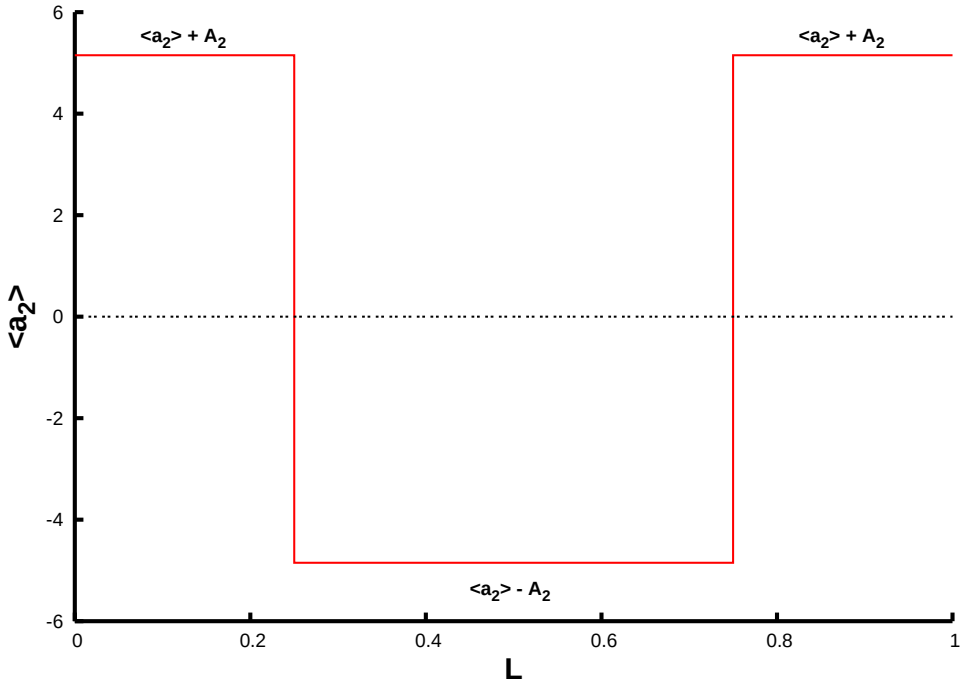

Figure 26: Sketch of a typical symmetric map for dispersion compensation. The map is composed by three segments consecutively positive, negative and positive group delay parameters.

where D $[\frac{ps}{mm\ Km}]$ has been already defined, and λ is the wavelength of a light pulse. The evolution of femtosecond optical pulses in fibers without damping and amplification is described by the following equation (see Sec. 1.4)

$$\psi_z = ia_2(z)\psi_{tt} + ib|\psi|^2\psi + a_3(z)\psi_{ttt} + a_4(|\psi|^2\psi)_t + a_5\psi(|\psi|^2)_t\ . \quad (116)$$

The meaning of the real coefficients a_i (i=2,3,4,5) and b have been previously discussed. The coefficients a_4, a_5 and b are constants along the whole map, while a_2 and a_3 depend on z according to relation (117) and (118)

$$a_2(z) = \begin{cases} < a_2 > + A_2 & \text{if } 0 \leq z \leq \frac{L}{4} \\ < a_2 > - A_2 & \text{if } \frac{L}{4} < z < \frac{L}{2} \\ < a_2 > + A_2 & \text{if } \frac{3}{4}L \leq z \leq L \end{cases} \tag{117}$$

$< a_2 >$ is the average value of the group velocity delay parameter, and A_2 represents the deviation of a_2 from its average value. In case of bright pulses the average dispersion $< a_2 >$ has been chosen bigger than zero, while for dark solitons smaller or equal zero. The dependency of the third order dispersion a_3 on z has been considered has follows

$$a_3(z) = \begin{cases} < a_3 > - A_3 & \text{if } 0 \leq z \leq \frac{L}{4} \\ < a_3 > + A_3 & \text{if } \frac{L}{4} < z < \frac{L}{2} \\ < a_3 > - A_3 & \text{if } \frac{3}{4}L \leq z \leq L \end{cases} \tag{118}$$

Having a look at (117) and (118), it can be noticed that a_2 and a_3 have always opposite singes, since A_2 and A_3 are much larger than $< a_2 >$ and $< a_3 >$, respectively.

5.1 Variational approach

This method was already successfully used in order to find periodic bright solutions in dispersion compensated transmission systems [79]. In this section we consider an approximate variational description for optical pulse evolution in fiber links with varying dispersion [70, 71, 72, 73, 79, 80].

This section is organized as follows. First, we present the equations governing the evolution of the parameters of the pulse along the map, then we compare the results of the ODE model with direct numerical simulation of Eq.(116).
As trial function we choose the following Gaussian form

$$\psi(z,t) = Ae^{-\frac{(t-T_0)^2}{2T^2}} e^{i(\lambda+\Omega(t-T_0)+\mu(t-T_0)^2)} . \quad (119)$$

The pulse is characterized by its amplitude A, width T, position T_0, phase λ, frequency shift Ω and chirp μ. Since all the terms in Eq.(116) are of dispersive type, we can use the energy conservation law in order to reduce the 6 degrees of freedom from to 5. The amplitude of the pulse A can be written as follows: $A = \frac{N}{\sqrt{T}}$, where N is a constant. Here, the last three terms on the right-hand side of Eq.(116) have been treated as perturbations. Following the procedure outlined in Sec. 3.2, we apply the variational approach to obtain a set of differential equations which describes the evolution of the pulse parameters along z

$$T_z = 4\mu T(a_2 + 3a_3\Omega) , \quad (120)$$

$$\mu_z = -\frac{\sqrt{2}N^2(b + a_4\Omega)T + 4(a_2 + 3a_3\Omega)(4\mu^2T^4 - 1)}{4T^4} , \quad (121)$$

$$\Omega_z = -\sqrt{2}\mu\frac{N^2}{T}(a_4 + a_5) , \quad (122)$$

$$\lambda_z = \frac{1}{8T^2}(-12a_3\Omega + \sqrt{2}T(5N^2(b + a_4\Omega) - 2N^2(3a_4 + 2a_5)\Omega) + 8(-a_2 + \Omega^2(a_2 + 2a_3\Omega)T^2 + 6a_3\mu^2\Omega T^4)) , \quad (123)$$

$$T_{0z} = 2a_2\Omega + \frac{3}{2}a_3(2\Omega^2 + \frac{1}{T^2} + 4\mu^2T^2) - \frac{N^2}{T}\frac{3a_4 + 2a_5}{2\sqrt{2}} . \quad (124)$$

It is important to notice that only the first three equations of the system are coupled. For given parameters N, b, a_i (i=2,3,4,5), and initial values ($z = 0$) Ω, T, and μ, we search for which width T the pulse (119) is periodic on a certain map.

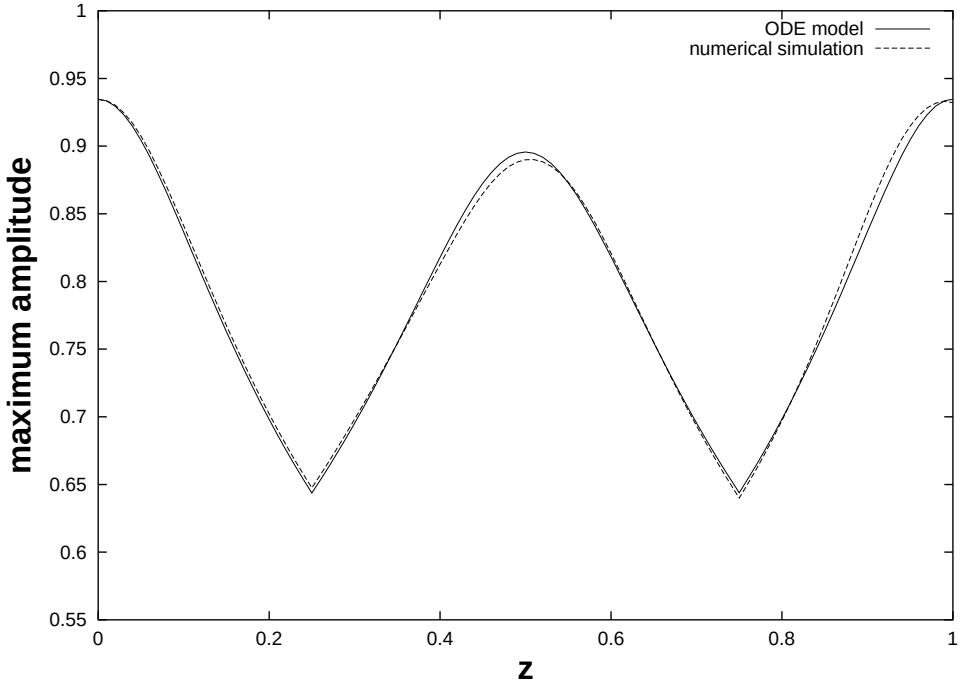

Figure 27: Comparison of the variational approach with direct numerical simulation of Eq.(116). The evolution of the maximum amplitude of a bright pulse along z is shown. The parameters of the map are: $< a_2 >= 0.1$, $A_2 = 5$, $< a_3 >= 0.0$, and $A_3 = 0.1$.

We fix all the parameters and we numerically integrate the system by using an arbitrary value of width $T = T_{initial}$. If the difference between the width at the beginning and at the end of the map, T and T_f respectively, is bigger than the error we would like to have, we increase or decreas T by a small factor δ, so that $T = T_{initial} \pm \delta$. We iterate the process until the difference $T - T_f$ approaches to zero. The periodic initial distribution (119) has been found by setting in Eqs.(120-122) the following coefficients: $< a_2 >= 0.1$, $A_2 = 5$, $b = 1$, $a_3 = 0.0$,

$A_3 = 0.1$, $a_4 = 0.05$ and $a_5 = 0.05$; and as initial parameters ($z = 0$): $T_0 = 0$, $\lambda = 0$, $\Omega = 0$, $\mu = 0$, $N = 1$. The whole map has length $L = 1$.

The periodicity has been found for $T = 1.14475$. To prove the validity of this method, we numerically integrate the Eq.(116) along the map by using the solution of the ODE model. The pulse which propagates along the three segments of the fiber must be periodically reproduced at the end of the map. In Fig. 27 the comparison of the variational approach with direct numerical simulation is shown. Depicted is the evolution of the maximum amplitude of the pulse with respect to z. The maximum initial amplitude is $A(z = 0) = \frac{N}{\sqrt{T}} = 0.935$, while the amplitude measured at the end of the map has value $A(z = L) = 0.932$.

By using this method we were not able to find any DM bright soliton next to the Sasa conditions (23) and (24). This result agrees with the stability analysis of Sec. 3.1, where we have seen that pulses under Sasa conditions are very sensitive to any variation of the linear coefficients (GVD and TOD). As long as the perturbation coefficients (a_3, a_4, a_5) are small compared to a_2 and b, and as long as the parameter N is not much larger than one, the agreement between ODE model and direct numerical simulation of Eq.(116) is very good.

This method is not appropriate to investigate DM dark solitons. While in bright case one can write an ansatz which well describes the propagation of a pulse along the map, for dark soliton this can not be done (at least not so easily). A bright pulse evolves along a dispersion map varying its amplitude, width, phase, and chirp. Numerical simulations of the NLS equation show that a dark soliton changes also its width, phase and chirp, but not its maximum amplitude, which is represented by the background, and its minimum value (in case of dark pulses equal zero). The three degrees of freedom, width, phase and chirp, appear to be not enough to describe the evolution of the pulse. On the left-hand side and on the right-hand side of a dispersion-managed dark soliton appears a tail which is part of the periodic pulse solution (see in the next Sec. 4.1.3, Fig. 30, and in

Sec. 4.1.4, Fig. 32). Along the map the tail changes its amplitude and width to represent periodically itself at the end of each map. Therefore an ansatz of the form

$$\psi = A \tanh(\eta(t-T_0))e^{i(\lambda+\Omega(t-T_0)+\gamma e^{-\mu t(t-t)^2})}, \quad (125)$$

is not appropriate to describe DM dark pulses. In the next section, we present another semi-analytical method based on an integral equation. Our aim will be to check whether this new approach can be used in order to find both DM bright and dark pulses for the Eq.(116).

5.2 Integral equation

In this section we propose an alternative method useful to find periodic solutions of an arbitrary map. The idea of the method is to write an integral equation for the following partial differential equation

$$\begin{aligned} \psi_z(z,t) = & ia_0\psi(z,t) - a_1\psi_t(z,t) + ia_2\psi_{tt}(z,t) + \\ & ib|\psi(z,t)|^2\psi(z,t) - a_3\psi_{ttt}(z,t) - a_5(|\psi(z,t)|^2)_t\psi(z,t) \\ & -a_4(|\psi(z,t)|^2\psi(z,t))_t , \end{aligned} \quad (126)$$

where all the coefficients are real numbers. The linear terms a_i (i=0,1,2,3) depend on z and can be written as

$$a_i = < a_i > + A_i . \quad (127)$$

$< a_i >$ (i=0,1,2,3) are the average values along the whole map, and the A_i represent the deviation of the linear terms from their average values. Substituting (127) into Eq.(126), we obtain

$$\begin{aligned} \psi_z(z,t) &= iA_0\psi(z,t) - A_1\psi_t(z,t) + iA_2\psi_{tt}(z,t) \\ &\quad -A_3\psi_{ttt}(z,t) + \epsilon g(z,t) \ , \end{aligned} \tag{128}$$

where

$$\begin{aligned} g(z,t) &= i < a_0 > \psi(z,t) - < a_1 > \psi_t(z,t) + \\ &\quad i < a_2 > \psi_{tt}(z,t) + ib|\psi(z,t)|^2\psi(z,t) - < a_3 > \psi_{ttt}(z,t) \\ &\quad -a_5(|\psi(z,t)|^2)_t\psi(z,t) - a_4(|\psi(z,t)|^2\psi(z,t))_t \ . \end{aligned} \tag{129}$$

The term $g(z,t)$ contains the average of the linear terms $< a_i >$ (i=0,1,2,3) and the three nonlinear terms b, a_4 and a_5, which have all been treated as perturbation. Next, we search for solutions of Eq.(116) in the perturbation series

$$\psi = \psi_0 + \epsilon\psi_1 + ... \ , \tag{130}$$

and we solve the equation up to the first order. Substituting (130) in Eq.(128), we obtain, at the zero order

$$\partial_z\psi_0 = iA_0\psi_0 - A_1\partial_t\psi_0 + iA_2\partial_{tt}\psi_0 - A_3\partial_{ttt}\psi_0 \ . \tag{131}$$

Replacing the differential operator $\frac{\partial}{\partial t}$ by $-i\omega$, and integrating between 0 and z, we have the zero order solution in Fourier space

$$\psi_0(z,\omega) = \psi_0(0,\omega)e^{i(A_0+A_1\omega-A_2\omega^2-A_3\omega^3)z} . \quad (132)$$

In Fourier space, the equation at the first order has form

$$\begin{aligned}\partial_z\psi_1(z,\omega) &= iA_0\psi_1(z,\omega)+i\omega A_1\psi_1(z,\omega)-i\omega^2A_2\psi_1(z,\omega) \quad (133)\\ &\quad -i\omega^3A_3\psi_1(z,\omega)+\epsilon g_0(z,\omega)\end{aligned}$$

where

$$\begin{aligned}g_0(z,\omega) &= i<a_0>\psi_0(z,\omega)+i<a_1>\omega\psi_0(z,\omega)- \quad (134)\\ &\quad i<a_2>\omega^2\psi_0(z,\omega)-i<a_3>\omega^3\psi_0(z,\omega)+\\ &\quad F[ib|\psi_0(z,t)|^2\psi_0(z,t)-a_5(|\psi_0(z,t)|^2)_t\psi_0(z,t)-\\ &\quad a_4(|\psi_0(z,t)|^2\psi_0(z,t))_t] .\end{aligned}$$

With F we have indicated the Fourier-transform operation and with F^{-1} its inverse. The Eq.(133) is easily solvable. The result is the following

$$\psi_1(z,\omega) = e^{iB(\omega)z}\int_0^L e^{-iB(\omega)z}g_0(z,\omega)dz , \quad (135)$$

where

$$B(\omega) = A_0+A_1\omega-A_2\omega^2-A_3\omega^3 . \quad (136)$$

At this stage, we discuss the periodicity of the first order solution. We require that the pulse at the beginning and at the end of the map has the same form:

$$\psi_1(z=L,\omega) \;=\; \psi_1(z=0,\omega), \tag{137}$$

and therefore, since the initial distribution is represented by $\psi_0(0,t)$, we obtain

$$\psi_1(z=L,\omega) = e^{iB(\omega)z}\int_0^L e^{-iB(\omega)z} g_0(z,\omega)dz \;=\; 0\;. \tag{138}$$

Replacing Eq.(134) into Eq.(138), we have

$$\begin{aligned} i\int_0^L e^{-iBz}(< a_0 > + < a_1 > \omega - < a_2 > \omega^2 - < a_3 > \omega^3)\psi_0(z,\omega) \qquad (139)\\ = \; -\int_0^L (e^{-iBz}F[N(\psi_0,\psi_0^*)])dz \qquad , \end{aligned}$$

where $N(\psi_0,\psi_0^*)$ contains the nonlinear terms

$$\begin{aligned} N(\psi_0,\psi_0^*) \;=\; & b|\psi_0(z,t)|^2\psi_0(z,t) + (r_1+r_2)\partial_t\psi_0^*(z,t)\psi^2(z,t) \qquad (140)\\ & +(r_1+2r_2)\partial_t\psi_0(z,t)|\psi_0(z,t)|^2\;. \end{aligned}$$

Substituting the solution at the zero order (132) into Eq.(139), we finally obtain

$$\psi_{0new}(0,\omega) \;=\; \int_0^L \frac{e^{-iBz}F[N(\psi_0,\psi_0^*)]}{- < a_0 > - < a_1 > \omega + < a_2 > \omega^2 + < a_3 > \omega^3}dz \tag{141}$$

Transforming back from ω space into t space the expression (141), we have the new initial distribution $\psi_{0new}(0,t)$. By using numerics, we iterate this procedure until the incoming distribution $\psi_0(0,t)$ and the new one $\psi_{0new}(0,t)$ are indistinguishable. If after n iterations the difference between the two distribution converge to zero, $\psi_{0new}(0,t)$ is taken as periodic solution of the map.

For our simulations, we have chosen as initial bright distribution $\psi_0(0,t)$ the Gaussian form

$$\psi_0(0,t) \;=\; Ae^{-\frac{t^2}{2T^2}}\;, \tag{142}$$

where A represents the amplitude of the pulse, and T is a parameter related to the width of the pulse. Here we have considered $A = T = 1$. As one can notice Eq.(141) requires that the average term $< a_0 >$ must be different than zero. The coefficients chosen for our simulation are the following: $< a_0 >= -1.0$, $A_0 = 0.0$, $< a_1 >= 0.0$, $A_1 = 0.0$, $< a_2 >= 0.15$, $A_2 = 5.0$, $< a_3 >= 0.0$, $A_3 = 0.2$, $b = 1.0$, $a_4 = 0.03$ and $a_5 = 0.02$. The lengths of the map L has been chosen equal one. The coefficients a_2 and a_3 depend on z and are defined by the Eqs.(117) and (118).

Similar to the previous section, we use the solution $\psi_{0_{new}}(0,t)$ as initial distribution for a direct numerical integration of Eq.(116). In Fig. 28 one can observe the results of the PDE simulation. Shown is the evolution of the maximum amplitude of the pulse along the map. The final amplitude of the pulse at the end of the map $A(z = L) = 1.00038$ is very close to its initial value $A(z = 0) = 1.0$.

The distribution obtained by using the integral equation can be represented as the sum of a real even function and an imaginary odd function (see Fig. 29). A good approximation of $\psi_{0_{new}}(0,t)$ is the following form

$$\psi(0,t) \;=\; Ae^{-\alpha t^2} + itBe^{-\beta t^2}\;. \tag{143}$$

The odd function on the right-hand side of Eq.(143) arises from the odd terms contained in Eq.(126). This method has been tested over a large range of map parameters. If the higher-order terms are small enough, $\epsilon << 1$, the distribution obtained by employing the integral equation is a good approximate solution of our

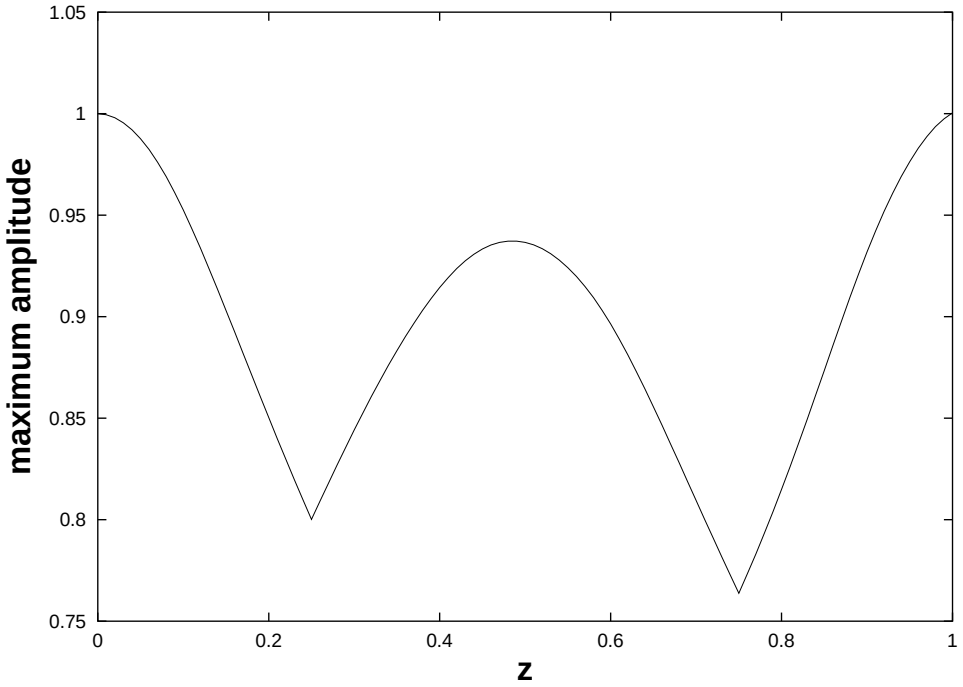

Figure 28: Maximum amplitude evolution of the periodic function obtained by using the integral equation. The pulse at the beginning of the fiber has maximum value $A(z=0)=1.0$ and at the end of the map $A(z=L)=1.00038$.

map. Important to mention is that when the coefficients of the equation almost satisfies the Hirota conditions, DM bright solitons exist. On the other hand, when the Sasa conditions are satisfy, no DM bright solutions have been found. This agrees with the results we have obtained in Sec. 3.2, where we have seen that pulses under Sasa conditions are very sensitive to variations on the linear terms of the master eqaution. The method has been applied in order to find DM dark solutions for the case of an unperturbed NLS equation. However, we have seen that an initial asymmetric pulse having a tanh-form, does not converge into a dark periodic solution of the map. Next, we present a method based on numerical simulations.

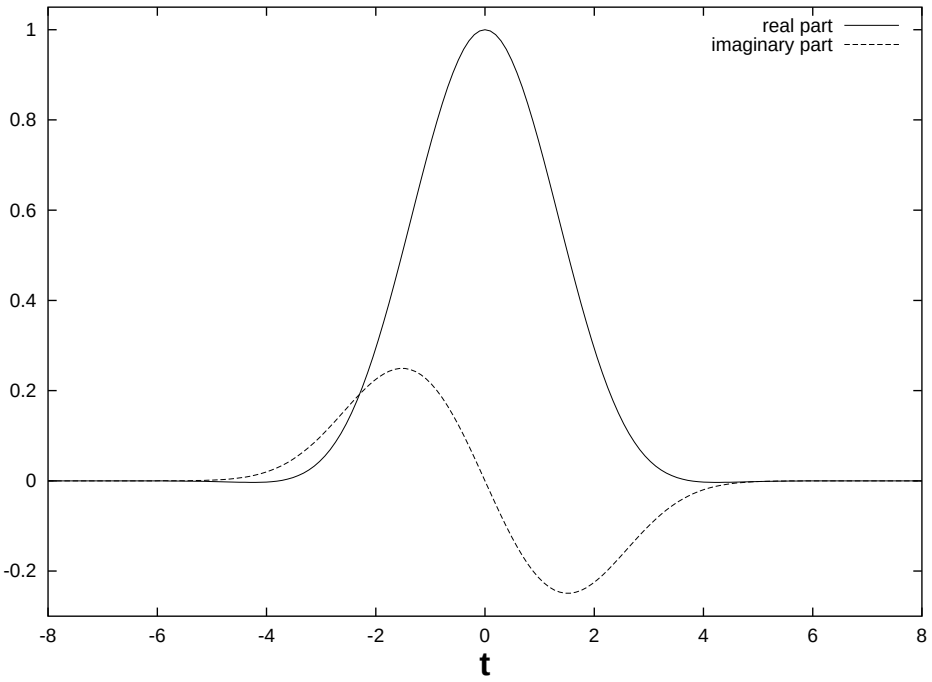

Figure 29: Real part and imaginary part of the periodic solution are shown. The parameters of the map are: $< a_0 >= 0.0$, $A_0 = -1.0$, $< a_1 >= 0$, $A_1 = 0.0$, $< a_2 >= 0.15$, $A_2 = 5$, $< a_3 >= 0.0$, $A_3 = 0.2$, $b = 1$, $a_4 = 0.03$, and $a_5 = 0.02$. $A = T = 1$

5.3 Numerical evaluation

In some particular parameter ranges, it is possible and relatively easy to find both DM bright and dark solitons. As an example we consider the map depicted in Fig. 26, with parameters $< a_2 >= -0.1$, $A_2 = 3.0$ and lenght of the map $L = 1.0$. The nonlinearity has value $b = 0.4$ and the higher-order terms have not been taken into account. As starting distribution we choose the following dark pulse

$$\psi(z,t) \;=\; A\,\tanh(\eta t)\,, \tag{144}$$

where $A = \eta = 1$. We use the expression (144) as starting distribution and we

propagate it along some tens maps by direct numerical simulation of Eq.(116). As long as the average dispersion is not too close to zero, or the parameter A_2 much larger than one, the initial distribution (144) evolves into a periodic solution of the map. During this process part of the exceeding energy is radiated away from the center of the soliton to the boundaries. In Fig. 30 one can see, that DM black pulses present, on the right-hand side and on the left-hand side of the central soliton, an oscillating tail. In case of DM bright solitons such humps can be noticeable only on a logarithmic scale. Important to note is, that while DM bright solitons are close to a Gaussian form, the central core of DM dark pulses are close to the classical case (tanh-form).

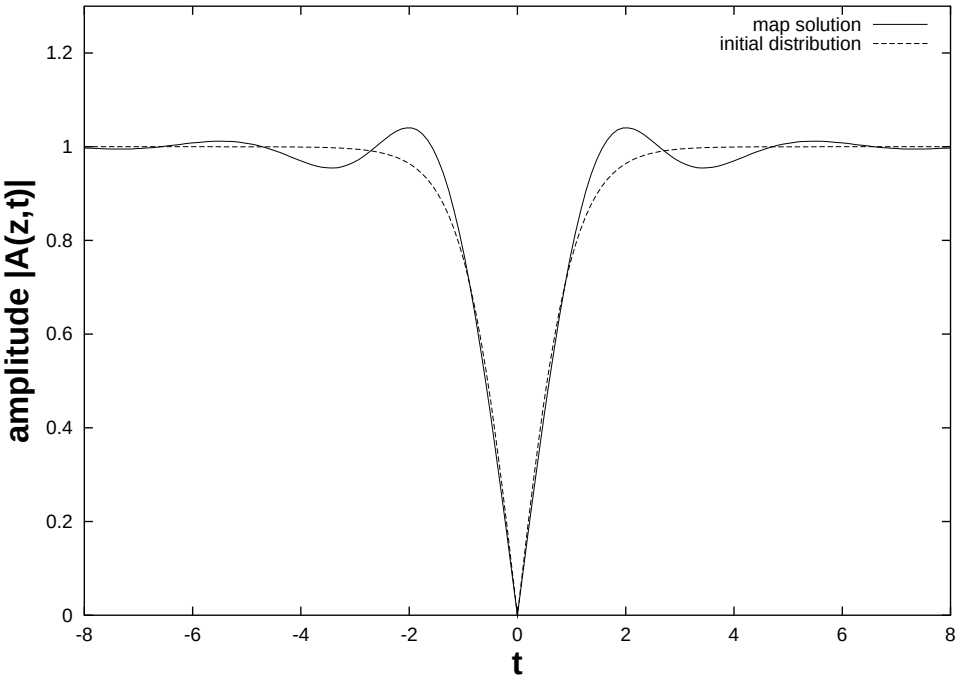

Figure 30: Initial distribution and periodic solution of the map are shown. The periodic solution has been obtained by using only numerical simulations. The parameters of the map are: $< a_2 >= -0.1$, $A_2 = 3$, and $b = 0.4$. The lenght of the map is $L = 1.0$.

The distribution depicted in Fig. 30 has been propagated over tens of dispersion lenghts and any changes in shape have been observed. A periodic solution can be obtained quite easily for different kind of maps. However, if we choose an average dispersion $< a_2 >$ very close to zero, or for large values of A_2, the radiations arising from the soliton are much more intense, and it becomes very difficult to obtain the periodic solution by using only numerics. To overcome this problem we'll present an alternative method in the next section.

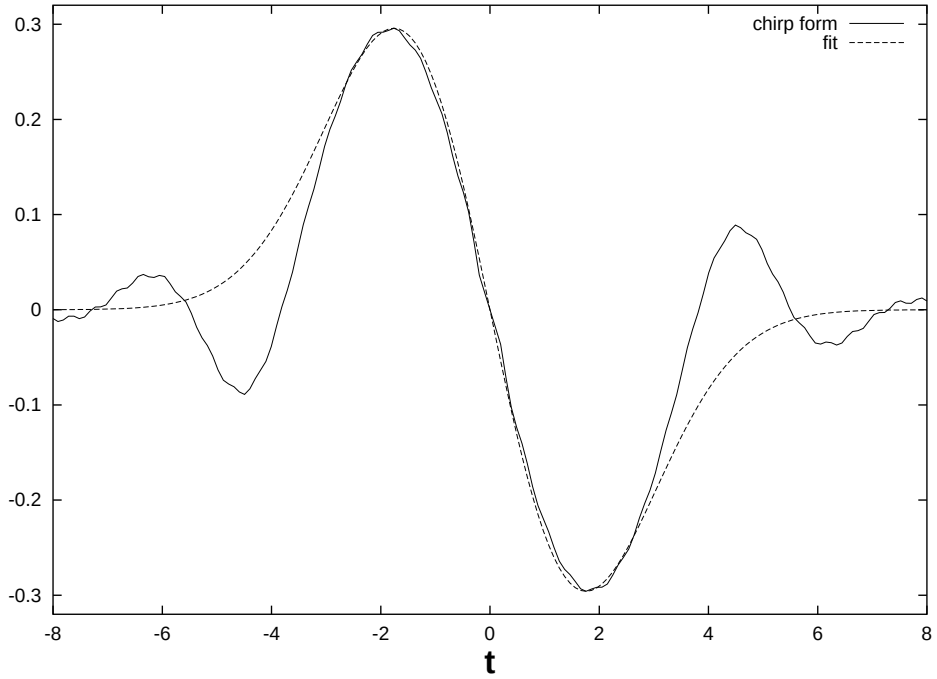

Figure 31: The first derivate in t of the chirp of the periodic solution at point ($z = \frac{3}{4}L$) and its fit function have been shown.

It is known that the phase of DM bright pulses as a quadratic time dependency ($e^{-i\mu t^2}$, where μ is called chirp). Here we show that in case of DM dark pulses the phase has Gaussian time dependency. This result has been obtained by employing numerical methods. What we have calculated is the first derivate in time of the pulse phase pulse depicted in Fig. 30.

$$e^{i\phi} = \frac{\psi}{|\psi|} \quad \longrightarrow \quad \phi_t = -ie^{-i\phi}(\frac{\psi}{|\psi|})_t \ . \tag{145}$$

By using as fit-function

$$f(z,t) = \mu e^{-\gamma t^2} \quad \longrightarrow \quad f(z,t)_t = -2\gamma\mu t e^{-\gamma t^2} \ , \tag{146}$$

we have calculated γ and μ (chirp). In Fig. 31 the function ϕ_t and its fit function $f(z,t)_t$ at the point $z = \frac{3}{4}L$ are shown. The periodic solution (see Fig. 30) has been propagated along the map and at the end of every piece of fiber both parameters γ and μ have been measured. At the beginning and at the end of the whole map the value of the chirp is very close to zero. At the end of the first and of the second segment of fiber, the chirp reaches its minimum and maximum value, respectively. At the distance $z = \frac{L}{4}$ we have measured $\mu = -0.86$, while at $z = \frac{3}{4}L$, $\mu = 0.86$. In both cases the parameter γ related to the width of the Gaussian has value 0.16.

This method can be employed also when higher-order terms are present. A DM dark solution have been found by using the following parameters: $< a_2 >= -0.1$, $A_2 = 3.0$, $b = 1.0$, $< a_3 >= -0.01$, $A_3 = 0.0$, $a_4 = -0.06$ and $a_5 = 0.06$. In the initial distribution (144) $A = \eta = 1$ have been chosen. Important is to point out that the coefficients are very close to satisfy the Hirota conditions (not exactly because a_2 depends on z). Here the periodic solution of the map is very similar to the one depicted in Fig. 30. The pulse acquires a velocity and the minimum of the hump grows from zero (initial value) up to 0.03. Even in this case it is not possible to find any solution of DM bright or dark solitons next to the Sasa conditions. In the next section we present a semi-analitical method usuful to obtain DM dark solitons in case of zero group velocity dispersion ($a_2 = 0$).

5.4 New map

Here, we present a new semi-analytical model which allows us to obtain periodic bright and dark solutions of an arbitrary map. At the end of the map, the wave can be written as the sum of the linear and nonlinear effects of Eq.(116) on the initial distribution $\psi(0,t)$

$$\psi(L,t) = e^{\mathcal{L}}\psi(0,t) + R\,. \tag{147}$$

$\mathcal{L}$ is the linear operator defined as

$$\mathcal{L} = \int_0^L (a_0(z) + a_1(z)\frac{\partial}{\partial t} + a_2(z)\frac{\partial^2}{\partial t^2} + a_3(z)\frac{\partial^3}{\partial t^3})dz\,, \tag{148}$$

and R is the contribution given by the three nonlinear terms on the right-hand side of Eq.(116). To search a periodic solution one has to look for a pulse which has same shape, amplitude and width at the beginning and at the end of the fiber. Therefore, our assumption is

$$\psi(L,t) = e^{i\phi}\psi(0,t)\,. \tag{149}$$

Now we can write the two pulses, $\psi(0,t)$ and $\psi(L,t)$, as a combination of the function at the n-map (ψ_n) and at the $n+1$-map (ψ_{n+1}) through two weight parameters α and β.

By using Eq.(149), Eq.(147) assumes the form

$$\begin{aligned} e^{i\phi_{n+1}}(\alpha\psi_{n+1}(0,t) + (1-\alpha)\psi_n(0,t)) &= \\ = e^{\mathcal{L}}(\beta\psi_{n+1}(0,t) + (1-\beta)\psi_n(0,t)) + R_n & \quad . \end{aligned} \tag{150}$$

Combining the expression (147) and Eq.(150), so that the term R_n vanishes, and recovering $\psi_{n+1}(0,t)$, we obtain

$$\psi_{n+1}(0,t) = \psi_n(0,t) + \frac{\psi_n(L,t) - e^{i\phi_{n+1}}\psi_n(0,t)}{\alpha e^{i\phi_{n+1}} - \beta e^{\mathcal{L}}} . \quad (151)$$

When the difference $\psi_{n+1}(0,t) - \psi_n(0,t)$ approaches to zero, we have the periodic solution of the map. Considering the numerator on the right-hand side of Eq.(151), we can easly see that such difference will be minimal when ϕ_{n+1} coincide with the difference in phase between $\psi_n(L,t)$ and $\psi_n(0,t)$.

We can prove it mathematically. Let us rename $g \equiv \psi_n(0,t)e^{i\phi_{n+1}}$, and $f \equiv \psi_n(L,t)$, we search for which ϕ the following integral becomes minimal

$$\int_0^L |fe^{i\phi} - g|^2 dt = \int_0^L (|f|^2 + |g|^2 - e^{i\phi}fg^* - e^{-i\phi}f^*g)dt . \quad (152)$$

The integral is minimal when the two last integrals are maximal.

$$Y(\phi) = \int_0^L e^{i\phi}fg^*dt + \int_0^L e^{-i\phi}f^*gdt = \delta e^{i\phi} + \delta^* e^{-i\phi} . \quad (153)$$

The function $Y(\phi)$ is maximal when

$$e^{i\phi}\delta = e^{-i\phi}\delta^* . \quad (154)$$

We can write $\delta = |\delta|e^{i\widetilde{\phi}}$ and $\delta^* = |\delta|e^{-i\widetilde{\phi}}$. Finally we found that the expression (152) is minimal when $\phi = -\widetilde{\phi}$. The phase ϕ as well as ψ_{n+1} have been calculated numerically.

Also the pulse at the end of the map $\psi(z = L, t)$ has been obtained by direct numerical simulation of Eq.(116). α and β are real number, and the only condition

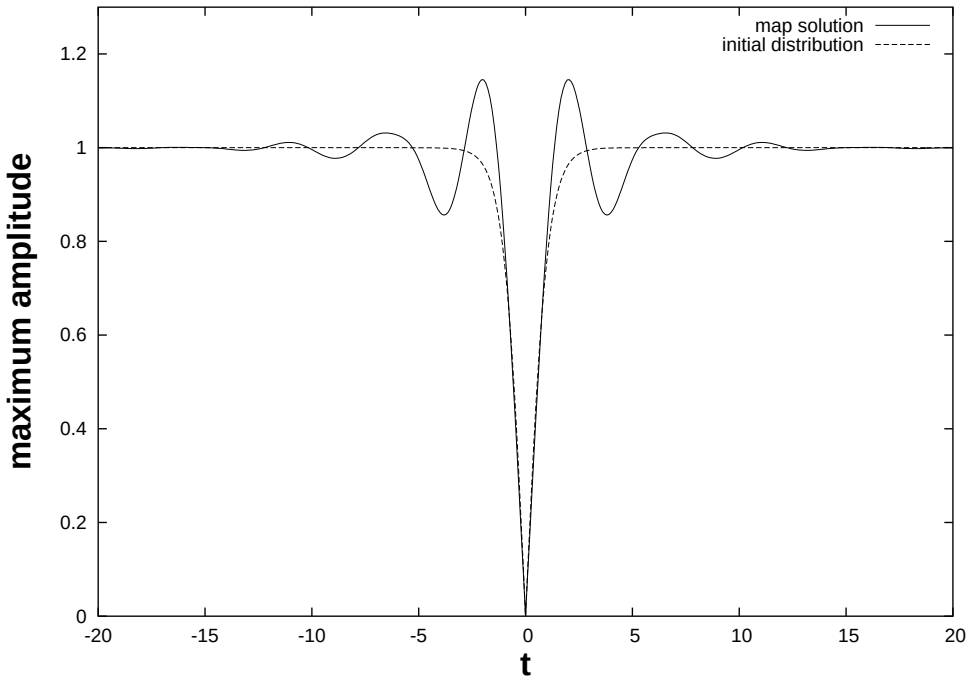

Figure 32: Absolute value of the initial distribution and of the periodic solution of the map are shown. The parameters of the map are: $< a_2 >= 0.0$, $A_2 = 5.0$, and $b = 0.4$

which they have to statisfy is, that they cannot be simultaneously equal zero. In order to test the goodness of the method, we consider the unperturbed NLS equation. This means that the higher-order terms in Eq.(116) have been set equal to zero. The two weight parameters α and β play a crucial role. In fact, the convergency of the initial distribution depends strongly on them. For every map and starting pulse, using a iterative proceeding, we search the right values of α and β. In the previous section we have discussed the difficulty to obtain a dark periodic solution of a map having average dispersion equal zero. Now we show the solution obtained for the following parameters of the map: $< a_2 >= 0.0$, $A_2 = 5.0$, and $b = 0.4$. As initial distribution $\psi(z = 0, t)_{n=0}$, we choose

$$\psi(z = 0, t)_{n=0} \quad = \quad A \tanh(\eta t) \; . \tag{155}$$

In our simulation $A = \eta = 1$ have been chosen. In Fig. 32 the absolute value of the initial distribution and the solution of the map are shown. As one can notice by a comparison of Fig. 30 with Fig. 32, the tails of the background next to the central solitons are much higher when the average dispersion is equal zero and when A_2 becomes larger. Because the complex form of our solution, it becomes difficult suggest an expression which could be used as trial function for analitic methods.

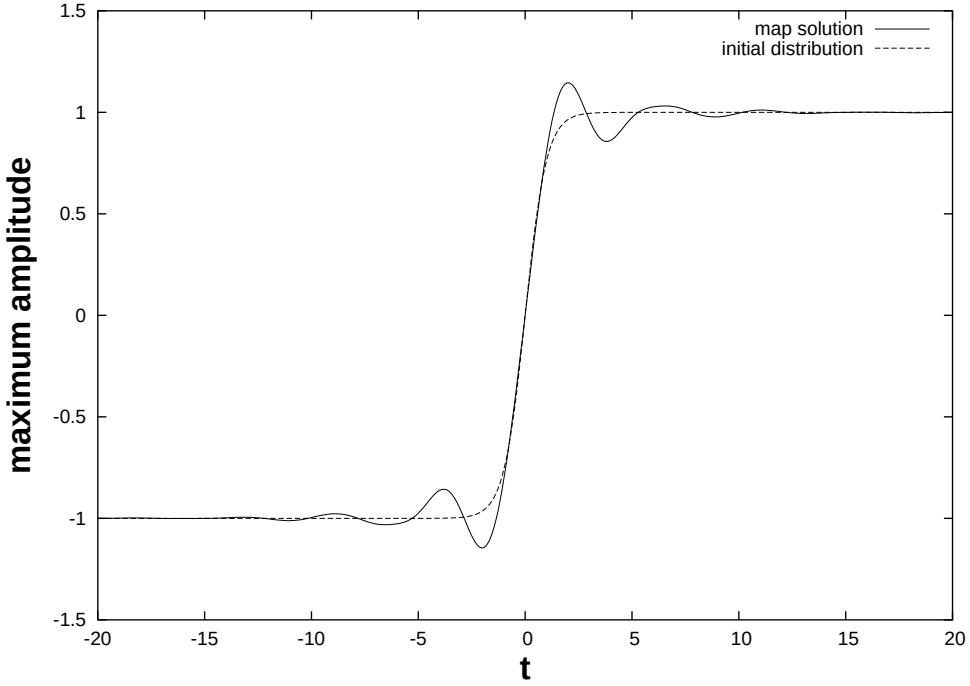

Figure 33: Real part of the initial distribution and of the periodic solution of the map are shown. The parameters of the map are: $< a_2 >= 0.0$, $A_2 = 5.0$, and $b = 0.4$.

Using this method we are able to obtain, after few hundreds iterations, DM bright and dark solitons. For this particular map the best results have been obtained by using $\alpha = -1.2$ and $\beta = -1.1$. The largest difference d between the absolute value of the pulse at the beginning and at the end of the map, was $d = 4.769\ 10^{-6}$, obtained after 300 iterations ($d = 9.028\ 10^{-7}$, after 1000

iterations). Fig. 33 shows the real part of the initial distribution and of the periodic solution. The imaginary part of both initial and final distribution are equal zero. The only condition that we have to fulfill for dark pulses is that the average dispersion $< a_2 >$ must be equal zero. Even if we include the higher-order terms in the discussion, this method shows us the existence of DM dark solutions. The higher-order terms have been setted: $< a_3 >= 0.0$, $A_3 = 0.05$, and $a_4 = a_5 = 0.01$. By using $\alpha = -1.2$ and $\beta = -1.1$, we have obtained a convergency after 300 iteractions. The biggest difference d between the absolute value of the input and output function have been estimeted of $\simeq 5 \cdot 10^{-5}$. The periodic solution has a form very similar to the one depicted in Fig. 32.

The same method has been used to calculate periodic bright solution when also higher-order terms are included. Fig. 34 shows the absolute value of the periodic pulse obtained by using the following map parameters: $< a_2 >= 0.15$, $A_2 = 5.0$, $b = 1.0$, $a_3 = -0.05$, $a_4 = -0.3$, $a_5 = 0.3$. The coefficients refer to Eq.(116). For bright pulses there are not restrictions on the average of dispersion $< a_2 >$ (for dark it has to be equal zero). $\alpha = 8$ and $\beta = 1$ have been used.

As initial distribution we have chosen a Gaussian form

$$\psi(z = 0, t)_{n=0} \quad = \quad Ae^{-\eta t^2} \ , \tag{156}$$

with $A = \eta = 1$.

Fig. 34 shows the periodic bright solution of the map. When higher-order terms are included, the pulse presents two little humps on both sides of the central core. In case of unperturbed NLS equation, such humps are noticeable only on a logarithmic scale. Both the DM bright and dark solitons has been propagated over tens maps and any changes in shape have been observed.

The last part of this work was dedicated to find out if Eq.(116) admits the exis-

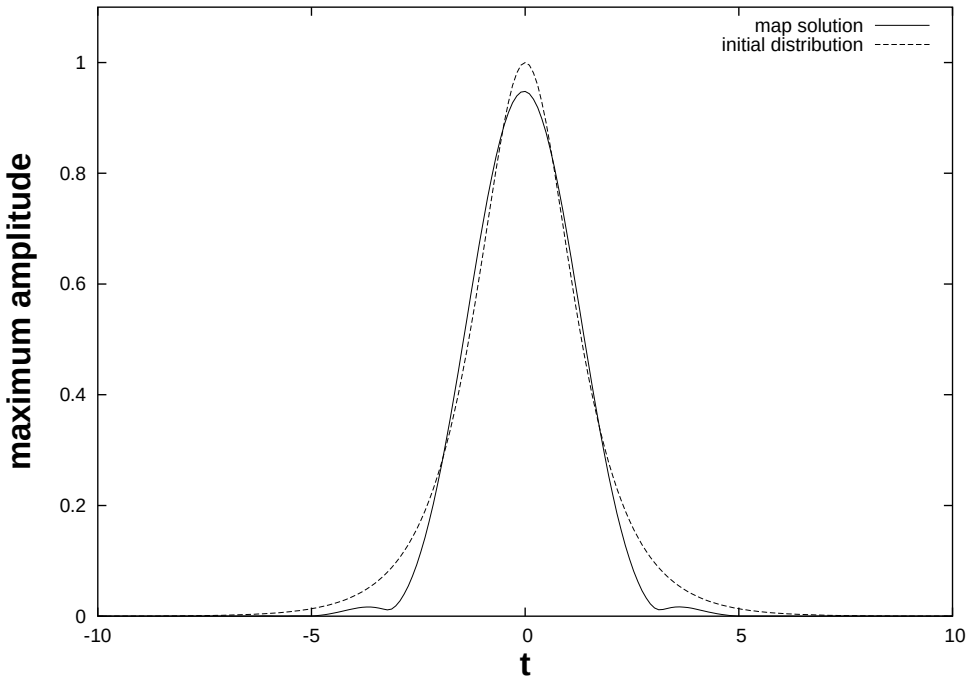

Figure 34: Absolute value of the initial distribution and of the periodic solution of the map are shown. The periodic bright pulse shows two humps on the right and lefth-hand side of the central pulse.

tence of DM bright and dark solitons. We have presented four different methods which can be succesfully used in this sense. In particular, the first two (variational approach and integral equation) have given good results for bright pulses, while the third and the fourth (numerical simulation and new map) can be applied in both bright and dark case. The main advatage of the last two with respect to the first two is, that higher-order terms have not been treated as perturbations. DM bright and dark solitons have been obtained in different parameter ranges, but we have seen that next to the Sasa conditions these solutions do not exist.

6 Summary

In this work the stability of new types of short-pulses, combinations of bright and dark solitons, have been investigated numerically. Such solutions have shown a very high robustness against amplitude, width, shape, chirp and noise perturbations. On the other hand, they become strongly unstable when the second and third order dispersion, GVD and TOD respectively, are disturbed. Results of particular interest have been obtained by disturbing one of the two Raman terms of the master equation. In fact, in case of bright-like pulses, the initial distribution changes its characteristics and evolves into a completely new type of solution. Significant results also come from the study of interaction and collision. We have observed that a repulsive force acts between bright-like pulses, while two dark-like pulses form a bound state. On the other hand, when we let both bright-like and dark-like pulses collide, we see, that they cross each other preserving their shape. Such particle-like behavior indicates, that the solitary waves behave like solitons.

Successively, we have presented analytical methods useful to investigate the stability of bright pulses and their interaction. In particular, we have confirmed the results concerning the stability analysis of bright pulses under Sasa conditions, and we have proved that when the Hirota conditions are fulfilled, bright pulses do not present any instability. The dynamics of the pulses interaction during their transmission in a fiber have been studied by employing the Karpman Solv'ev approach (KSA).

In the last part of the work, we have presented four different methods which can be used in order to find periodic solutions of a given DM map: variational approach, integral equation, numerical simulation and a new semi-analytic map. All of them take into account higher-order terms. Some of these methods can be used only for bright pulses, but others have been successfully adopted also in dark case. Both DM bright and dark solitons can be easily obtained in coefficient

ranges far from Sasa conditions.

7 Bibliography

References

[1] A. Hasegawa, Physics and Applications of Optical Solitons in Fibers'95, (Kluwer Academic Publishers, 1996).

[2] D. Marcuse, Light Transmission Optics (Van Nostrand Reinhold, New York, 1982), Chaps. 8 and 12.

[3] V. Ramaswamy, I. P. Kaminow, P. Kaiser, and W. G. French, Appl. Phys. Lett. **33**, 814 (1978).

[4] I. P. Kaminow, IEEE J. Quantum Electron. **QE-17**, 15 (1981).

[5] D. N. Pyne, A. J. Barlow, and J. J. R. Hansen, IEEE J. Quantum Electron. **QE-18**, 477 (1982).

[6] S. C. Rashleigh, J. Lightwave Technol. **LT-1**, 312 (1983).

[7] J. Noda, K. Okamoto, and Y. Sasaki, J. Lightwave Technol. **LT-4**, 1071 (1986).

[8] N. Bloembergen, Nonlinear Optics (Benjamin, reading, MA, 1977), Chap. 1.

[9] Y. R. Shen, Principles of Nonlinear Optics (Wiley, New york, 1984).

[10] P. N. Butcher and D. N. Cotter, The Elementes of Nonlinear Optics (Cambridge University Press, cambridge, UK, 1990).

[11] R. W. Boyd, Nonlinear Optics (Academic Press, San Diego, CA, 1992).

[12] R. H. Stolen and C. Lin, Phys. Rev. A **17**, 1448 (1978).

[13] A. Hasegawa and F. Tappert, Appl. Phys. Lett. **23**, 142 (1973).

[14] R. H. Stolen, E. P. Ippen, and A. R. Tynes, Appl. Phys. Lett. **20**, 62 (1972).

[15] E. P. Ippen and R. H. Stolen, Appl. Phys. Lett. **21**, 539 (1972).

[16] R. G. Smith, Appl. Opt. **11**, 2489 (1972).

[17] K. Porsezian and K. Nakkeeran, Phys. Rev. Lett. 76, 3955 (1996).

[18] J. Kim, Q.H. Park and H.J. Shin, Phys. Rev. E 58, 6746 (1998).

[19] Kodama, Y. (1985). On integrable system with higher order correction. Phys. Lett. A, 107, 245-249.

[20] Kodama, Y. (1985). Optical solitons in a monomode fiber. J. Stat. Phys., 39, 597-614.

[21] F. DeMartini, C. H. Townes, T. K Gustavson, and P. L. Kelley, Phys. rev. 164, 312 (1967)

[22] D. Grischkowsky, E. Courtens, and J. A. Armstrong, Phys. rev. Lett. 31,422 (1973).

[23] N. Tzoar and M. Jain, Phys. Rev. A 23, 1266 (1981).

[24] D. Anderson and M. Lisak, Phys. Rev. A 27, 1393 (1983).

[25] G. Yang and Y. R. Shen, Opt. Lett. 9, 510 (1984).

[26] J. T. Manassah, M. A. Mustafa, R. A. Alfano, and P. P. Ho, IEEEJ. Quantum Electron. QE-22, 197 (1986).

[27] E. A. Golovchenko, E. M. Dianov, A. M. Prokhorov, and V. N. Serkin, Sov. Phys. Dokl. 31, 494, (1986).

[28] K. Ohkuma, Y. H. Ichikawa, and Y. Abe, Opt. Lett. 22, 516 (1987).

[29] Y. Kodama and K. Nozaki, Opt. Lett. 12, 1038 (1987).

[30] F. M. Mitschke and L. F. Mollenauer, Opt Lett. 11, 659 (1986).

[31] J. P. Gordon, Opt. Lett. 11, 662 (1986).

[32] P. Beau, W. Hodel, B. Zysset, and H. P. Weber, IEEE J. Quantum Electron. QE-23, 1938 (1987).

[33] K. Tai, A. Hasegawa, and N. Bekki, Opt. Lett. 13, 392 (1988).

[34] A. B. Grudinin, E. M. Dianov, D. V. Korobkin, A. M. Prokhorov, V. N. Serkin, and D. V. Khaidarov, JEPT Lett. 46, 221 (1987).

[35] See, for example, G.P. Agrawal, *NonlinearFiberOptics* (Academic Press, New York, 1995).

[36] K. J. Blow, N. J. Doran, and David Wood, J. Opt. Soc. Am. B 6, 1301 (1988).

[37] Z. Li, Lu Li, H. Tian, G. Zhou, and K. H. Spatschek, Phys. Rev. Lett., Vol 89, Nr 26, (2002)

[38] A. Hasegawa and Y. Kodama, *Solitons in Optical Communications* (Oxford University Press, Oxford, 1995).

[39] Y.Kodama and A.Hasegawa, IEEE J. Quantum Electron. 23, 510 (1987).

[40] R. Hirota, J. Math. Phys. **14**, 805 (1973).

[41] N. Sasa and J. Satsuma, J. Phys. Soc. Jpn. **60**, 409 (1991).

[42] M. J. Potasek and M. Tabor, Phys. Lett. A **154**, 449 (1991).

[43] D. Mihalache, N. Truta, and L.-C. Crasovan, Phys. Rev. E **56**, 1064 (1997).

[44] M. Gedalin, T. C. Scott, and Y. B. Band, Phys. Rev. Lett. **78**, 448 (1997).

[45] J. Kim, Q.H. Park and H.J. Shin, Phys. Rev. E 58, 6746 (1998).

[46] E. M. Gromov, L. V. Piskunova, and V. V. Tyutin, Phys. Lett. A **256**, 153 (1999).

[47] S. L. Palacios, A. Guinea, J. M. Fenández-Díaz, and R. D. Crespo, Phys. Rev. E **60**, R45 (1999).

[48] V. I. Karpman, Phys. Rev. E **62**, 5678 (2000).

[49] Z.H. Li, L. Li, H.P. Tian and G.S. Zhou, Phys. Rev. Lett. **84** 4096 (2000).

[50] J. A. Fleck, J. R. Morris, and M. D. Feit, Appl. Phys. **10**, 129 (1976).

[51] J. W. Cooley and J. W. Tukey, Math. Comput. **19**, 297, (1965).

[52] T. R. Taha and M. J. Ablowitz, J. Comp. Phys. **55**, 203 (1984).

[53] M. Lax, J. H. Batteh, and G. P. Agrawal, J. Appl. Phys. **52**, 109 (1981).

[54] M. D. Feit and J. A. Fleck, Appl. Opt **17**, 3990 (1978).

[55] M. D. Feit and J. A. Fleck, Appl. Opt **18**, 2843 (1979).

[56] G. P. Agrawal, J. Appl. Phys. **56**, 3100, (1984).

[57] P. Meissner, E. Patzak, and D. Yevick, IEEE J. Quantum Electron. **QE-20**, 899 (1984).

[58] G. P. Agrawal, J. Lightwave Technol. **LT-2**, 537 (1984).

[59] E. A. Sziklas and A. E. Siegman, Appl. Opt. **14**, 1874 (1975).

[60] M. Lax, G. P. Agrawal, M. Belic, B. J. Coffey, and W. H. Louisell, J. Opt. Soc. Am. A **2**, 732 (1985).

[61] B. Hermansson, D. Yevick, and P. Danielsen, IEEE J. Quantum Electronic **QE-19**, 1246 (1983).

[62] L. Thylen, E. M. Wright, G. I. Stegeman, C. T. Seaton , and J. V. Moloney, Opt. Lett. **11**, 739 (1986).

[63] D. Yevick and B. Hermansson, Opt. Commun. **47**, 101 (1983).

[64] V. A. Vysloukh, Sov J. Quantum Electron. **13**, 1113 (1983).

[65] R. H. Hardin and F. D. Tappert, SIAM Rev. Chronicle **15**, 423 (1973).

[66] V. I. Karpman, J. J. Rasmussen, and A. G. Shagalov, Phys. Rev. E **64**, 026614 (2001).

[67] A. Mahalingam and K. Porsezian, Phys. Rev. E **64**, 046608 (2001).

[68] L. Li, Z.H. Li, Z.Y. Xu, G.S. Zhou, and K.H. Spatschek, Phys. Rev. E **66**, 046616 (2002).

[69] Z.H. Li, G.S. Zhou, and D.C. Su, SPIE Proceedings (SPIE, Bellingham, 1998), Vol 3552, p. 226.

[70] I. Gabitov, S.K. Turitsyn, Optics Lett. 21 (1996) 327; Pisma ZETP 63 (1996) 814.

[71] J.N. Kutz, P. Holmes, S.G. Evangelides Jr., J.P. Gordon, J. Opt. Soc. Am. B 22 (1997) 372.

[72] A. Berntson, D. Anderson, M. Lisak, M.L. Quiroga-Teixeiro, M. Karlsson, Optics. Comm. 130 (1996) 153.

[73] I. Gabitov, E.G. Shapiro, S.K. Turitsyn, Optics Comm. 134 (1996) 317; Phys. Rev. E 55 (1997) 3624.

[74] D. Anderson, Phys. Rev. A 27 (1983) 3135.

[75] V.I. Karpamn and V.V. Solov'ev, Physica D **3**, 487 (1981).

[76] V. S. Gerdjikov, I. M. Uzunov, E. G. Evstatiev and G. L. Diankov, Phys. Rev. E **55**, 6039 (1997).

[77] I.M. Uzunov, M. Gölles, and F. Lederer, Phys. Rev. E 52, 1059 (1995).

[78] A.B. Aceves, C. De Angelis, G. Nalesso. and M. Santagiustina, Opt. Lett. **19**, 2104 (1994).

[79] S. K. Turitsyn, I. Gabitov, E. W. Laedke, V. K. Mezentsev, S. L. Musher, E. G. Shapiro, T. Shäfer, K. H. Spatschek, Opt. Comm. **151**, 117-135 (1998).

[80] E. Shapiro, S. K. Turitsyn, Phys. Rev. E (Rpid Communications) 56 (1997).

[81] M. Suzuki, I. Morita, S. Yamamoto, H. Taga, and S. Akiba, Electro. Lett. Vol. 31, 2027-2028 (1995).

[82] M. Nakazawa, and H. Kubota, Electron. Lett., Vol. 31, 216-217 (1995).

[83] N. J. Smith, F. M. Knox, N. J. Doran, K. J. Blow, and I. Bennion, Electron. Lett., Vol. 32, 54-55 (1996).

[84] T. Yu, E. A. Golovchenko, A. N. Pilipetskii, and C. R. Menyuk, Opt. Lett., Vol. 22, 793-795 (1997).

[85] J. M. Jacob, E. A. Golovchenko, A. N. Pilipetskii, G. M. Carter, and C. R. Menyuk, IEEE Photon. Technol. Lett., Vol. 9, 130-132 (1997).

[86] L.F. Molleauer, S. G. Evangelides Jr., H. A. Haus, IEEE J. Lightwave Technol. 9 (1994) 194.

[87] L.F. Molleauer, P. V. Mamyushev, M. J. Neubelt, Optics Lett. 19 (1995) 704.

[88] A. Hasegawa, Y. Kodama, Optics Lett. 15 (1990) 1444; Phys. Rev. Lett. 66 (1991) 161.

[89] Y. S. Kivshar, K. H. Spatschek, M. L. Quiroga Teixeiro, S. K. Turitsyn, Pure Appl. Optics 4 (1995) 281.

[90] M. J. Ablowitz and G. Bondini, Opt. Lett. 21, 327 (1996).

8 Acknowledgments

The work was carried out at the Institut für Theoretische Phusik I, Heinrich-Heine-Universität Düsseldorf.

I thank Herr Prof. Dr. K.- H. Spatschek for providing me with a valuable support during these years; his willingness to discuss the results and careful reading of the manuscript which helped to refine it considerably.

I am thankful to Prof. Dr. Christos N. Likos for evaluating my work.

To Dr. Zhonghao Li for the interesting and stimulating discussions and for the revision of the manuscript.

A special thanks to Dr. Laedke for introducing me to the world of programming and for his help in innumerable situations.

I am very thankful to Frau Gröters and Frau Gerardi for their constant solar presence and their invaluable help in the resolution of numerous organizational and bureaucratic problems.

To Alexander Posth (with whom I shared the office) for the help he gave me from the very beginning in solving many little problems, and to Dr. Wenk for administration of the network and computer serviceability.

I am thankful to Herr Zügge for his always positive mood and because he tried to learn Italian so that I could feel a bit (more like) at home.

To Dmitri Lesnik and Prof. Dr. Sydora for revising the manuscript and to Christoph Karle, Sylvie Defrasne, Marcus Neuer, Andreas Wingen, Kolja Kauder and Zelimir Marojevic for contributing to the pleasant working atmosphere.

I thank all the friends who have helped me during this time in numerous situations.

I gratefully thank my parents, my brother, my grandmother and all the relatives

who gave me support and I always felt them next to me.

And of course a very special thanks to my girlfriend, Annegret, who encouraged me during these last years and for her help in revising the manuscript.